2017

Catalytic Hydrotreatment for the Development of Renewable Transportation Fuels

LiLu Funkenbusch
Michigan Technological University, ltfunken@mtu.edu

CATALYTIC HYDROTREATMENT FOR THE DEVELOPMENT OF RENEWABLE TRANSPORTATION FUELS

By

LiLu Tian Funkenbusch

A DISSERTATION

Submitted in partial fulfillment of the requirements for the degree of

DOCTOR OF PHILOSOPHY

In Chemical Engineering

MICHIGAN TECHNOLOGICAL UNIVERSITY

2017

This dissertation has been approved in partial fulfillment of the requirements for the Degree of DOCTOR OF PHILOSOPHY in Chemical Engineering.

Department of Chemical Engineering

Dissertation Advisor:	*Dr. Michael E. Mullins*
Committee Member:	*Dr. David R. Shonnard*
Committee Member:	*Dr. Tony N. Rogers*
Committee Member:	*Dr. Audrey L. Mayer*
Department Chair:	*Dr. Pradeep Agrawal*

Table of Contents

List of Figures

List of Tables

Preface

The work contained in this dissertation was conducted in the department of Chemical Engineering at Michigan Technological University from August 2012 to October 2017. Some of the chapters in this dissertation are journal articles that have been submitted or are being prepared for submission (Chapters 2, 4, 5, and 6).

This dissertation was written by LiLu Tian Funkenbusch. All experiments and measurements discussed within this dissertation were performed by LiLu Tian Funkenbusch with the assistance of collaborators acknowledged in the acknowledgement section of this dissertation.

Acknowledgements

Thank you to my advisor Dr. Michael E. Mullins for his guidance and insight throughout this project. I would also like to thank my committee members, Dr. Audrey Mayer, Dr. Tony Rogers, and Dr. David Shonnard, for their time and input. Thank you to our collaborators: Dr. David Shonnard, Janet C. Metsa, Dr. Louise Olsson, Muhammad Abdus Salam, Dr. Lennart Vamling, Tallal Belkheiri, Nattapol Srettiwat, and Dr. Olumide Winjobi. Many thanks to our machinist, Jerry Norkol, and the rest of the staff in our department, without whom this project would not have been possible. Thank you to my undergraduate researchers as well.

The bulk of this research was funded by the National Science Foundation through a Sustainable Energy Pathways Grant (MSP/CHE-ENG/ECCS-1230803). Funding also came from the Department of Energy Argonne National Laboratory (Contract #3F-31321) and the King-Chavez-Parks Future Faculty Fellowship. Support was also provided by Dr. Louise Olsson at Chalmers University.

To Dylan, for always making me smile. To MayLin, Dan, William, and George, for always being there for me. To my mother, for your strength and inspiration. To my father, for your help and guidance. Your love and support mean the world to me. I love you all more than words can express. Thank you.

Abstract

Biologically-derived feedstocks are a highly desirable source of renewable transportation fuel. They can be grown renewably and can produce fuels similar in composition to conventional fossil fuels. They are also versatile and wide-ranging. Plant oils can produce renewable diesel and wood-based pyrolysis oils can be made into renewable gasoline. Catalytic hydrotreatment can be used to reduce the oxygen content of the oils and increase their viability as a "drop-in" transportation fuel, since they can then easily be blended with existing petroleum-based fuels. However, product distribution depends strongly on feedstock composition and processing parameters, especially temperature and type of catalyst. Current literature contains relatively little relevant information for predicting process-level data in a way that can be used for proper life cycle or techno-economic assessment. For pyrolysis oil, the associated reaction pathways have been explored via experimental studies on model compounds in a bench scale hydrotreatment reactor. The reaction kinetics of each compound were studied as a function of temperature and catalyst. This experimental data is used to determine rate constants for a hybrid, lumped-parameter kinetic model of paradigm compounds and pyrolysis oil, which can be used to scale-up this process to simulate larger, pilot-scale reactors. For plant oils, some appropriate data was found in the literature and adapted for a preliminary model, while some experimental data was also collected using the same reactor constructed for the pyrolysis oil studies. With a systematic collection of kinetic data, hydrotreatment models can be developed that can predict important life cycle assessment inputs, such as hydrogen consumption, energy consumption and greenhouse gas production, which are necessary for regulatory and assessment purposes. As a demonstration of how this model can be incorporated into assessment tools, a technoeconomic analysis was performed on the hydrothermal liquefaction of lignin from a pulp mill, with some of the products sent to a refinery to create biofuel and some of the products used to create BTEX. The process-level model developed earlier was used to model hydrotreatment reactors used to generate commodity chemical co-products from phenolic compounds. Overall, this process showed promise and, with improving separations technology, could be a valuable source of revenue for pulp mills and refiners. However, in order to be truly profitable, the minimum selling price of the biofuel would need to be between $3.52 and $3.96 per gallon.

1. Introduction & Motivation

Biofuels, such as plant oil, algal oil, waste cooking oils, pyrolysis oil, tall oils, and tallow, are attractive, renewable fuel sources because they can yield hydrocarbon products with chemical and physical properties similar to and compatible with traditional fossil fuels. This allows producers to blend the products with fossil fuels easily and take advantage of existing infrastructure. Because these biofuels are derived from renewable, abundant and more environmentally-friendly sources, significant research efforts have been focused on the optimal production of feedstocks and conversion method. Interest is especially high in areas that are relatively undeveloped in the fuels market. Relatively little focus, however, has been placed on treating these fuels after the initial conversion step. Due to the organic nature of these feedstocks, biofuels typically contain a high level of oxygen, even after conversion, making them incompatible with existing fuel. The presence of oxygen creates blending issues, lowers the heating value of the fuel and makes biofuels unstable in storage.[1,2]

A similar issue arises with crude oil, which contains heavy metals, sulfur and nitrogen. In the petroleum industry, crude oil is catalytically hydrotreated using sulfided cobalt/molybdenum or nickel/molybdenum catalysts to remove these contaminants. A comparable approach can be taken by considering oxygen as a contaminant and hydrotreating the biofuels over a catalyst to remove the oxygen and produce a hydrocarbon product that can be blended in any proportion with existing fuel.

The pyrolysis of woody biomass can produce a bio-oil (also called pyrolysis oil) that is a complex mixture of oxygenated hydrocarbons, mostly C_4 to C_8.[3] Pyrolysis oil can include water, light acids, aldehydes, furans and phenolic compounds.[4] In its crude form, a high amount of oxygen, up to 40%, is retained in the fuel and can cause compatibility issues.[5] Oxygenated compounds also make the crude bio-oil viscous, corrosive, and can form waxy deposits during storage, as well as lowering the heating value of the oil as a fuel, which lowers its economic value and viability as a fuel source.[2] However, a significant portion of the bio-oil is within the desired range of hydrocarbons for gasoline and, with catalytic hydrotreatment, a hydrocarbon fuel that is fully compatible with petroleum-based gasoline can be produced.[6] An example of catalytic hydrotreatment of phenol on platinum on alumina is shown in Figure 1-1 below.

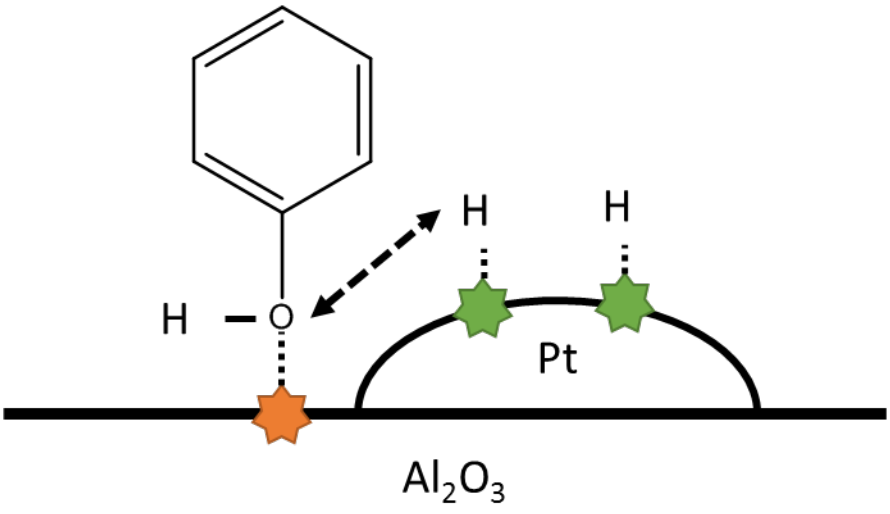

Figure 1-1. Catalytic hydrodeoyxgenation of phenol on platinum on alumina

Similarly, plant oils are composed of triglycerides: three long-chain fatty acids, with varying degrees of unsaturation, attached by a "backbone". Fortunately, the fatty acids that comprise plant oils typically range from C_8 to C_{22}, primarily C_{16} and C_{18}, ideal for the production of diesel and jet fuel.[2] Traditionally, once the backbone of the triglyceride is removed, usually in the form of glycerin, the plant oil undergoes transesterification, where it is transformed into a fatty acid methyl ester (FAME) or fatty acid ethyl ester (FAEE) fuel called "biodiesel". However, biodiesel still contains oxygen and is not easily blendable with traditional diesel. Alternatively, fatty acids can instead undergo catalytic hydrotreatment, which yields a simple hydrocarbon fuel that can be blended in any proportion with diesel fuel. After the removal of the backbone in the form of propane, hydrotreatment in the form of hydrodeoxygenation, decarbonylation, and/or decarboxylation, along with secondary reactions, result in either long-chain or branched hydrocarbons that are identical to compounds frequently found in petroleum-based diesel.

While the catalytic hydrotreatment process has perhaps the most significant environmental impact of the entire process from biological feedstocks to fuel in terms of greenhouse gas (GHG) production, energy and hydrogen consumption, it is also the most poorly understood step in the process. Based on the current literature, there is little coherent data available on reaction kinetics that would allow for proper LCA or scaling up of a process.[7] Instead, most life cycle assessments rely on proprietary data from

industrial sources or make stoichiometric assumptions without considering process conditions and resulting selectivities.

Considering the importance of the hydrotreatment step, it is surprising that there has been no systematic study of reaction kinetics and process-level analysis of important environmental assessment factors.[8] Kinetic studies of this process are necessary to understand these fundamental factors. Once the kinetics of the hydrotreatment reactor are understood, the process can be simulated using a kinetic reactor model, generating process-level details and allowing for easy scale-up of the process without expensive testing. The petroleum industry has used this approach with traditional crude oil, which differs even from location to location and can contain hundreds of components. Mapping every reaction pathway and obtaining all of the kinetic data for every one of those compounds is impractical, leading to lumped-parameter kinetic models. These lumped models group reaction pathways and/or compounds together. This vastly simplifies the models when predicting product compositions, yields, catalyst, energy, and hydrogen input, requiring a much smaller number of kinetic rate constants. By focusing only on observed compounds and not hypothesized intermediates, the reaction network can be further simplified and the number of initial tests can be significantly reduced. Instead of all possible components and reaction pathways of these biological oils, a small number of representative model compounds can be selected, and relevant experimental data can be collected on their lumped reaction pathways. With enough experimental data, a model can be constructed that can work with any inlet composition, including pure, individual

components, biological oil (of varying sources and composition), and even different blends of those oils.

The overall goal of this project was to further the understanding of the catalytic hydrotreatment of alternative fuels through the development of a kinetic model to improve the hydrotreatment upgrading process. The research was organized in the manner shown below:

1. Literature Review – Plant & Pyrolysis Oils (Chapters 2 & 3)
2. Batch Reactor Studies – Pyrolysis Oils (Chapter 4)
3. Differential Reactor Studies – Pyrolysis Oils (Chapter 5)
4. Pilot Reactor Studies – Plant & Pyrolysis Oils (Chapters 2 & 5)
5. Technoeconomic Assessment – HTL Oils (Chapter 6)

However, four of the chapters in this dissertation are intended for publication. Therefore, this document is organized in the following manner:

- Chapter 1: Introduction & Motivation
- Chapter 2: Kinetic Modeling of the Hydrotreatment of Oleic Acid over a Pt/Al_2O_3 Catalyst
- Chapter 3: Catalytic Hydrotreatment of Pyrolysis Oil Literature Review

- Chapter 4: Catalytic Hydrotreatment of Pyrolysis Oil Model Compounds over Pt/Al_2O_3 and Pd/C: Part I: Batch Reactors
- Chapter 5: Catalytic Hydrotreatment of Pyrolysis Oil Model Compounds over Pt/Al_2O_3 and Pd/C: Part II: Continuous Reactors
- Chapter 6: Assessment of Hydrothermal Liquefaction Oil with Catalytic Upgrading for Renewable Fuel and Chemical Production
- Chapter 7: Conclusions & Future Work

1.1 References

[1] A. Bridgwater, "Review of fast pyrolysis of biomass and product upgrading," Biomass and Bioenergy, vol. 38, pp. 68-94, 2012.

[2] E. Furimsky, "Hydroprocessing challenges in biofuels production," Catalysis Today, 2013.

[3] J. Adjaye and N. Bakhshi, "Catalytic conversion of a biomass-derived oil to fuels and chemicals I: model compound studies and reaction pathways," Biomass and Bioenergy, vol. 8, pp. 131-149, 1995.

[4] R. J. Evans and T. A. Milne, "Molecular characterization of the pyrolysis of biomass," Energy & Fuels, vol. 1, pp. 123-137, 1987/03/01 1987.

[5] Q. Zhang, J. Chang, T. Wang, and Y. Xu, "Review of biomass pyrolysis oil properties and upgrading research," Energy Conversion and Management, vol. 48, pp. 87-92, 2007.

[6] Asphaug, S. (2013). "Catalytic Hydrodeoxygenation of Bio-oils with Supported MoP-Catalysts.

[7] Kalnes, T., et al. (2007). "Green diesel: a second generation biofuel." International Journal of Chemical Reactor Engineering 5(1).

[8] Mortensen, P. M., et al. (2011). "A review of catalytic upgrading of bio-oil to engine fuels." Applied Catalysis A: General 407(1–2): 1-19.

2. Kinetic Modeling of the Hydrotreatment of Oleic Acid over a Pt/Al_2O_3 Catalyst[1]

2.1 Introduction

Direct catalytic upgrading of plant oils to transportation fuels is straightforward compared to treating fossil fuels. Since the initial feedstock is less complex, sulfur content is low, and the presence of other catalyst poisons is rare.[1] Feedstocks for direct catalytic upgrading may originate from a variety of materials, including seed oils, tall oil from pulp processing, or even waste cooking oils.[2] However, such oils are highly oxygenated mixtures of triglycerides and fatty acids, making them unsuitable for replacing traditional fuels without an intermediate upgrading step.

Recently, these oils have been reacted with alcohols in the presence of base catalysts to produce fatty acid methyl ether (FAME) biodiesel, which is typically blended with fossil fuels. Unfortunately, biodiesel can only be blended in limited amounts with pure hydrocarbon fuels, typically 5-20%, due to clogging issues in filters and poor cold flow properties caused by oxygen still present in the fuel.[1] Direct catalytic hydrotreatment of plant oils to paraffinic hydrocarbons is more attractive, since the process can yield products which are readily blended with petroleum-based fuels.[3] These hydrotreated

[1] This work is in preparation for resubmission to Energy & Fuels, and is a collaboration with Dr. David Shonnard, J.C. Metsa, and Jennifer Robinson.

fuels are frequently referred to as hydrorenewable diesel (HRD) or green diesel, and can easily take advantage of existing infrastructure.[4]

A key challenge in renewable fuel analysis is the lack of supporting process level data.[5,6] One of the most important and costly stages is the hydroprocessing upgrading step. There is a lack of knowledge of how process conditions and the molecular characteristics of plant oils can affect hydrogen and energy requirements for this step.[6] This results in dependence on empirical data. The models developed for analysis of the hydrotreatment of bio-oil feedstocks are largely based upon stoichiometric yields predicted via process simulators or other "black box" models, which can overpredict fuel production and performance by a large margin. Relevant reaction pathway data from the literature have been compiled and adapted to a multiphase reactor model, but insufficient experimental data was reported to fit the reactor model parameters. To fill this gap in data for model validation, we have conducted bench-scale studies on the hydrotreatment of oleic acid, a surrogate compound for plant oils, in a continuous trickle bed reactor. The result is a process-level model that more realistically predicts the product distribution, hydrogen consumption, GHG emissions, and energy requirements for the HDT of bio-oils. This process-level model may then be incorporated into an overall process simulation to provide a higher confidence technoeconomic analysis (TEA) or life cycle assessment (LCA) for a biomass-to-fuels facility. This paper provides a proof-of-concept study for a specific feedstock and catalyst for a range of process conditions

that can be readily extended to other bio-oil feedstocks and catalyst given a limited preliminary analysis of the reaction kinetics.

2.2 Literature Review

A literature review was conducted to determine the state of research and find comparison points for the kinetic model. Studies on the rate kinetics of upgrading reactors were limited. Fortunately, limited relevant data on the hydrotreatment of triglycerides and fatty acids, specifically oleic acid, stearic acid, and similar compounds, were found. These results were used as the basis for our experiments and for comparison and validation of the model.

Veriansyah et al. (2012) studied the conversion of soybean oil over a variety of supported metal catalysts.[7] Madsen et al. (2011) studied oleic acid and tripalmitin as model compounds for waste cooking fats and oils over platinum on alumina and nickel on alumina.[8] Both theorized reaction networks for the conversion of triglycerides and fatty acids (FA) to hydrocarbons, which specify three different reaction pathways for fatty acids: decarbonylation (Eqn. 2-1), decarboxylation (Eqn. 2-2), and HDO (Eqn. 2-3). While these networks are relatively generic, they can be used as the first steps towards a more detailed reaction network.

Decarbonylation	$FA\ (n) + H_2 \rightarrow Paraffin\ (n - 1) + CO + H_2O$	(Eqn. 2-1)
Decarboxylation	$FA\ (n) \rightarrow Paraffin\ (n - 1) + CO_2$	(Eqn. 2-2)

Hydrodeoxygenation $FA\ (n) + 3\ H_2 \rightarrow Paraffin\ (n) + 2\ H_2O$ (Eqn. 2-3)

*n = number of carbons

Rozmyslowicz et al. (2010) explored the conversion of tall oil fatty acids (TOFA), specifically linoleic (C_{18}, 2 unsaturated) and oleic acid (C_{18}, 1 unsaturated), over palladium on mesoporous carbon (Pd/C). A preference for saturation reactions over HDO or DeCOx reactions was shown in a hydrogen-starved environment, where stearic acid (C_{18}, fully saturated) was the primary product.[9] This allows the extension of the reaction network to include a triglyceride saturation reaction, a necessity since unsaturated fatty acids are primary components in many vegetable oils.[10] This is further supported by Immer et al. (2010), who looked at how hydrogen concentrations affected reaction rates and selectivity. It was shown that oleic acid decarboxylation was significantly slower in the absence of hydrogen, and therefore without the initial saturation reaction to stearic acid.[11]

Snare et al. (2007) considered Pd/C for the HDT of ethyl stearate, a fatty acid ethyl ester (FAEE) which is commonly found in biodiesel. While upgrading biodiesel is outside the scope of this paper, stearic acid is one of the primary products in ethyl stearate's HDT network and the reaction network for triglyceride HDT can be further extended here. Most importantly, an unsaturation reaction from n-heptadecane to olefins and a subsequent aromatization reaction can be added.[4] This paper also provides rate constants for a decarboxylation reaction (stearic acid to n-heptadecane), as well as the unsaturation and aromatization reactions.

Kumar et al. (2013) presents a reaction network for stearic acid over nickel catalysts on a variety of supports. Nickel catalysts are a more robust hydrogenation catalyst than platinum or palladium, however, they are not as effective. A dehydration reaction from an alcohol intermediate, octadecanol, to an olefin, octadecene, occurs over their catalyst set, which provides another possible pathway for the consumption of alcohol and the creation of olefins during hydrotreatment. Arrhenius rate constants, activation energies, and pre-exponential factors for their reaction network are also provided.[12]

Finally, Vam (2013) describes a more complete reaction network for the HDT of stearic acid in the presence of hydrogen. Here, the optimal reaction conditions for production of paraffinic products were chosen to be Pd/C at 300°C and low H_2 conditions. Rate kinetics were also studied as a function of temperature and other process conditions, and rate constants from this paper were adapted for the model.[13] Low hydrogen concentrations were selected based on Immer et al. (2010), who noted a significant decrease in conversion under pure hydrogen environments. This is most likely due to competitive adsorption on the surface of the catalyst between the fatty acid and the hydrogen.[11] Some hydrogen is necessary to maintain the activity of the catalyst.[11,14]

2.3 Proposed Reaction Network

2.3.1. Lumped Parameter Approach

The lumped parameter approach has long been used in the petroleum industry for HDT of crude oil feedstocks that often consist of hundreds of different compounds. Modeling each compound and all of its possible reactions and intermediates is not feasible. Essentially, compounds with similar characteristics, such as functional groups or hydrocarbon chain length, are assumed to behave similarly. For example, monounsaturated fatty acids would be grouped together, regardless of the length of the hydrocarbon chain or specific placement of the double bond, and assumed to follow the same reaction pathway, undergoing a saturation reaction to fully saturated fatty acids, another "lump". This proven approach has been adapted in the model presented here for plant oils. This reduces the number of reactants and products to be modeled down to a manageable number. Since there are a relatively small number of fatty acids associated with plant oils, most of which vary only in degree of unsaturation and carbon chain length, they may reasonably be modeled in this fashion.[10] A set of ten reaction pathways has been selected from the literature, as discussed above, and are shown in Figure 2-1. It should be noted that not all reactions will be relevant for each catalyst, feedstock, or set of processing conditions.

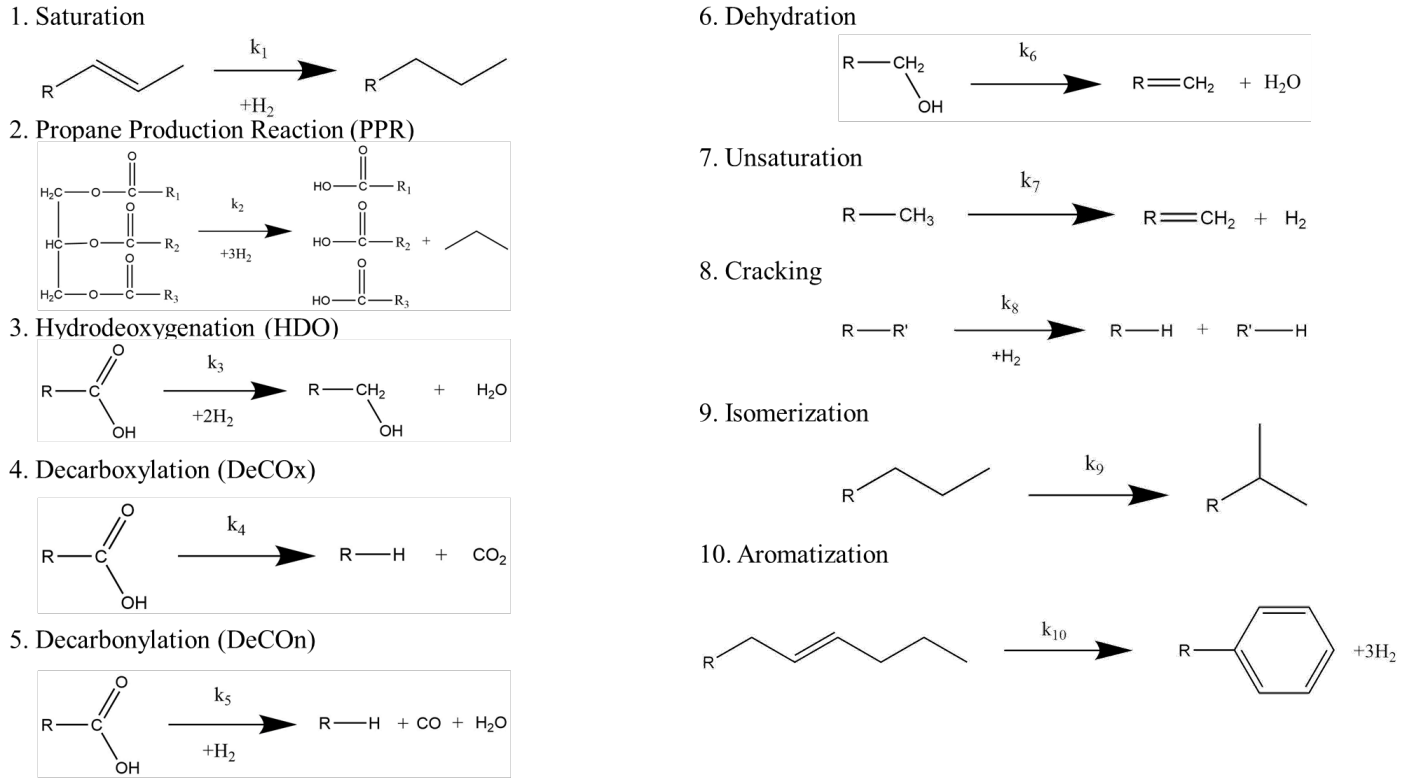

Figure 2-1. Lumped reaction pathways included in model

2.3.2. Reaction Network

Based on these sources and using the lumped parameter approach, a proposed reaction network was created for use in the model, as shown in Figure 2-2. The initial feedstock is a plant oil containing unsaturated triglycerides, a molecule containing three fatty acids (with varying degrees of unsaturation) tied together by a glycol backbone. The triglyceride molecule then undergoes a propane production reaction, where the glycol backbone is removed as propane and three fatty acids are liberated. These fatty acids can undergo three possible reaction pathways: a hydrodeoxygenation reaction to a long-chain alcohol, a decarboxylation reaction to a long-chain paraffin, or a decarbonylation reaction to a long-chain paraffin. The long-chain alcohols undergo either a hydrodeoxygenation reaction to paraffins or a dehydration reaction to olefins. The long-chain paraffins are typically considered the desired fuel products of this process, but can undergo an unsaturation reaction, a cracking reaction, or an isomerization reaction, leading to other possible desired products. Olefins can also be a desired product, and can subsequently undergo a saturation reaction, an isomerization reaction, or an aromatization reaction. In Figure 2-2, the reactions for which literature with usable kinetic data was found are shown with normal lines. Reactions for which there was evidence, but no experimental rate data are shown with dashed lines.

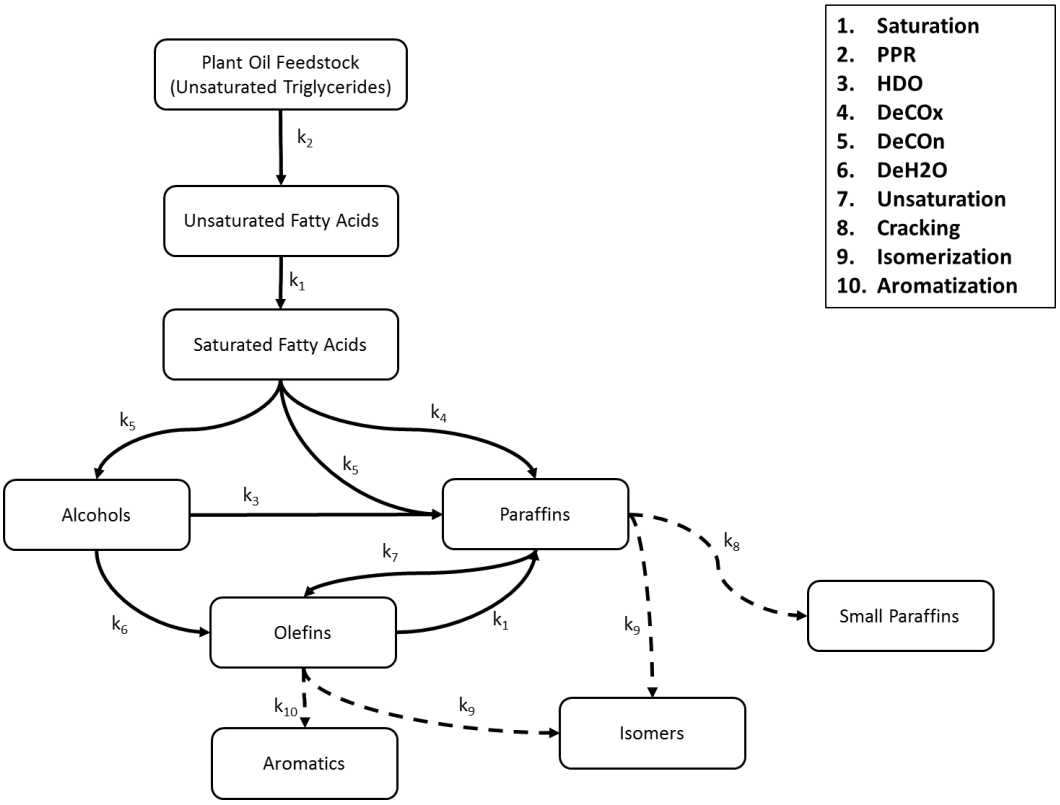

Figure 2-2. Proposed reaction pathways for hydrotreatment of a triglyceride

Most studies reported are in batch reactors at elevated pressures or continuous reactors near atmospheric pressure. Because of this gap in relevant data, a continuous reactor was constructed, as discussed below, to run at 5-8 bar and temperatures comparable to industrial reactors.

2.4 Materials & Methods

Oleic acid (99%, Alfa Aesar), n-dodecane (99+%, Alfa Aesar), and analytical standards were obtained commercially. Hydrogen and argon were purchased from American

Welding & Gas. As described in a previous study, the Pt/Al_2O_3 catalyst was synthesized via incipient wetness impregnation, using hexachloroplatinic acid and alumina (10-25 mesh), and then reduced under hydrogen, resulting in a catalyst with 4.95% metal loading.[15] HDT was conducted in a trickle bed reactor system with a 20.3 mm inner diameter reactor bed. For each test, 4.65 g of catalyst was placed inside the reactor, held in place with a stainless steel mesh screen inside a catalyst bed. The reactor was then heated to the desired temperature with 5 mole % hydrogen flowing, with argon as a carrier gas at 0.5 L/min, controlled by a mass flow controller, to achieve a desired stoichiometric ratio. A system pressure of 6.7 bar was maintained to keep the principal reactants and products in the liquid phase, except for hydrogen and any gaseous byproducts formed. The reactor was heated using a Thermolyne F21100 tube furnace set at 250, 300, 350, or 375°C. Once the system reached steady state, liquid reactant and solvent were fed to the system at a flowrate of 0.5 mL/min using a custom high pressure liquid chromatography (HPLC) pump (Series I Plus, Supercritical Fluid Technologies). Liquid flowrates in the reactor were set to produce a packed bed residence time of 30 seconds using liquid hourly space velocity (LHSV) calculations. The liquid feed was 5 mole percent oleic acid in dodecane (0.22 mol/L). Dodecane was used as an inert solvent to control the reactor. Products were cooled and depressurized to atmospheric pressure downstream via a stainless steel shell and coil condenser and back-pressure regulator (Novaspect) before splitting in a gas-liquid separator. Gaseous products, excess hydrogen and argon were vented. A reactor schematic is shown in Figure 2-3.

Liquid products were collected for offline analysis. After heating the sample to 60°C for thirty minutes, 0.2 mL pyridine (>99.9%, Sigma-Aldrich) was added to 1 mL of sample. 0.2 mL of this solution was then placed in the auto-sampler vial and 30 microliters of BSTFA (w/ 1% TCMS, Cerilliant) was added. The vials were then left overnight to fully derivatize and were analyzed the following day in a HP5890 GC/FID. LC/MS analysis was also performed to confirm the GC/FID analysis and product identities, using a Thermo Finnegan LCQ Advantage Ion-Trap.

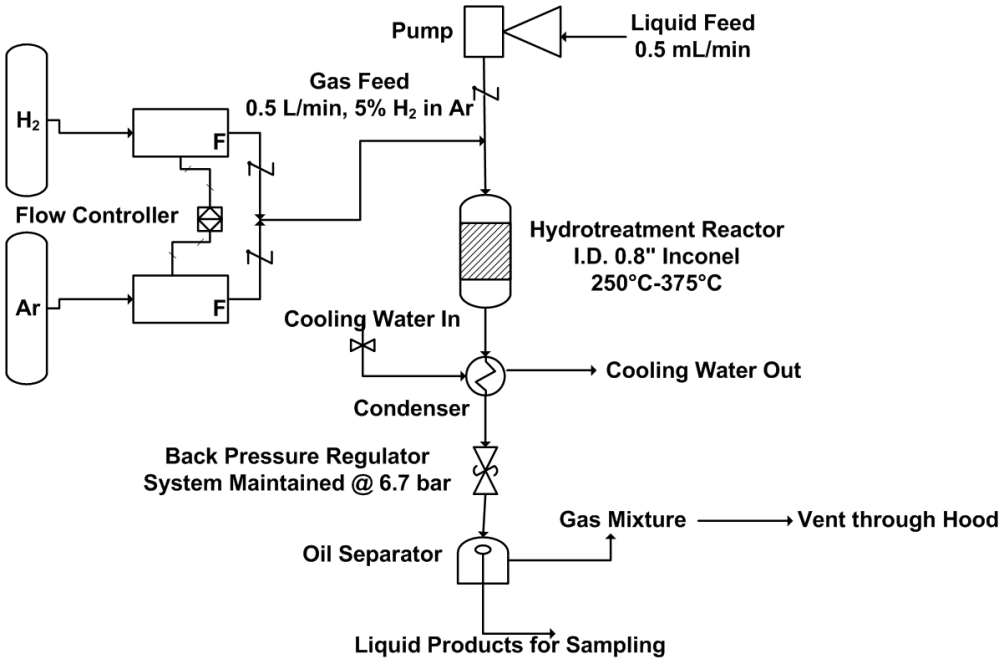

Figure 2-3. Reactor schematic for pilot-scale trickle bed reactor

2.5 Experimental Results

Oleic acid conversion increased with increasing temperature, with a large jump in conversion from 350°C to 375°C, possibly indicating a shift in the dominant mechanism. Stearic acid, octadecanol, and heptadecanol were the primary products indicated by the GC/FID, with some minor peaks, which were tentatively identified using the LC/MS results. LC/MS analysis showed other fatty acids, such as linoleic acid, hydrocarbons, such as octadecane and heptadecane, and fatty acid methyl or ethyl esters (FAME or FAEE), such as methyl oleate. In the LC/MS results, shown in Table 2-1, heptadecanol concentration is less than 1% from 250°C to 350°C, but increases to almost 12% at 375°C. This probably occurs via a decarbonylation reaction from stearic acid, which indicates a high activation energy for this particular reaction. The traces of FAME and FAEE compounds also indicate possible cracking in the system and subsequent esterification at 375°C, and to minimize this, the reactor was not operated over 375°C. Fully deoxygenated products, such as octadecane, are not observed until most of the oleic acid is consumed, indicating a suppression of oxygen removal reactions until the oleic acid is saturated. The products identified are consistent with the proposed reaction network and this mechanism is a starting point for a process-level kinetic model.

These results are consistent with literature sources, where noble metal, alumina-supported catalysts have a strong preference for decarboxylation and decarbonylation reactions. Gong et al. compared a bimetallic $PtPd/Al_2O_3$ catalyst and more traditional $NiMo/Al_2O_3$ catalysts, and showed a higher amount of DeCOx and DeCOn for the noble metal catalyst and a preference for the HDO pathway with the NiMo catalyst.[16] Hengst

et al. and Madsen et al. both observed heptadecane as a product of oleic acid HDT over noble metal catalysts supported on alumina.[17,18]

Table 2-1. LC/MS Analysis Results

		% Abundance				
Compound	**Formula**	**blank**	**250°C**	**300°C**	**350°C**	**375°C**
Ethyl Oleate	$C_{20}H_{38}O_2$	0.01	0.02	0.02	0.02	1.71
Methyl Oleate	$C_{19}H_{36}O_2$	0.01	0.00	0.01	0.01	0.96
Stearic Acid	$C_{18}H_{36}O_2$	0.00	3.23	3.75	4.03	39.82
Oleic Acid	$C_{18}H_{34}O_2$	99.83	96.42	95.94	94.25	39.50
Linoleic Acid	$C_{18}H_{32}O_2$	0.07	0.03	0.03	0.04	4.08
Octadecanol	$C_{18}H_{38}O$	0.00	0.00	0.00	0.01	0.19
Methyl Palmitoleate	$C_{17}H_{32}O_2$	0.01	0.00	0.00	0.00	0.69
Heptadecanol	$C_{17}H_{36}O$	0.05	0.21	0.24	0.96	11.73
Octadecane	$C_{18}H_{38}$	0.00	0.00	0.00	0.01	0.54
Heptadecane	$C_{17}H_{36}$	0.00	0.00	0.00	0.01	0.17
*Exp m/z is the mass to charge ratio, and represents the molecular weight minus a hydrogen						

2.6 Process Modeling

2.6.1. Background

A realistic reactor model is necessary for optimizing and evaluating plant oil HDT. This model should be able to predict product composition, hydrogen input requirements, and energy needs for use in analyses, over a range of operating conditions and feed compositions. Such a model is essential, considering the complex behavior of multiphase catalytic reactors. Commercial programs, such as Aspen® or Unisim®, cannot perform the detailed analyses required for an in-depth, process level optimization or analysis. Such “black box” simulators cannot accurately account for multiphase conditions and

are not sensitive to the effect of reactor conditions on reaction pathways. At a minimum, a good model should incorporate the effects of the hydrogen/oil ratio, interphase mass transfer, temperature, residence time, intrinsic reaction kinetics, etc. and be able to predict process input requirements and product outputs. The model presented here focuses on the yield and selectivity of products, energy consumption, and total hydrogen demand. Additional factors, such as cooling water requirements, waste minimization, and recycling of excess hydrogen, could be included in later versions.

2.6.2. Model Parameters

The reactor model created for this exploratory study was generated in MathCAD®, and is a co-current, trickle-bed reactor with a gas phase consisting of hydrogen and an inert carrier gas, a liquid phase with the plant oil, triglycerides, or fatty acids, and a stationary solid phase of a catalyst. In almost every study found in the literature and in our experiments, multiphase reactors, either trickle-bed or slurry, were used. The type of reactor and process conditions used as an experimental test case were selected to accurately model a HDT reactor operating at parameters commonly cited in the literature as yielding a good conversion and selectivity for diesel. The basic model system is shown in Figure 2-4.

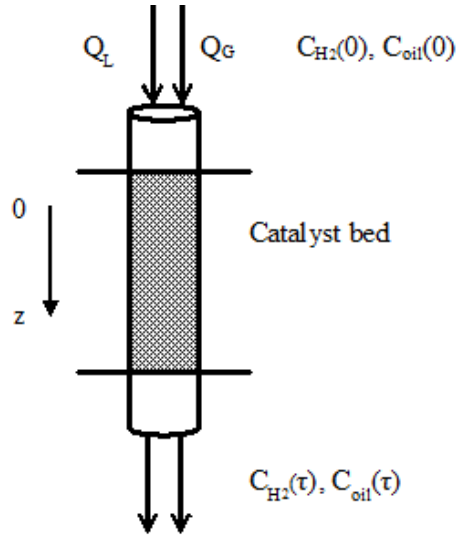

Figure 2-4. Model system of plug-flow trickle-bed reactor

Some simplifying assumptions include no axial mixing, uniform radial concentrations, no resistance to mass transfer through the gas phase, isothermal operation, negligible pressure drop across the reactor, and constant gas phase volumetric flowrates. Products were assumed to stay in the liquid phase, except for any hydrogen, carbon dioxide, or carbon monoxide generated, which go into the vapor phase. The rate of mass transfer of hydrogen from the gas-liquid interface to the bulk liquid and mass transfer of both reactants from the bulk liquid to the catalyst surface were incorporated, but it was assumed that there were no mass transfer limitations within each phase. Empirically derived correlations for trickle-bed reactors may be used to determine the k_La and k_sa values.[19,20] A liquid hold-up of 0.3 was also assumed, based on previous work done in a similar reactor.[20] The Henry's Law constant for the partitioning of hydrogen (H_{H2}) into the liquid organic phase can be found from the literature or determined experimentally.

Incremental material balances can then be made in each phase with respect to either residence time (τ) or length (z) of the reactor. The only terms that differ are the reaction rate constants, which vary mostly with temperature and catalyst. This makes the model both flexible and robust.

Material balances are derived for the two principal reactants, as shown in Table 2-2. These equations are generic; the model contains a separate incremental balance for each "lump" in the oil. This resulted in a set of ordinary differential equations to be solved simultaneously as an initial value problem. The solution to these equations, in terms of the concentration of each species as a function of residence time, is shown in the results.

Table 2-2. Differential Reactor Equations & Associated Nomenclature

$$H_2, gas: \; -\frac{dC_{H2,G}}{d\tau} - \{k_{La}\}_{H2}\left(H_{H2}C_{H2,G} - C_{H2,L}\right) = 0 \qquad \text{(Eqn. 2-5)}$$

$$H_2, liq.: -\frac{dC_{H2,L}}{d\tau} + \{k_{La}\}_{H2}\left(H_{H2}C_{H2,G} - C_{H2,L}\right) - \{k_{Sa}\}_{H2}\left(C_{H2,L} - C_{H2,S}\right) = 0 \qquad \text{(Eqn. 2-6)}$$

$$oil, liq.: -\frac{dC_{oil,L}}{d\tau} - \{k_{La}\}_{oil}\left(C_{oil,L} - H_{oil}C_{oil,G}\right) - \{k_{Sa}\}_{oil}\left(C_{oil,L} - C_{oil,S}\right) = 0 \qquad \text{(Eqn. 2-7)}$$

$$H_2, surface: \; -\frac{dC_{H2,S}}{d\tau} = \{k_{Sa}\}_{H2}\left(C_{H2,L} - C_{H2,S}\right) - \sum_i \frac{\eta k_i C_{H2,S}^m C_{oil,S}^n}{1 + K_C C_{oil,S}^n} \qquad \text{(Eqn. 2-8)}$$

$$oil, surface: \; -\frac{dC_{oil,S}}{d\tau} = \{k_{Sa}\}_{oil}\left(C_{oil,L} - C_{oil,S}\right) - \sum_i \frac{\eta k_i C_{H2,S}^m C_{oil,S}^n}{1 + K_C C_{oil,S}^n} \qquad \text{(Eqn. 2-9)}$$

Table 2-3. Definitions & Values for Differential Equation Parameters

Term	Definition	Source
$\{k_La\}_i$	Mass transfer coefficient for gas-liquid ($time^{-1}$)	[18]
$\{k_ca\}_i$	Mass transfer coefficient for liquid-surface of the catalyst ($time^{-1}$)	[18]
K_A	Surface adsorption coefficient	Fit
$C_{H2,G}$	Concentration of hydrogen in the gas phase (gmols/volume)	--
$C_{H2,L}$	Concentration of hydrogen in the liquid phase (gmols/volume)	--
$C_{H2,S}$	Concentration of hydrogen in the solid phase (gmols/volume)	--
$C_{oil,L}$	Concentration of bio-oil in the liquid phase (gmols/volume)	--
$C_{oil,S}$	Concentration of bio-oil in the solid phase (gmols/volume)	--
H_C	Henry's Law constant, $C^* = C_g / H$ (mole/mole)	[20]
k	Reaction rate constant ($time^{-1}$)	Fit
τ	Residence time (time)	--
m, n	Order of reaction	Fit
Q_G	Gas volumetric flow rate (volume/time)	--
Q_L	Liquid volumetric flow rate (volume/time)	--
A_c	Column cross sectional area (area)	--
η	Catalyst effectiveness factor	[19]

The rate expressions for these paths can be simple power law expressions, or more complicated forms, such as Langmuir-Hinshelwood kinetics, as shown in Table 2-3.[21,22,23] Based upon the observed oleic acid conversions, rate constants were fitted to each kinetic model. For this range of temperatures, apparent activation energies were determined: 51.2 kJ/mol for saturation, 34.2 kJ/mol for HDO, and 80.6 kJ/mol for decarbonylation. Regardless of the form of the rate expressions, the resulting set of equations may readily be solved simultaneously using integration methods such as

Runga-Kutta or commercial programs such as MatLab® or MathCAD®. The product composition may be fitted with the model to calculate rate constants for each reaction pathway. With these, the reactor performance for a wide range of plant oil feedstocks and their constituent fatty acids can be predicted. The model can also be used to scale up the process or examine the effect of changing process conditions without performing difficult pilot scale tests.

2.6.3. Data Comparison to Model

The data from the HDT of oleic acid over Pt/Al_2O_3 was incorporated into the kinetic model developed above. Table 2-3 shows the actual versus predicted conversions of oleic acid in the reactor using the fitted Arrhenius rate constants. All conversions predicted by the model are within 0.3% of the experimental values.

Table 2-4. Data vs. Model Comparison for Conversion of Oleic Acid on Pt/Al_2O_3

Temperature	Data	Model
250°C	3.7%	3.8%
300°C	7.9%	7.9%
350°C	11.5%	11.6%
375°C	56.7%	56.5%

2.7 Model Test Cases

2.7.1. Base Case

While rate constants and other parameters vary for different catalysts, feedstocks and reactor conditions, the basic model is suitable to extend and compare to literature values for hydrogen consumption. To best compare to literature values for hydrogen consumption, a test case was generated that assumes a feed of soybean oil, a common feedstock in industrial operations and literature. The liquid flowrate was set at 100 mL/min, temperature was set at 300°C, and inlet hydrogen concentration was 5% volume with an overall gas flowrate of 10 L/min, giving a hydrogen to oil molar ratio of roughly 10 to 1. These conditions were selected based on literature, as discussed earlier, and yield a one minute liquid residence time in the reactor.[11,13] Rate constants for the reaction network shown in Figure 1 were adapted from experiments and literature; the primary reaction kinetics observed in the pilot-scale reactor were used for most of the modeling, but secondary reaction kinetics such as cracking were adapted from literature sources. [4, 20, 21, 22] The results quantitatively describe what one would expect for the proposed reaction network and are shown in Figure 2-5. There is over 90% conversion, as expected, with approximately 97% selectivity for paraffinic hydrocarbons. A steady, monotonic decline in the concentration of the unsaturated triglyceride in the liquid phase (unsatTAGL) is seen, with a rapid propane production reaction matching its disappearance rate. Unsaturated triglyceride on the catalyst (unsatTAGC) as well as fatty acid (FA) concentration rise briefly, as most of the hydrogen present goes towards the propane production reaction, but after the first few seconds, the conversion of those compounds is instantaneous under the excess of hydrogen. Most importantly, perhaps, is the ratio between the competing HDO, DeCOx and DeCOn reactions. This can be

determined from the end concentrations of water, carbon dioxide (co2), and carbon monoxide (co), although it should be noted that the DeCOn reaction produces both water and carbon monoxide, and this is taken into account when calculating ratios. At 300°C, a preference for the DeCOx reaction can be seen, with some DeCOn and little HDO. To test the flexibility of the model, two sets of test cases were generated by changing temperature or hydrogen to oil ratios.

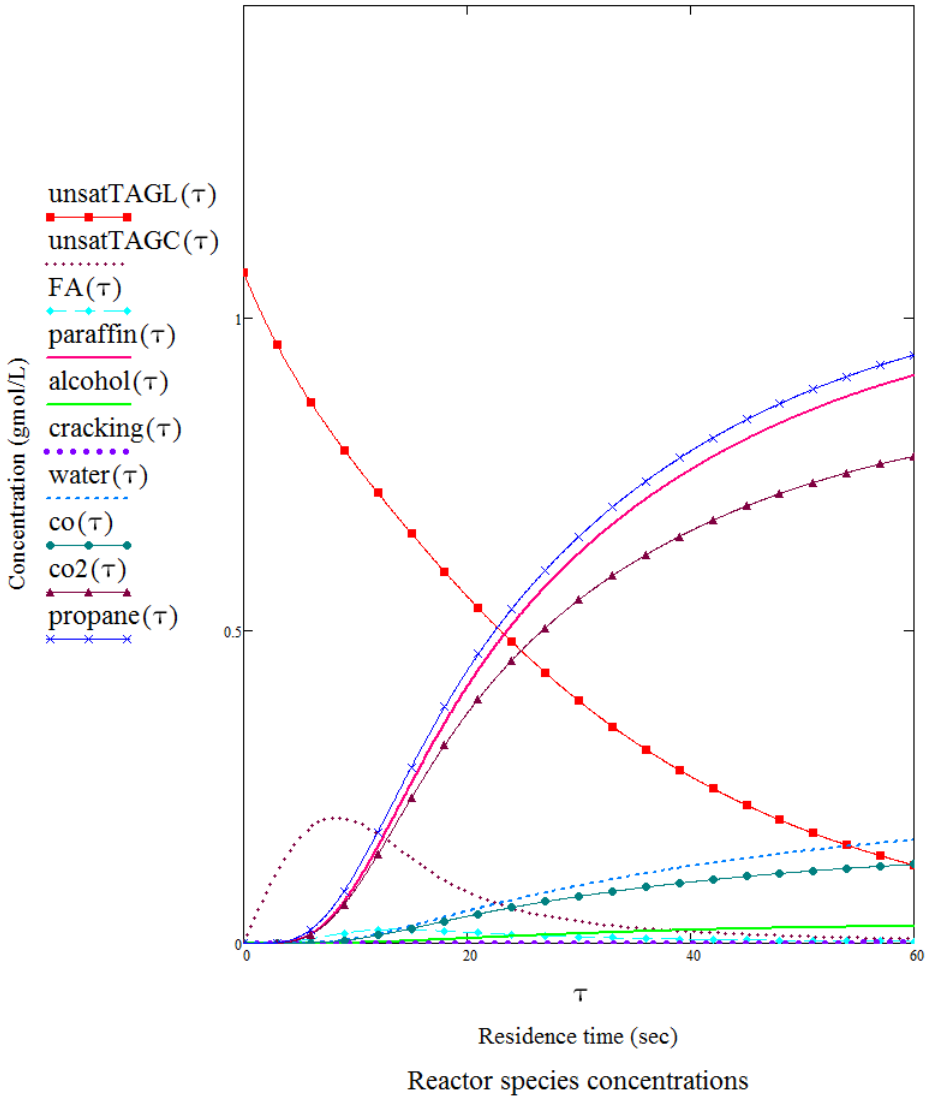

Reactor species concentrations

Figure 2-5. Basic test case product distribution and yield at 300°C, 10:1 hydrogen to oil ratio, 1 min residence time

2.7.2. Temperature dependence

The model was run at 250°C and 300°C to test the typical range of HDT reactors and at 500°C to force cracking reactions to occur in the reactor, as a more extreme example of pathway shift. The results are shown in Figure 2-6. The lowest temperature, 250°C, shows a prevalence of DeCOx, almost no DeCOn and HDO. While there is about 90% overall conversion of the unsaturated triglycerides, the fatty acid concentration is slower to disappear than in the basic 300°C case shown earlier, and even the unsaturated triglycerides on the surface of the catalyst take a little longer to disappear. The basic case at 300°C is as described before, with a preference for DeCOx and 90% conversion of the triglycerides. The primary desired product in both of these cases are long chain paraffins, with propane, carbon dioxide, carbon monoxide, and water as byproducts. At 500°C, there is a strong preference for DeCOn and HDO with a low amount of DeCOx. This clearly demonstrates the shift in reaction pathway that can occur at different temperatures. This temperature case also exhibits cracking reactions in the system, which break down the long paraffins into shorter chains. This can be a desired reaction, depending on the targeted product, but it is important to carefully control the extent of cracking. These reaction pathway preferences are critical when optimizing reactor conditions for a particular product or determining hydrogen consumption for an LCA or TEA. At 250°C, hydrogen consumption is slightly higher than at 300°C, most likely due

to incomplete deoxygenation of some of the fatty acids, indicated by the presence of some alcohol in the system. At 500°C, however, the hydrogen consumption is even lower, since cracking reactions, which consume only one mole of hydrogen, begin to stifle other reactions, such as the propane production reaction, which consumes three moles of hydrogen. The results here are comparable to those seen in literature, as are the trends in pathway preference.[23,24,25]

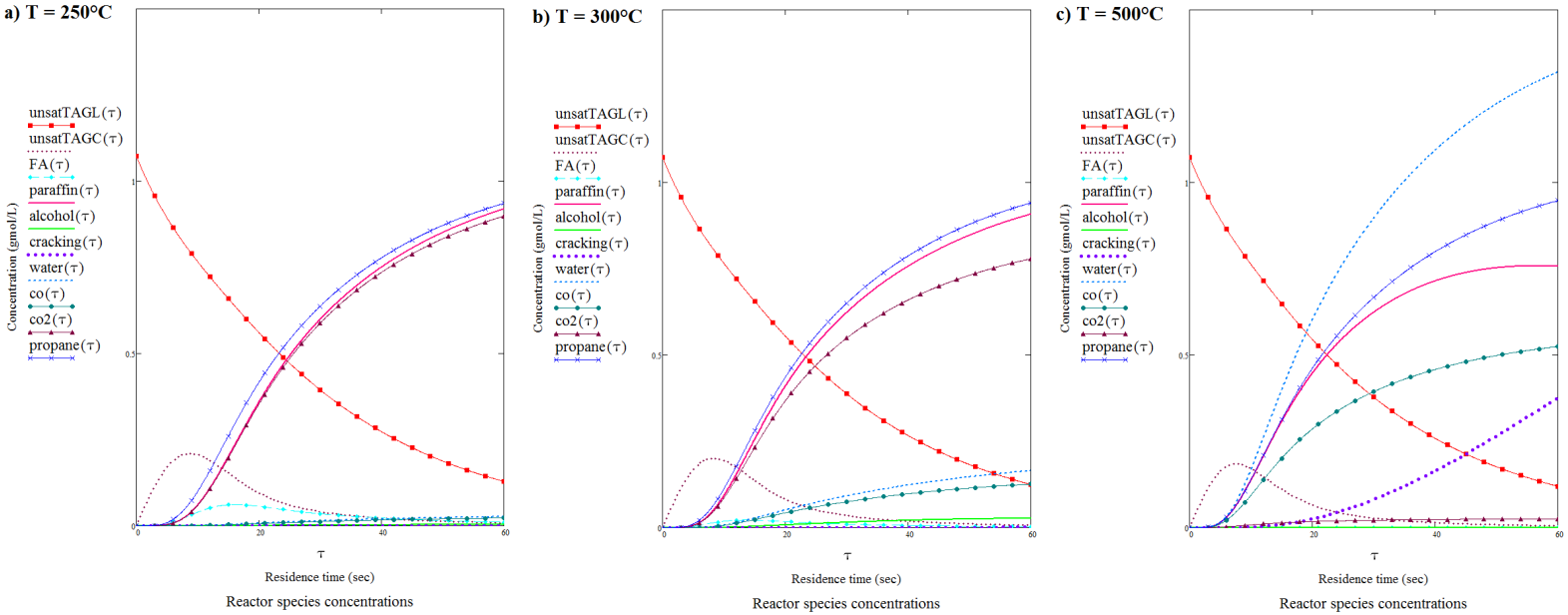

Figure 2-6. Effect of temperature on product distribution and yield at 1 minute residence time and 10:1 hydrogen to oil ratio. (a) 250°C, (b) 300°C, (c) 500°C.

2.7.3. Hydrogen to oil ratio dependence

Figure 2-7 shows the effect of hydrogen to oil ratios on the product distribution and yields at 2:1 and 10:1 ratios. Reduction of the hydrogen ratio has a severe impact on overall conversion, with only 43% conversion at the lower ratio. The reactions are also forced along the DeCOx pathway, which does not consume hydrogen, while there are no DeCOn or HDO reactions at all. Unreacted, unsaturated triglycerides on the surface of the catalyst are also prevalent in the system. These are all indicators of a hydrogen-starved environment.

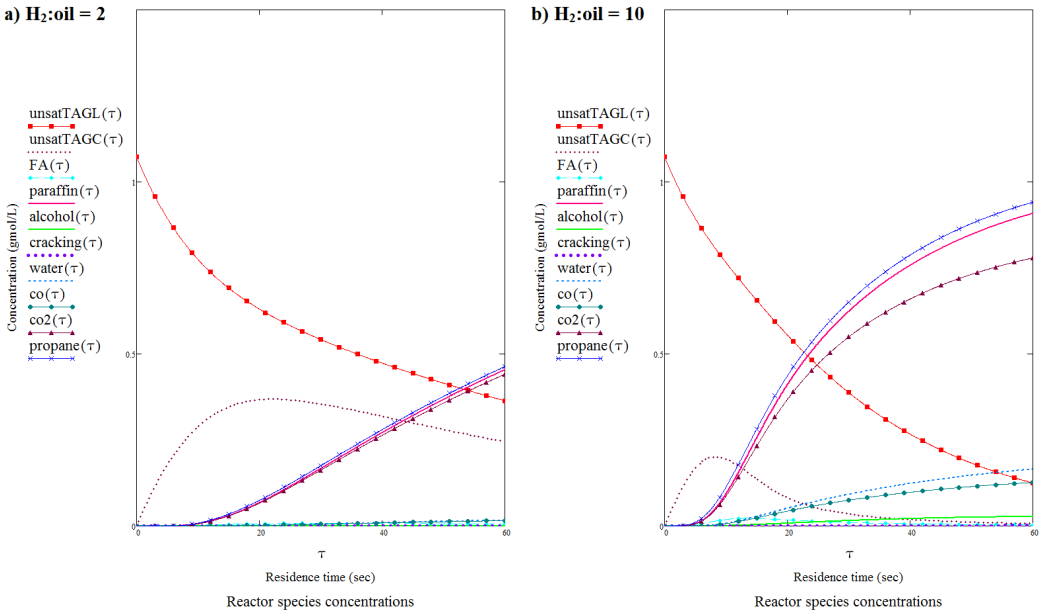

Figure 2-7. Effect of hydrogen to oil ratio on HDT product distribution at 60s residence time and 300°C. (a) ratio of 2:1, (b) ratio of 10:1

2.7.4. Heating/cooling load

The model can be used to determine several process outcomes. The total energy required for the process is calculated via an energy balance based on feed conversion, product concentrations, molar flowrates of gas and liquid, and associated heats of formation. For an isothermal reactor, the heat removal (or addition) required, q, is determined from the model product distribution as follows.

$$q = Q_L \sum v_i C_i \Delta H_i \qquad \text{(Eqn. 2-10)}$$

Where Q_L is the liquid flowrate, v_i is the stoichiometric coefficient, C_i is the product concentration, and ΔH is the heat of formation for each compound. From the basic test case above, the sum of the reactions was found to be mildly exothermic at 300°C, with about 0.92 kJ of cooling per liter of plant oil processed needed to maintain the reactor isothermally. A non-isothermal case could also be considered in future work, but represents a much more complicated set of calculations.[26]

2.7.5. Hydrogen consumption

Similarly, based upon the volumetric flowrates of hydrogen in the gas and liquid phases (assuming that hydrogen adsorbed on the catalyst stays in the reactor), the total consumption of hydrogen for the process is determined by a simple material balance across the reactor, as seen in Equation 11. The high cost and environmental impact of hydrogen makes the ability to predict this information a necessity. Certain reactions consume hydrogen (saturation, HDO), others are hydrogen-neutral (DeCOx), and some

reactions produce hydrogen (aromatization).[27] This model can account for pathway preference between these reactions based on process conditions. Consumption and production can be similarly measured for any of the species accounted for in the reaction pathways.

$$Q_G \left(H_{2\ gas}(0) - H_{2\ gas}(z)\right) - Q_L\, H_{2\ liq.}(z) = H_2\ consumption\ rate\ \left(\frac{mol}{time}\right)$$

(Eqn. 2-11)

Regrettably, few systematic studies on hydrogen requirements for the hydroprocessing step were found in the literature. Most analyses rely on industrial pilot plant data, Aspen® or other "black box" simulations, or experiments performed using batch reactors, which cannot accurately reflect process conditions in commercial facilities.[28,29,30,31] Some, however, can be used to provide comparisons and validation for the model developed here.

An LCA publication from Kalnes et al. (2007) provides a range of required hydrogen input for different plant oils that include varying degrees of unsaturation and hydrocarbon tail lengths.[31] The article describes the production of branched, paraffin-rich diesel fuel using hydrodeoxygenation (HDO), decarboxylation (DeCOx), and isomerization reactions. Results were based on experimental conversions of different oils at a range of operating conditions. Depending on isomerization severity and extent of HDO versus DeCOx, the hydrogen input requirement ranged between 1.5 to 3.8 kg

hydrogen per 100 kg plant oil input. The report states that this range is due to different oil inputs as well as different operating conditions, and therefore differing ratios of DeCOx to HDO. Unfortunately, these conditions were not explicitly stated. Nonetheless, as a test of the model's validity, the model was run using an unsaturated triglyceride at 300°C over a noble metal catalyst under 5% hydrogen, as discussed earlier. To simulate literature sources, conditions were set to achieve total conversion with paraffins as the primary product. This yielded a hydrogen consumption of 3.8 kg H_2 consumed per 100 kg of unsaturated triglyceride fed into the reactor. While this is on the higher end of the values found in Kalnes et al. (2007), only one kind of oil (soybean oil) was modeled, rather than a range of feedstocks.[31] The test case also does not include any isomerization, which may have an effect on overall hydrogen use.

Another report by Huo et al. (2008) considers the production of three types of renewable fuel from soybean oil: two different renewable diesels and one renewable gasoline. The major difference between the two renewable diesel fuels is the extent of HDO to DeCOx, as shown by different carbon dioxide output values. Only one type of renewable diesel showed propane production. The hydrogen input requirement was calculated as 0.030 and 0.032 pounds of hydrogen per pound of final fuel product.[29] These values were derived from an Aspen® model that simulated conditions present in a UOP plant. Again, the final composition of the renewable diesels is not discussed, and neither are the processing conditions, making exact comparison difficult. At test case conditions, our model shows higher hydrogen consumption, with a value of 0.347 pounds of

hydrogen per pound of final fuel product. However, due to the lack of compositional data, the final fuel product was assumed as heptadecane for this calculation, which may or may not accurately reflect the per pound basis of the paper's results, and the assumption of soybean oil as the initial feedstock may not be the best match for their calculations.

2.8 Conclusions

The lumped parameter, Langmuir-Hinshelwood model presented here is the simplest model that captures the details of the reaction kinetics, and when combined with a trickle-bed model, is able to robustly simulate a plant oil HDT reactor as a function of process conditions. It can predict hydrogen and energy consumption for a specific feedstock and set of operating conditions in a way that "black box" simulation programs such as Aspen® and Unisim® cannot. Given a relatively limited amount of data, it can accurately predict HDT product composition for a known feedstock and set of reactor conditions, as demonstrated using our test pilot data. Apparent activation energies were determined over this range of temperatures: 51.2 kJ/mol for saturation, 34.2 kJ/mol for HDO, and 80.5 kJ/mol for decarbonylation. This was then modeled and fit the experimental data well. For the test case of a triglyceride feedstock with three unsaturated double bonds at 300°C over a noble metal catalyst, the model predicts a hydrogen consumption of 3.8 kg per 100 kg oil feedstock, which shows good agreement with literature values.[29,31] A cooling load of 0.92 kJ per liter of plant oil was also calculated for the test case. Test cases were also run at 250°C and 500°C to demonstrate

the reaction pathway shifts from decarboxylation to decarbonylation and cracking. These outputs can be utilized in plant design, LCAs, TEAs, and other analyses of a particular feedstock or fuel product. The major obstacle to this model is the lack of necessary kinetic and reaction information. While there are many studies on the HDT of plant oils and their substituent compounds, there are few that consider the reaction kinetics in a way that can be used for modeling without expensive pilot-scale testing. To improve upon this model, further studies need to be conducted that determine the reaction kinetics of common triglycerides and fatty acids found in plant oils. The same modeling approach could also be used for other types of biologically derived feedstocks, including tall oils, pyrolysis oil, or even algal oil.[2] This process-level analysis could even be expanded to provide a set of detailed process design modules for a complete biorefinery design.

2.9. References

[1] J. G. Holmgren, C; Marinangeli, R; Marker, T; Faraci, G; Perego, C, "New Developments in Renewable Fuels Offer More Choices," Hydrocarbon Processing, vol. September 2007, pp. 67-72.

[2] E. Santillan-Jimenez and M. Crocker, "Catalytic deoxygenation of fatty acids and their derivatives to hydrocarbon fuels via decarboxylation/decarbonylation," Journal of Chemical Technology and Biotechnology, vol. 87, pp. 1041-1050, 2012.

[3] P. Šimáček, D. Kubička, G. Šebor, and M. Pospíšil, "Fuel properties of hydroprocessed rapeseed oil," Fuel, vol. 89, pp. 611-615, 2010.

[4] M. Snåre, I. Kubičková, P. Mäki-Arvela, K. Eränen, J. Wärnå, and D. Y. Murzin, "Production of diesel fuel from renewable feeds: kinetics of ethyl stearate decarboxylation," Chemical Engineering Journal, vol. 134, pp. 29-34, 2007.

[5] D. B. Agusdinata, F. Zhao, K. Ileleji, and D. DeLaurentis, "Life cycle assessment of potential biojet fuel production in the United States," Environmental science & technology, vol. 45, pp. 9133-9143, 2011.

[6] P. Šimáček, D. Kubička, I. Kubičková, F. Homola, M. Pospíšil, and J. Chudoba, "Premium quality renewable diesel fuel by hydroprocessing of sunflower oil," Fuel, vol. 90, pp. 2473-2479, 2011.

[7] B. Veriansyah, J. Y. Han, S. K. Kim, S.-A. Hong, Y. J. Kim, J. S. Lim, et al., "Production of renewable diesel by hydroprocessing of soybean oil: Effect of catalysts," Fuel, vol. 94, pp. 578-585, 2012.

[8] T. Madsen, E. H. Ahmed, C. H. Christensen, R. Fehrmann, and A. Riisager, "Hydrodeoxygenation of waste fat for diesel production: Study on model feed with Pt/alumina catalyst," Fuel, vol. 90, pp. 3433-3438, 2011.

[9] Rozmysłowicz, P. Mäki-Arvela, S. Lestari, O. A. Simakova, K. Eränen, I. L. Simakova, et al., "Catalytic deoxygenation of tall oil fatty acids over a palladium-mesoporous carbon catalyst: a new source of biofuels," Topics in Catalysis, vol. 53, pp. 1274-1277, 2010.

[10] K. Suslick, "Kirk-Othmer encyclopedia of chemical technology," J. Wiley&Sons: New York, vol. 26, pp. 517-541, 1998.

[11] J. G. Immer, M. J. Kelly, and H. H. Lamb, "Catalytic reaction pathways in liquid-phase deoxygenation of C18 free fatty acids," Applied Catalysis A: General, vol. 375, pp. 134-139, 2010.

[12] P. Kumar, S. R. Yenumala, S. K. Maity, and D. Shee, "Kinetics of hydrodeoxygenation of stearic acid using supported nickel catalysts: Effects of supports," Applied Catalysis A: General, vol. 471, pp. 28-38, 2014.

[13] Vam, "Kinetics of the Hydro-Deoxygenation of Stearic Acid over Palladium on Carbon Catalyst in Fixed-Bed Reactor for the Production of Renewable Diesel," University of Dayton, 2013.

[14] Peng, C. Zhao, S. Kasakov, S. Foraita, and J. A. Lercher, "Manipulating catalytic pathways: deoxygenation of palmitic acid on multifunctional catalysts," Chemistry–A European Journal, vol. 19, pp. 4732-4741, 2013.

[15] Funkenbusch, L.T., Mullins, M.E., “Hydrotreatment of Pyrolysis Oil Model Compounds over Pt/Al2O3 and Pd/C Catalysts: Part II: Trickle Bed Reactors,” Industrial & Engineering Chemistry Research, in preparation for submission August 2017.

[16] S. Gong, A. Shinozaki, M. Shi, and E. W. Qian, "Hydrotreating of Jatropha Oil over Alumina Based Catalysts," Energy & Fuels, vol. 26, pp. 2394-2399, 2012/04/19 2012.

[17] K. Hengst, M. Arend, R. Pfützenreuter, and W. F. Hoelderich, "Deoxygenation and cracking of free fatty acids over acidic catalysts by single step conversion for the production of diesel fuel and fuel blends," Applied Catalysis B: Environmental, vol. 174, pp. 383-394, 2015.

[18] A. T. Madsen, E. H. Ahmed, C. H. Christensen, R. Fehrmann, and A. Riisager, "Hydrodeoxygenation of waste fat for diesel production: Study on model feed with Pt/alumina catalyst," Fuel, vol. 90, pp. 3433-3438, 2011.

[19] H. S. Fogler, "Elements of chemical reaction engineering," 1999.

[20] L. M. Kindt, M. E. Mullins, D. W. Hand, A. A. Kline, D. L. Carter, and J. D. Garr, "Catalytic oxidation model development of the volatile reactor assembly unit of the international space station water processor," SAE Technical Paper0148-7191, 1995.

[21] S. Berenblyum, T. A. Podoplelova, R. S. Shamsiev, E. A. Katsman, V. Y. Danyushevsky, and V. R. Flid, "Catalytic chemistry of preparation of hydrocarbon fuels from vegetable oils and fats," Catalysis in Industry, vol. 4, pp. 209-214, 2012.

[22] E. Furimsky, "Catalytic hydrodeoxygenation," Applied Catalysis A: General, vol. 199, pp. 147-190, 2000.

[23] S. Shah, S. Sharma, and M. Gupta, "Biodiesel preparation by lipase-catalyzed transesterification of Jatropha oil," Energy & Fuels, vol. 18, pp. 154-159, 2004.

[24] W. Charusiri and T. Vitidsant, "Kinetic study of used vegetable oil to liquid fuels over sulfated zirconia," Energy & fuels, vol. 19, pp. 1783-1789, 2005.

[25] R. Sharma, M. Anand, B. Rana, R. Kumar, S. Farooqui, M. Sibi, et al., "Jatropha-oil conversion to liquid hydrocarbon fuels using mesoporous titanosilicate supported sulfide catalysts," Catalysis Today, 2012.

[26] M. Anand and A. K. Sinha, "Temperature-dependent reaction pathways for the anomalous hydrocracking of triglycerides in the presence of sulfided Co–Mo-catalyst," Bioresource technology, vol. 126, pp. 148-155, 2012.

[27] Y. Murzin, I. Kubickova, M. Snåre, P. Mäki-Arvela, and J. Myllyoja, "Method for the manufacture of hydrocarbons," ed: Google Patents, 2009.

[28] S. Bezergianni, A. Dimitriadis, A. Kalogianni, and P. A. Pilavachi, "Hydrotreating of waste cooking oil for biodiesel production. Part I: Effect of temperature on product yields and heteroatom removal," Bioresource technology, vol. 101, pp. 6651-6656, 2010.

[29] S. Bezergianni, A. Dimitriadis, T. Sfetsas, and A. Kalogianni, "Hydrotreating of waste cooking oil for biodiesel production. Part II: effect of

temperature on hydrocarbon composition," Bioresource technology, vol. 101, pp. 7658-7660, 2010.

[30] C. Elliott, "Historical developments in hydroprocessing bio-oils," Energy & Fuels, vol. 21, pp. 1792-1815, 2007.

[31] Sebos, A. Matsoukas, V. Apostolopoulos, and N. Papayannakos, "Catalytic hydroprocessing of cottonseed oil in petroleum diesel mixtures for production of renewable diesel," Fuel, vol. 88, pp. 145-149, 2009.

[32] P. Miller and A. Kumar, "Techno-economic assessment of hydrogenation-derived renewable diesel production from canola and camelina," Sustainable Energy Technologies and Assessments, vol. 6, pp. 105-115, 2014.

[33] H. Huo, M. Wang, C. Bloyd, and V. Putsche, "Life-Cycle Assessment of Energy and Greenhouse Gas Effects of Soybean-Derived Biodiesel and Renewable Fuels (No. ANL/ESD/08-2)," Argonne National Laboratory, Argonne, IL, 2008.

[34] R. W. Stratton, H. M. Wong, and J. I. Hileman, "Life cycle greenhouse gas emissions from alternative jet fuels," Partnership for AiR Transportation Noise and Emissions Reduction. Massachusetts Institute of Technology, Cambridge, MA, 2010.

[35] T. Kalnes, T. Marker, and D. R. Shonnard, "Green diesel: a second generation biofuel," International Journal of Chemical Reactor Engineering, vol. 5, 2007.

3. Catalytic Hydrotreatment of Pyrolysis Oil Literature Review

Over 100 papers were reviewed to assess the state of research in this area. Unfortunately, few papers considered reaction kinetics in a way that could be used for proper sustainability assessments of the conversion of wood to renewable gasoline. Instead, background information was collected on research trends, such as reactor types, pressures, temperatures, catalysts used, and model compounds, and this information was used to direct the experimental research plan. Tabulated results are shown in Chapter 8.

3.1 Pyrolysis Oil

While there are many different feedstocks that can be used in pyrolysis, including old tires, plant residues, and algae, the research presented here focuses on woody feedstocks or lignocellulosic biomass, specifically debarked virgin wood.[1] While the same concepts can be applied to forest residues, and other wood byproducts, there are issues with ash content and other contaminants that were not within the scope of this project. Lignocellulosic biomass has three primary components: cellulose, hemicellulose, and lignin. Cellulose and hemicellulose are polysaccharides and decompose during pyrolysis in a predictable manner, over a definitive temperature range.[2] Lignin, however, is a heterogeneous biopolymer with three different "building blocks": p-coumaryl alcohol, coniferyl alcohol, and sinapyl alcohol, which decompose across a wide range of

temperatures (100-900°C).[2,3] Product ratios and compositions can vary significantly depending on processing conditions and original feedstock.

Pyrolysis is a thermochemical decomposition process that breaks substances down at a high heat in the absence of oxygen. There are two main types of pyrolysis: slow and fast, or flash, pyrolysis. Slow pyrolysis involves heating materials to high temperatures slowly, mostly to ensure the correct consistency and remove moisture. This process can be used to generate a type of coal, called bio-char, which is typically used to sequester carbon and remediate soil. Fast or flash pyrolysis is almost instantaneous, with a high heating rate and final temperatures that are usually over 500°C.[4]

Pyrolysis releases a gaseous product, a solid char product, and a vapor that is condensed into a dark brown liquid, called bio-oil or pyrolysis oil. The exact composition of pyrolysis oil depends on a wide range of factors, especially original feedstock and pyrolysis conditions. However, pyrolysis oil is generally described as a complex mixture of oxygenated hydrocarbons that includes water, light acids, aldehydes, furans and phenolic compounds.[5] Most of these compounds are highly oxygenated and cause issues with viscosity and corrosiveness and are unstable in storage.[6,7] The pH of pyrolysis oil is typically 2-3, water content can range from 15-30%, which significantly lowers the heating value of pyrolysis oil as a fuel, and oxygen content can range from 35-40%.[8]

The wide range of compounds in pyrolysis oil makes filtration and separation necessary before utilization as a fuel. Filtration simply separates out any char and large oligomers that remain in the oil. Separation typically separates out different soluble fractions using solvents. Unfortunately, the exact composition of any bio-oil has not yet been fully understood, even with multiple analytical techniques.[9] Instead, researchers in this area rely on grouping compounds, typically into chemical families that exhibit similar properties and, conveniently, have similar retention times when run through analytical equipment such as a GC/MS or HPLC.[9] Depending on the final purpose of the pyrolysis oil, different solvents and fractions are necessary. For the purpose of biofuel, monomers and dimers of the phenolic compounds that come from the breakdown of lignin are the desired component. These are large enough to be in the gasoline range for fuel, even with treatment to remove the oxygenated groups. Typically, these compounds separate into solvents like ether and dichloromethane.[9,10]

3.2 Model Compounds

Given the complex and largely unknown nature of pyrolysis oil, it is necessary to choose surrogate compounds to represent the desired phenolic fraction. By carefully selecting just a few model compounds, the major functional groups are represented and the thermodynamic properties of the pyrolysis oil can be approximated. Based on a review of the literature, anisole, m-cresol and guaiacol were chosen to represent the phenolic fraction, and furfural was chosen to represent the larger holocellulosic compounds. This suite of compounds are found, in varying percentages, in pyrolysis oil and can be used to

reasonably simulate the behavior of phenolic pyrolysis fractions during the hydrotreatment process.[11,12,13] Chemical structures for all of these compounds can be seen in Figure 3-1.

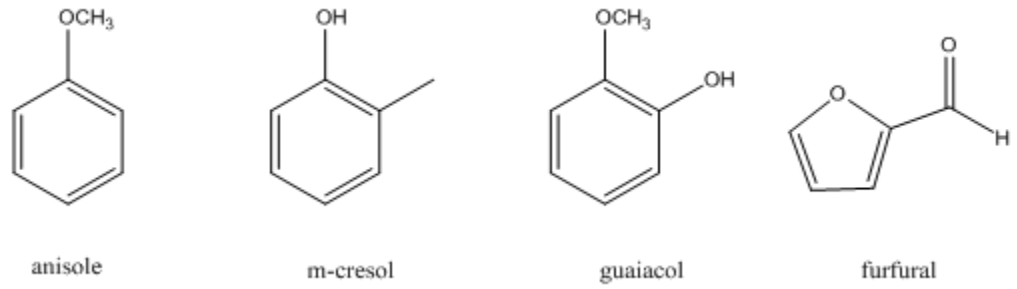

Figure 3-1. Phenolic Model Compounds

Anisole presents an ether bond that makes its properties somewhat different from regular phenolic compounds. In the presence of a catalyst and hydrogen, hydrodeoxygenation and saturation reactions occur that lead to the primary desired products, benzene and cyclohexane. Other products with less deoxygenation or with transalkylation were also observed, such as cresol isomers and phenol.[14,15,16,17]

M-cresol has a phenol base, but also has a methyl group on the ring, which allows better investigation of cracking and rearrangement functionalities on the catalyst. Here, the final desired products are toluene and methylcyclohexane. However, significant amounts of transalkylation occur and different cresol isomers, phenol, and xylenol, which has two methyl groups on the ring, are common products as well.[18,19,20,21,22,23]

Guaiacol has two oxygenated groups, one methoxyl and one hydroxyl group. This provides insight into reaction preference for functional groups, as well as how the dual oxygenation affects the catalyst. Because both of the functional groups are oxygenated, the final desired products are once again benzene and cyclohexane.[15,20,24,25,26,27,28,29,30,31,32,33] However, the double oxygen groups can lead to re-polymerization of the compounds that then form coke on the catalyst.[34,35] Coke will rapidly clog the active sites on the catalyst and result in catalyst deactivation. The catalyst can be regenerated under high heat and hydrogen, but this is costly and requires the process to be shut down for at least a few hours.

Phenol was used in later experiments, but was not seen in many literature sources, probably due to the fact that it is crystalline at room temperature. Most of the model compounds used in experiments are liquid at room temperature; these are simply easier to work with. Phenol, as the basic phenolic building block, has easily predictable behavior when hydrotreated.[49,57]

Furfural is a carbohydrate-based component that comes from the holocellulosic compounds in pyrolysis oil. While the phenolic, lignin-based compounds are the target reactants, there is no clear fractionation method to selectively separate them out. Therefore, it is necessary to understand how the holocellulosic compounds will react under hydrotreatment as well. Furfural typically proceeds via a decarbonylation and

subsequent ring opening route or via a hydrogenation and subsequent hydrodeoxygenation route.[12] It is more difficult to remove the oxygen from the furfural compound because it is contained inside the ring.

3.3 Catalytic Hydrotreatment

Crude oil used in the petroleum industry contains sulfur, nitrogen and low levels of oxygen. These contaminants are removed in hydrotreatment fixed bed reactors at high temperatures and pressures under hydrogen, typically over a sulfided cobalt-molybdenum (CoMo) or nickel-molybdenum (NiMo) catalyst supported on alumina. The remaining sulfur is removed in a stripper unit to prevent poisoning of the noble metal catalysts contained in reforming and isomerization units further down the line.

A similar approach can be taken with removing the oxygen from pyrolysis oil. By running the oil through a hydrotreatment unit, oxygen is removed from the compounds and the thermal and physical properties of the product oil are brought closer to that of petroleum-based gasoline. The oil becomes less viscous and corrosive, the heating value increases, and the color even lightens from dark brown to yellow or even clear, if the hydrotreatment is carried to completion.

When catalytically hydrotreating phenolic compounds on a commercial scale, a primary concern is hydrogen consumption. Reacting a compound like phenol, for example, can

use anywhere from one to four hydrogen molecules per phenol molecule, depending on the extent of reaction, as shown in Figure 3-2.

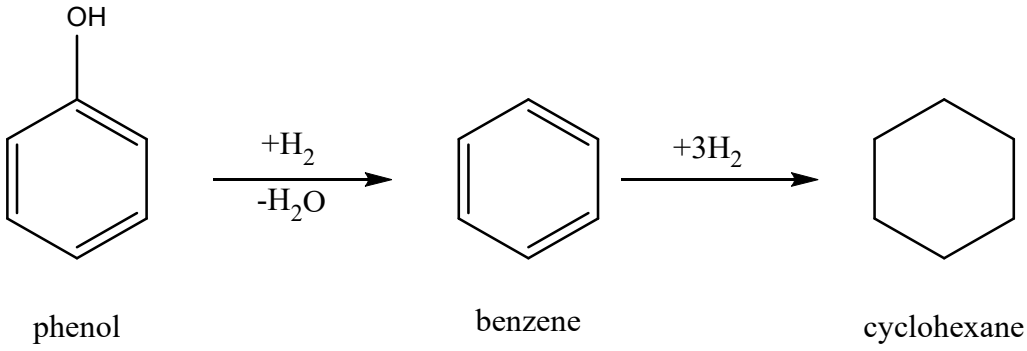

Figure 3-2. First Possible Reaction Pathway for Hydrotreatment of Phenol

However, the removal of the hydroxyl group is often difficult, as the carbon to oxygen bond off the aromatic ring is quite strong.[18] Instead, it is often necessary to saturate the ring prior to removal of the hydroxyl group, as shown in Figure 3-3.

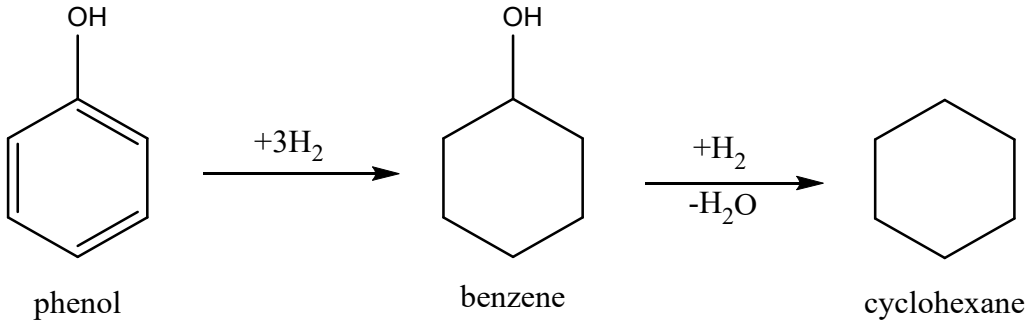

Figure 3-3. Second Possible Reaction Pathway for Hydrotreatment of Phenol

The ability to predict this can be critical when commercializing this process and, because most hydrogen today is sourced from natural gas reforming, can also have a huge impact on the sustainability of the process. Different catalysts, reactor temperatures, and hydrogen to oil ratios can direct which pathway the process will take, what the final product composition will be, and how much hydrogen is consumed.

3.4 Reactor Types

Although continuous hydrotreatment reactors are standard in industry, most literature sources use batch reactors.[23,26,27,28,32,33,35,36,37,38,39,40,41] This is most likely because batch reactors allow laboratory scale equipment to reach the high pressures present in industrial equipment without presenting a costly safety hazard. While this can provide insight into reaction pathways and mechanisms at the elevated pressures, it does not provide a proper understanding of the reaction kinetics, mainly due to the start-up time necessary for the batch reactor to reach the set temperature and pressure once the reactants and catalyst are placed inside.

The continuous flow reactor experiments conducted in literature are performed at lower pressures, sometimes even atmospheric, and, as a result, the reactants are often in the vapor phase. While the fixed bed design more accurately reflects industrial hydroprocessing units, mass transfer coefficients and limitations for vapor phase reactants will be different from the liquid phase reactants found in industry.[21,24,25,29,30,31,42,43,44]

3.5 Reactor Pressures & Temperatures

Industrial hydrotreatment reactors for petroleum are typically fixed bed, continuous reactors between 50 and 100 bar and 300-400°C. Ideally, pyrolysis oil hydrotreatment reactors would be run at the same conditions so that co-processing pyrolysis oil and other more renewable fuels with crude oil would be possible.[45,46]

Pressures in hydrotreatment reactors vary drastically across literature sources, but can be sorted into two general categories, high and low. Batch reactors can maintain a much higher pressure than laboratory scale continuous reactors, and experimental designs typically reflect this. Lower pressure reactors are run at near atmospheric pressures, and the model compounds are typically in the vapor phase.[29,30,31,36,44] Unfortunately, because of the difference between these operating conditions and those found in industry, mass transfer concerns cannot be properly accounted for.

The main feature of higher pressure reactors is that the reactants are at liquid phase. While there is little or no vapor pressure data for common pyrolysis oil compounds at elevated temperatures, most reactants remain in the liquid phase when the pressure is over 4 or 5 bar. From that point, high pressures can range anywhere up to 200 bar.[26,27,35,39,40,41] These pressures more accurately simulate industrial conditions, however, the highest pressure experiments are usually performed in batch reactors, which still do not accurately simulate the hydrotreatment reactors found in industry.

The typical temperature for a catalytic hydrotreatment reactor is between 250 and 400°C. Almost every source in literature uses temperatures in this range. Such temperatures are essentially necessary for hydrotreatment reactions and, as a result, literature sources match industrial conditions very closely.

3.6 Hydrotreatment Catalysts

Traditional petroleum hydroprocessing catalysts, specifically sulfided cobalt-molybdenum (CoMo) or nickel-molybdenum (NiMo) on a support such as alumina, are a logical place to start, and there is a large amount of literature available. These catalysts are excellent for hydrotreatment of organic compounds and show promising results overall.[19,21,23,24,25,27,35,47,48] However, these catalysts require a small amount of sulfur to be present in the feed in order to remain active.[49,50] For petroleum, which has large amounts of sulfur in it already, there is always enough sulfur present to maintain catalyst activity. For biological feedstocks such as pyrolysis oil, however, there is little to no initial sulfur present, and the use of sulfided catalysts requires the addition of sulfur, usually in the form of hydrogen disulfide or dimethyl disulfide.[51] This sulfur can leach into the oil, contaminating it and forcing further treatment later in the process. While this limits the potential for processing pure pyrolysis oil with the sulfided catalyst, this line of research can be used to expand on co-processing pyrolysis oil with crude oil.

Due to the sulfur leaching issue, more recent research trends have been away from the traditional sulfided catalysts. Instead, acidic zeolite catalysts, noble metal or nickel catalysts, and bifunctional catalysts have gained popularity. Unfortunately, many of these catalysts can be poisoned very quickly by nitrogen- or sulfur-containing compounds and are therefore incompatible with petroleum feeds.

Acidic catalysts, such as ZSM-5 and other zeolites, have cracking and isomerization functionalities. While they can readily remove oxygen, these catalysts also tend to crack carbons off of the primary chain and result in smaller molecular weight products.[41,42,52,53,54,55,56,57,58]

Noble metal and nickel catalysts have a hydrogenation functionality, which can be used for hydrodeoxygenation, but also tends to saturate the aromatic carbon bonds.[28,40,59,60] Ring saturation is hydrogen intensive, and noble metals are expensive, even at only 1-5% weight loading, making pilot or commercial scale use of noble metal catalysts costly and impractical. Instead, nickel catalysts have been suggested as substitutes. Nickel exhibits a similar hydrogenation functionality to noble metals. As with the noble metal catalysts, the primary function is to saturate or reduce the ring.[26]

The optimal catalyst depends on the desired product. For producing biofuels from renewable feedstocks, there is a need for both the acidic and hydrogenation functionalities, leading to the rise in popularity of bifunctional catalysts. These catalysts

are typically a hydrogenation metal or bimetallic catalyst on an acidic ceramic support. When used in hydrotreating, they still have a tendency to saturate the aromatic ring, but will also remove oxygenated groups without breaking the ring.[15,22,29,30,31,32,33,36,40,43,44,59,61,62,63]

In order to fully investigate the range of catalysts, all types except for the sulfided catalysts were investigated. A representative catalyst from each type was selected: ZSM-5, an acidic zeolite catalyst, palladium on carbon (Pd/C), a noble metal hydrogenation catalyst, and platinum on alumina (Pt/Al_2O_3).

3.7 References

[1] K. Chaiwong, T. Kiatsiriroat, N. Vorayos, and C. Thararax, "Study of bio-oil and bio-char production from algae by slow pyrolysis," Biomass and Bioenergy, vol. 56, pp. 600-606, 9// 2013.

[2] H. Yang, R. Yan, H. Chen, D. H. Lee, and C. Zheng, "Characteristics of hemicellulose, cellulose and lignin pyrolysis," Fuel, vol. 86, pp. 1781-1788, 2007.

[3] J. Zakzeski, P. C. Bruijnincx, A. L. Jongerius, and B. M. Weckhuysen, "The catalytic valorization of lignin for the production of renewable chemicals," Chemical Reviews, vol. 110, pp. 3552-3599, 2010.

[4] A. Bridgwater and G. Peacocke, "Fast pyrolysis processes for biomass," Renewable and Sustainable Energy Reviews, vol. 4, pp. 1-73, 2000.

[5] R. J. Evans and T. A. Milne, "Molecular characterization of the pyrolysis of biomass," Energy & Fuels, vol. 1, pp. 123-137, 1987/03/01 1987.

[6] S. Czernik and A. V. Bridgwater, "Overview of Applications of Biomass Fast Pyrolysis Oil," Energy & Fuels, vol. 18, pp. 590-598, 2004/03/01 2004.

[7] J. P. Diebold, A review of the chemical and physical mechanisms of the storage stability of fast pyrolysis bio-oils: National Renewable Energy Laboratory Golden, CO, 2000.

[8] Q. Zhang, J. Chang, T. Wang, and Y. Xu, "Review of biomass pyrolysis oil properties and upgrading research," Energy Conversion and Management, vol. 48, pp. 87-92, 2007.

[9] M. Garcia-Perez, A. Chaala, H. Pakdel, D. Kretschmer, and C. Roy, "Characterization of bio-oils in chemical families," Biomass and Bioenergy, vol. 31, pp. 222-242, 2007.

[10] R. H. Venderbosch, A. R. Ardiyanti, J. Wildschut, A. Oasmaa, and H. J. Heeres, "Stabilization of biomass-derived pyrolysis oils," Journal of Chemical Technology & Biotechnology, vol. 85, pp. 674-686, 2010.

[11] M. H. El-barbary, P. H. Steele, and L. Ingram, "Characterization of fast pyrolysis bio-oils produced from pretreated pine wood," Applied biochemistry and biotechnology, vol. 154, pp. 3-13, 2009.

[12] Z. W. He, Xianqin, "Hydrodeoxygenation of model compounds and catalytic systems for pyrolysis bio-oils upgrading," Catalysis for Sustainable Energy, vol. 1, pp. 28–52, 2012-09-14 2013.

[13] M. Saidi, F. Samimi, D. Karimipourfard, T. Nimmanwudipong, B. C. Gates, and M. R. Rahimpour, "Upgrading of lignin-derived bio-oils by catalytic hydrodeoxygenation," Energy & Environmental Science, vol. 7, pp. 103-129, 2014.

[14] R. C. Runnebaum, R. J. Lobo-Lapidus, T. Nimmanwudipong, D. E. Block, and B. C. Gates, "Conversion of anisole catalyzed by platinum supported on alumina: The reaction network," Energy & fuels, vol. 25, pp. 4776-4785, 2011.

[15] R. C. Runnebaum, T. Nimmanwudipong, D. E. Block, and B. C. Gates, "Catalytic conversion of compounds representative of lignin-derived bio-oils: a reaction network for guaiacol, anisole, 4-methylanisole, and cyclohexanone

conversion catalysed by Pt/γ-Al2O3," Catalysis Science & Technology, vol. 2, pp. 113-118, 2012.

[16] Y. Yang, C. Ochoa-Hernández, A. Víctor, P. Pizarro, J. M. Coronado, and D. P. Serrano, "Effect of metal–support interaction on the selective hydrodeoxygenation of anisole to aromatics over Ni-based catalysts," Applied Catalysis B: Environmental, vol. 145, pp. 91-100, 2014.

[17] X. Zhu, R. G. Mallinson, and D. E. Resasco, "Role of transalkylation reactions in the conversion of anisole over HZSM-5," Applied Catalysis A: General, vol. 379, pp. 172-181, 2010.

[18] A. J. Foster, P. T. Do, and R. F. Lobo, "The synergy of the support acid function and the metal function in the catalytic hydrodeoxygenation of m-cresol," Topics in Catalysis, vol. 55, pp. 118-128, 2012.

[19] B. Gevert, J. Otterstedt, and F. Massoth, "Kinetics of the HDO of methyl-substituted phenols," Applied catalysis, vol. 31, pp. 119-131, 1987.

[20] J. Horáček, G. Šťávová, V. Kelbichová, and D. Kubička, "Zeolite-Beta-supported platinum catalysts for hydrogenation/hydrodeoxygenation of pyrolysis oil model compounds," Catalysis Today, vol. 204, pp. 38-45, 2013.

[21] F. Massoth, P. Politzer, M. Concha, J. Murray, J. Jakowski, and J. Simons, "Catalytic hydrodeoxygenation of methyl-substituted phenols: Correlations of kinetic parameters with molecular properties," The Journal of Physical Chemistry B, vol. 110, pp. 14283-14291, 2006.

[22] L. Nie and D. E. Resasco, "Kinetics and mechanism of m-cresol hydrodeoxygenation on a Pt/SiO 2 catalyst," Journal of Catalysis, vol. 317, pp. 22-29, 2014.

[23] Y. Yang, H. a. Luo, G. Tong, K. J. Smith, and C. T. Tye, "Hydrodeoxygenation of Phenolic Model Compounds over MoS< sub> 2</sub> Catalysts with Different Structures," Chinese Journal of Chemical Engineering, vol. 16, pp. 733-739, 2008.

[24] V. N. Bui, D. Laurenti, P. Afanasiev, and C. Geantet, "Hydrodeoxygenation of guaiacol with CoMo catalysts. Part I: Promoting effect of cobalt on HDO selectivity and activity," Applied Catalysis B: Environmental, vol. 101, pp. 239-245, 2011.

[25] V. N. Bui, D. Laurenti, P. Delichère, and C. Geantet, "Hydrodeoxygenation of guaiacol: Part II: Support effect for CoMoS catalysts on HDO activity and selectivity," Applied Catalysis B: Environmental, vol. 101, pp. 246-255, 2011.

[26] M. Bykova, O. Bulavchenko, D. Y. Ermakov, M. Y. Lebedev, V. Yakovlev, and V. Parmon, "Guaiacol hydrodeoxygenation in the presence of Ni-containing catalysts," Catalysis in Industry, vol. 3, pp. 15-22, 2011.

[27] A. Centeno, E. Laurent, and B. Delmon, "Influence of the Support of CoMo Sulfide Catalysts and of the Addition of Potassium and Platinum on the Catalytic Performances for the Hydrodeoxygenation of Carbonyl, Carboxyl, and Guaiacol-Type Molecules," Journal of Catalysis, vol. 154, pp. 288-298, 7// 1995.

[28] A. Gutierrez, R. K. Kaila, M. L. Honkela, R. Slioor, and A. O. I. Krause, "Hydrodeoxygenation of guaiacol on noble metal catalysts," Catalysis Today, vol. 147, pp. 239-246, 10/15/ 2009.

[29] T. Nimmanwudipong, R. C. Runnebaum, D. E. Block, and B. C. Gates, "Catalytic conversion of guaiacol catalyzed by platinum supported on alumina: reaction network including hydrodeoxygenation reactions," Energy & fuels, vol. 25, pp. 3417-3427, 2011.

[30] T. Nimmanwudipong, R. C. Runnebaum, D. E. Block, and B. C. Gates, "Catalytic reactions of guaiacol: reaction network and evidence of oxygen removal in reactions with hydrogen," Catalysis letters, vol. 141, pp. 779-783, 2011.

[31] T. Nimmanwudipong, C. Aydin, J. Lu, R. C. Runnebaum, K. C. Brodwater, N. D. Browning, et al., "Selective Hydrodeoxygenation of Guaiacol Catalyzed by Platinum Supported on Magnesium Oxide," Catalysis letters, vol. 142, pp. 1190-1196, 2012.

[32] X. Zhang, T. Wang, L. Ma, Q. Zhang, and T. Jiang, "Hydrotreatment of bio-oil over Ni-based catalyst," Bioresource technology, vol. 127, pp. 306-311, 2013.

[33] X. Zhang, T. Wang, L. Ma, Q. Zhang, Y. Yu, and Q. Liu, "Characterization and catalytic properties of Ni and NiCu catalysts supported on ZrO2–SiO2 for guaiacol hydrodeoxygenation," Catalysis Communications, vol. 33, pp. 15-19, 3/5/ 2013.

[34] A. G. Gayubo, A. T. Aguayo, A. Atutxa, R. Aguado, and J. Bilbao, "Transformation of Oxygenate Components of Biomass Pyrolysis Oil on a HZSM-5 Zeolite. I. Alcohols and Phenols," Industrial & Engineering Chemistry Research, vol. 43, pp. 2610-2618, 2004/05/01 2004.

[35] E. Laurent and B. Delmon, "Study of the hydrodeoxygenation of carbonyl, carboxylic and guaiacyl groups over sulfided CoMo/γ-Al2O3 and NiMo/γ-Al2O3 catalysts. I: Catalytic reaction schemes," Applied catalysis. A, General, vol. 109, pp. 77-96, 1994.

[36] A. R. Ardiyanti, S. A. Khromova, R. H. Venderbosch, V. A. Yakovlev, and H. J. Heeres, "Catalytic hydrotreatment of fast-pyrolysis oil using non-sulfided bimetallic Ni-Cu catalysts on a δ-Al2O3 support," Applied Catalysis B: Environmental, vol. 117–118, pp. 105-117, 5/18/ 2012.

[37] S. J. Hurff and M. T. Klein, "Reaction pathway analysis of thermal and catalytic lignin fragmentation by use of model compounds," Industrial & engineering chemistry fundamentals, vol. 22, pp. 426-430, 1983.

[38] C. J. Richard, B. Patel, D. Chadwick, and K. Hellgardt, "Hydrothermal deoxygenation of pyrolysis oil from Norwegian spruce: Picea abies," Biomass and Bioenergy, vol. 56, pp. 446-455, 9// 2013.

[39] E.-M. Ryymin, M. L. Honkela, T.-R. Viljava, and A. O. I. Krause, "Competitive reactions and mechanisms in the simultaneous HDO of phenol and methyl heptanoate over sulphided NiMo/γ-Al< sub> 2</sub> O< sub> 3</sub>," Applied Catalysis A: General, vol. 389, pp. 114-121, 2010.

[40] J. Wildschut, F. H. Mahfud, R. H. Venderbosch, and H. J. Heeres, "Hydrotreatment of fast pyrolysis oil using heterogeneous noble-metal catalysts," Industrial & Engineering Chemistry Research, vol. 48, pp. 10324-10334, 2009.

[41] X. Zhang, Q. Zhang, T. Wang, L. Ma, Y. Yu, and L. Chen, "Hydrodeoxygenation of lignin-derived phenolic compounds to hydrocarbons over Ni/SiO 2–ZrO 2 catalysts," Bioresource technology, vol. 134, pp. 73-80, 2013.

[42] J. D. Adjaye and N. N. Bakhshi, "Production of hydrocarbons by catalytic upgrading of a fast pyrolysis bio-oil. Part I: Conversion over various catalysts," Fuel Processing Technology, vol. 45, pp. 161-183, 12// 1995.

[43] S. Leng, X. Wang, X. He, L. Liu, Y. e. Liu, X. Zhong, et al., "NiFe/γ-Al2O3: A universal catalyst for the hydrodeoxygenation of bio-oil and its model compounds," Catalysis Communications, vol. 41, pp. 34-37, 11/5/ 2013.

[44] X. Zhu, L. L. Lobban, R. G. Mallinson, and D. E. Resasco, "Bifunctional transalkylation and hydrodeoxygenation of anisole over a Pt/HBeta catalyst," Journal of Catalysis, vol. 281, pp. 21-29, 2011.

[45] A. Bridgwater, "Review of fast pyrolysis of biomass and product upgrading," Biomass and Bioenergy, vol. 38, pp. 68-94, 2012.

[46] ,V. N. Bui, G. Toussaint, D. Laurenti, C. Mirodatos, and C. Geantet, "Co-processing of pyrolisis bio oils and gas oil for new generation of bio-fuels: Hydrodeoxygenation of guaïacol and SRGO mixed feed," Catalysis Today, vol. 143, pp. 172-178, 5/15/ 2009.

[47] E. G. Baker and D. C. Elliott, "Catalytic hydrotreating of biomass-derived oils," ACD, Div. Fuel Chem, vol. 32, pp. 257-263, 1987.

[48] E. Furimsky, "Catalytic hydrodeoxygenation," Applied Catalysis A: General, vol. 199, pp. 147-190, 2000.

[49] W.-y. Wang, Y.-q. Yang, J.-g. Bao, and H.-a. Luo, "Characterization and catalytic properties of Ni–Mo–B amorphous catalysts for phenol hydrodeoxygenation," Catalysis Communications, vol. 11, pp. 100-105, 2009.

[50] W. Wang, Y. Yang, H. Luo, T. Hu, and W. Liu, "Amorphous Co–Mo–B catalyst with high activity for the hydrodeoxygenation of bio-oil," Catalysis Communications, vol. 12, pp. 436-440, 2011.

[51] E. Furimsky, "Hydroprocessing challenges in biofuels production," Catalysis Today, 2013.

[52] J. D. Adjaye and N. N. Bakhshi, "Production of hydrocarbons by catalytic upgrading of a fast pyrolysis bio-oil. Part II: Comparative catalyst performance and reaction pathways," Fuel Processing Technology, vol. 45, pp. 185-202, 12// 1995.

[53] K. L. Hew, A. M. Tamidi, S. Yusup, K. T. Lee, and M. M. Ahmad, "Catalytic cracking of bio-oil to organic liquid product (OLP)," Bioresource technology, vol. 101, pp. 8855-8858, 11// 2010.

[54] A. J. Maia, B. Louis, Y. L. Lam, and M. M. Pereira, "Ni-ZSM-5 catalysts: Detailed characterization of metal sites for proper catalyst design," Journal of Catalysis, vol. 269, pp. 103-109, 1/1/ 2010.

[55] T. Nimmanwudipong, R. C. Runnebaum, S. E. Ebeler, D. E. Block, and B. C. Gates, "Upgrading of Lignin-Derived Compounds: Reactions of Eugenol Catalyzed by HY Zeolite and by Pt/γ-Al2O3," Catalysis letters, vol. 142, pp. 151-160, 2012.

[56] S. Vitolo, M. Seggiani, P. Frediani, G. Ambrosini, and L. Politi, "Catalytic upgrading of pyrolytic oils to fuel over different zeolites," Fuel, vol. 78, pp. 1147-1159, 1999.

[57] C. Zhao, S. Kasakov, J. He, and J. A. Lercher, "Comparison of kinetics, activity and stability of Ni/HZSM-5 and Ni/Al< sub> 2</sub> O< sub> 3</sub>-HZSM-5 for phenol hydrodeoxygenation," Journal of Catalysis, vol. 296, pp. 12-23, 2012.

[58] C. Zhao and J. A. Lercher, "Upgrading Pyrolysis Oil over Ni/HZSM-5 by Cascade Reactions," Angewandte Chemie, vol. 124, pp. 6037-6042, 2012.

[59] J. Wildschut, I. Melian-Cabrera, and H. Heeres, "Catalyst studies on the hydrotreatment of fast pyrolysis oil," Applied Catalysis B: Environmental, vol. 99, pp. 298-306, 2010.

[60] H. Zhao, D. Li, P. Bui, and S. Oyama, "Hydrodeoxygenation of guaiacol as model compound for pyrolysis oil on transition metal phosphide hydroprocessing catalysts," Applied catalysis A: general, vol. 391, pp. 305-310, 2011.

[61] A. R. Ardiyanti, S. A. Khromova, R. H. Venderbosch, V. A. Yakovlev, I. V. Melián-Cabrera, and H. J. Heeres, "Catalytic hydrotreatment of fast pyrolysis

oil using bimetallic Ni–Cu catalysts on various supports," Applied catalysis A: general, vol. 449, pp. 121-130, 12/27/ 2012.

[62] C. Zhao, Y. Kou, A. A. Lemonidou, X. Li, and J. A. Lercher, "Hydrodeoxygenation of bio-derived phenols to hydrocarbons using RANEY® Ni and Nafion/SiO2 catalysts," Chemical Communications, vol. 46, pp. 412-414, 2010.

[63] C. Zhao, J. He, A. A. Lemonidou, X. Li, and J. A. Lercher, "Aqueous-phase hydrodeoxygenation of bio-derived phenols to cycloalkanes," Journal of Catalysis, vol. 280, pp. 8-16, 2011.

4. Catalytic Hydrotreatment of Pyrolysis Oil Model Compounds over Pt/Al_2O_3 and Pd/C

Part I: Batch Reactors[2]

4.1 Introduction

Biofuels are attractive renewable fuel sources because they can yield products similar to petroleum-based fuels. Because these fuels are derived from renewable and more eco-friendly feedstocks, significant efforts have been focused on researching optimal feedstocks and conversion methods.[1] Relatively little focus, however, has been placed on treating these fuels after the initial conversion step. Due to the biological nature of the feedstocks, biofuels usually contain oxygen, making them incompatible with petroleum-based fuel.[2] The high oxygenation of the biofuels creates miscibility issues, lowers the heating value, and makes them unstable in storage.[3,4] The pyrolysis of woody biomass produces pyrolysis oil, which is a highly complex mixture of oxygenated hydrocarbons.[5] Pyrolysis oil can include water, acids, aldehydes, furans and phenolic compounds, but exact composition varies drastically, based on original feedstock species, growing location and conditions, and conversion method.[6] In its crude form, a high amount of oxygen is retained in the oil, up to 40%.[7] Similar issues arise with crude oil, which contains heavy metals, sulfur, nitrogen, and oxygen. In a petroleum refinery, crude oil is hydrotreated, typically using sulfided cobalt/molybdenum (CoMo) or

[2] This work has been submitted to Industrial & Engineering Chemistry Research, and is a collaboration with Dr. Louise Olsson and Muhammad Abdus Salam.

nickel/molybdenum (NiMo) catalysts, to remove contaminants.[8] A comparable approach can be taken with biofuels to remove oxygen and produce a pure hydrocarbon product that can be blended in any proportion with traditional fuel. A significant portion of pyrolysis oil is within the desired range of hydrocarbons (C_6-C_8) for gasoline and, with catalytic hydrotreatment (HDT), a hydrocarbon fuel that is fully compatible with petroleum-based gasoline can be produced.[9]

While catalytic hydrotreatment has perhaps the most significant environmental impact of the entire process from biological feedstocks to fuel in terms of greenhouse gas (GHG) production, energy and hydrogen consumption, it is also the most poorly understood step in the process.[10] Based on current literature, there is little appropriate data available on reaction kinetics that would allow for proper life cycle assessment or scaling up of a process.[11,12] Instead, most life cycle assessments rely on proprietary data from industrial sources or make stoichiometric assumptions without considering process conditions and resulting pathway selectivities.

Once the reaction kinetics are understood, the process can be simulated using a reactor model, generating process-level details and allowing for simple scale-up of the process without expensive testing. The petroleum industry has used this approach with traditional crude oil, which differs from location to location and can contain hundreds of components. Mapping every kinetic pathway and obtaining data for every one of the compounds present is impractical, leading to lumped parameter models, which group

reaction pathways and/or compounds together. This streamlines modeling when predicting product compositions, yields, optimal catalyst, and energy and hydrogen input, and requires a more reasonable number of parameters. By focusing only on observed compounds and not hypothetical intermediates, the reaction network can be further simplified. With enough experimental data, a model can be constructed for any known inlet composition, including individual components, oil (of varying sources and composition), and even different blends of those oils. This model should yield accurate predictions for life cycle and techno-economic assessments, which will further the development of the technology and allow for faster screening of potential feedstocks.

4.2 Materials & Methods

Anisole, m-cresol, phenol, and n-dodecane (all 99+%) were obtained from Sigma Aldrich. Dodecane was used as an inert solvent for the phenolic compounds to limit the exothermic reactions and enable better quantification of the results. Palladium on carbon (Pd/C, powder, 5% metal loading) and platinum on alumina (Pt/Al_2O_3, powder, 5% metal loading) catalysts were also obtained from Sigma Aldrich, with particle sizes of roughly 1 micron, which were reduced in the Parr reactor for six hours under 10 bar hydrogen at 300°C. HDT studies were conducted in a batch slurry reactor system (Parr 4848B) with a maximum volume of 150 mL, as shown in Figure 4-1. Prior to each test, 120 mL solution of 5 mole percent model compound in dodecane were loaded into the reactor, along with 500 mg of catalyst. A baffle was inserted to ensure turbulent flow, and the reactor was sealed. After flushing with nitrogen, 10 bar of hydrogen was

maintained while the reactor achieved the set temperature (250, 300, or 350°C). The hydrogen pressure was then increased to 50 bar. A high pressure, pure hydrogen environment with high conversions was used to simulate commercial reactor conditions and product composition. Once the desired pressure and temperature were reached, time was set as 0 hours and an initial sample was taken. A sample was taken once every hour for four hours. Unfortunately, because the reactor could not be heated instantaneously, there is a pre-heating period prior to sampling during which some amount of conversion occurs. The reactor was stirred at 1000 rpm throughout the start-up and reaction times. The reactor was re-pressurized with hydrogen as necessary to compensate for any losses during sampling. Liquid samples were analyzed using a GC/MS-FID (Agilent 5977A MSD & Agilent 7890B GC), with calibrations performed on both for all observed compounds.

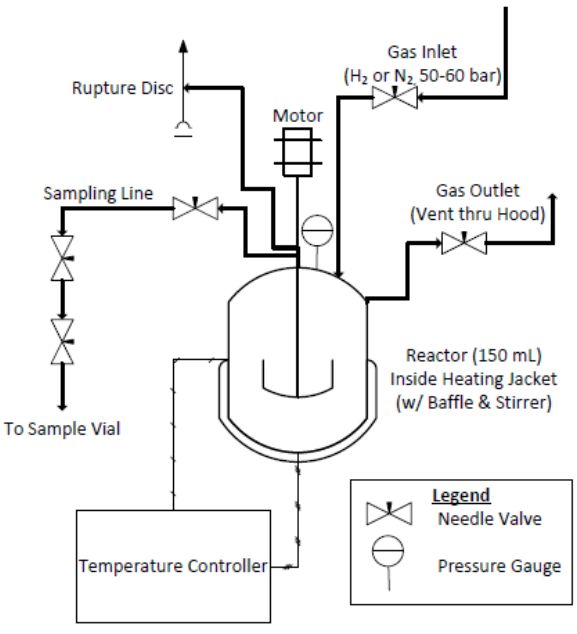

Figure 4-1. Parr Batch Reactor Photograph and Diagram

In previous work, we have studied relevant hydrotreatment mechanisms and pathways in a continuous micro-reactor system at low conversions.[13] As a result, for this study, anisole, m-cresol and phenol (shown in Figure 4-2) were chosen as model compounds for the lignin fraction of pyrolysis oil, which is 10-25% of crude pyrolysis oil, depending on specific feedstock.[14] They represent a variety of phenolic groups commonly found in pyrolysis oil, including methoxyl, methyl, and hydroxyl groups. The majority of the experiments were performed using Pt/Al_2O_3, but a set of tests was performed with Pd/C to examine differences due to catalyst functionality. Two dosages (200 and 500 mg) of Pt/Al_2O_3 catalyst were used to test for any mass transfer limitations.

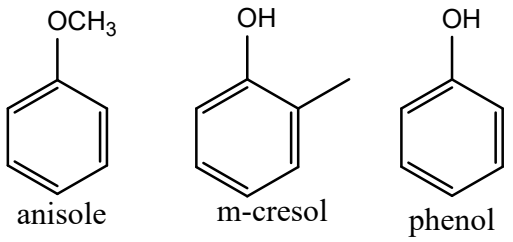

Figure 4-2. Pyrolysis Oil Lignin Fraction Model Compounds

4.3 Results

The analytical results were converted to absolute concentrations, and all analysis was performed accordingly. The reaction products and intermediates were used to propose a

simple reaction network. The rate constants for this network were then fitted to the experimental data, as discussed in the next section.

4.3.1. Individual Surrogate Compounds

For anisole, an increase in conversion and a pathway shift from ring saturation to demethylation were evident with increasing temperature. At 250°C, there was 57.7% conversion of anisole, with a pathway preference for ring saturation leading to methoxycyclohexane. At 300°C, there was 76.7% conversion, and a higher preference for the initial demethylation reaction that generates phenol from anisole. At 350°C, as shown in Figure 4-3, 99.0% conversion was attained, and the pathway almost completely shifted to the initial demethylation reaction. There was also more conversion of oxygenated intermediates to cyclohexane at the higher temperature. Four replicate experiments were performed with anisole at 300°C. After normalizing the results to the 0^{th} hour concentration of the original data set, standard deviations were calculated for each compound at each sampling time. The average standard deviation was 0.02 mol/L, approximately ±5% of the starting concentration. These results were quite similar to previous studies for anisole HDO over more traditional hydrotreatment catalysts, which yielded cyclohexane with phenol as the primary intermediate.[15]

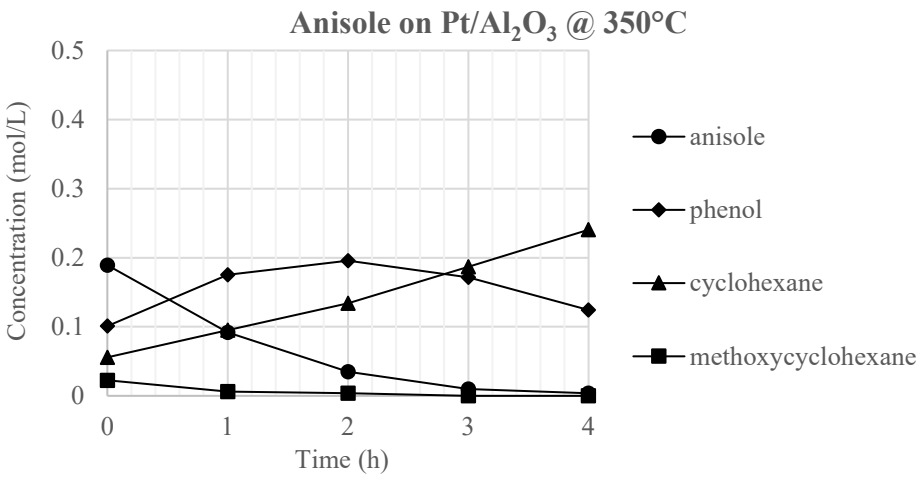

Figure 4-3. Anisole on Pt/Al_2O_3 results – Concentration vs. Time at 350°C

With m-cresol, there appears to be just one pathway, where m-cresol is hydrodeoxygenated to toluene, and then the ring is saturated to methylcyclohexane. There appears to be a significant conversion of m-cresol prior to the first sampling while the reactor is coming to temperature, yielding variability in overall conversion over four hours. At 250°C, the slowest reaction rate is seen, even though conversion prior to sampling is high. Due to the high initial conversion, however, complete conversion is achieved by the end of the four hour reaction period. At 300°C, there is no conversion prior to sampling, and the first conversion is noted after one hour. Once the reactions are initiated, the reaction rate is higher than at 250°C, but conversion of m-cresol is still only about 78% at the end of four hours. At 350°C (Figure 4-4), the highest reaction rate is observed, and 93% conversion of m-cresol is achieved by the end of the test, although there is less conversion prior to sampling than at 250°C. It is worth noting that toluene concentrations are consistently low over the entire four hours at all temperatures,

indicating either a rapid conversion of toluene to methylcyclohexane or an equilibrium between those species.[16] At 250°C, the concentration of toluene is ~5%, at 300°C, it is ~3%, and at 350°C, concentration is ~1% throughout the four hours. The concentration of toluene in the system is temperature dependent, but may also depend on hydrogen pressure or catalyst type. Another study, where the HDO of 4-methylphenol (p-cresol) over a sulfided molybdenum catalyst at 28 bar was examined, resulting in an almost 50% conversion to toluene after 5 hours at 350°C and almost 60% conversion to toluene at 330°C.[17]

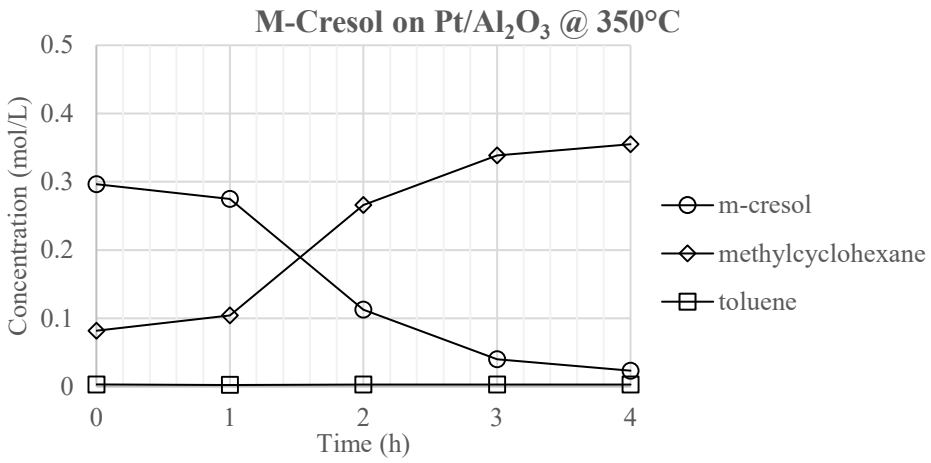

Figure 4-4. M-Cresol on Pt/Al_2O_3 results – Concentration vs. Time at 350°C

With phenol, we see a similar pathway as with anisole, where phenol is converted directly to cyclohexane. At 250°C, there is an hour long delay before conversion begins, but than a reasonable reaction rate and total conversion, ending at 79.5%. At 300°C, there is total conversion by the end and a 49.5% startup period conversion. At 350°C,

shown in Figure 4-5, there seems to be some suppression of the reactions; conversion is only at 71% by the end of the reaction period. However, the reaction rate for pure phenol at 350°C is almost the same as the phenol intermediate in the anisole reaction, once the consumption of anisole is complete. Based upon these results, the hydrodeoxygenation and ring saturation occur so rapidly that no intermediates are observed. A previous study with a similar system using petroluem hydrotreatment catalysts showed that phenol primarily forms cyclohexane in HDO systems, without any primary intermediates.[18]

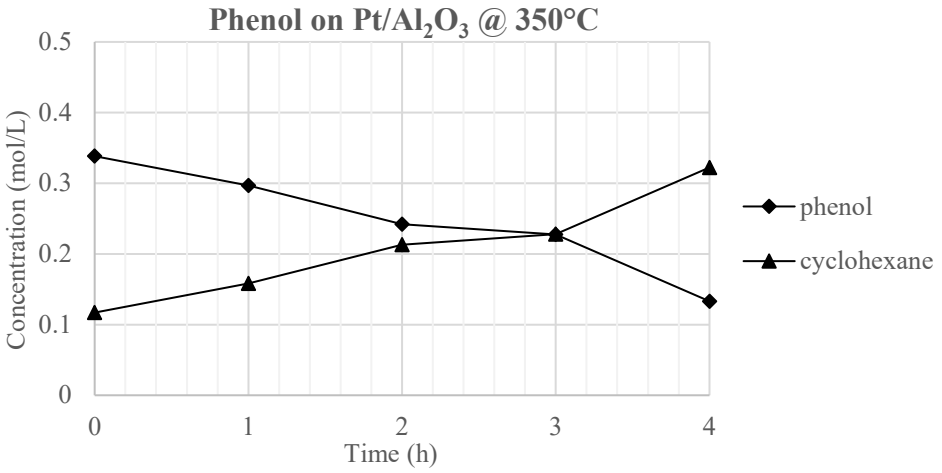

Figure 4-5. Phenol on Pt/Al_2O_3 results – Concentration vs. Time at 350°C

4.3.2. Catalyst Dosage Experiments

A set of trials were also performed using a smaller 200 mg dosage of the Pt/Al_2O_3 catalyst to investigate the effect of catalyst loading in the system, while all other reactor conditions were kept the same. As with the 500 mg tests, the preferred reaction pathway shifted from an initial ring saturation reaction to an initial demethylation reaction with

increasing temperature. At 250°C, the difference in total conversion of anisole between the two catalyst dosages was statistically insignificant. However, at 300°C, the four hour conversion over 500 mg was 76.7% versus 66.0% over 200 mg, and at 350°C, shown in Figure 4-6, conversion of anisole on 500 mg was 99.0% versus 88.8% over 200 mg. Although one might expect to have a linear relationship between conversion and catalyst mass, the results show that the change in conversion is not proportional to the catalyst mass. This may be due to mass transfer limitations or a more complex surface reaction order than we have assumed. Moreover, for a first order reaction in a batch reactor, Vdc/dt=-kcW. Solving this results in X=1-exp(-kWt/V). For low conversions, this will appear linear, but not for the higher conversions that we have used in this study.

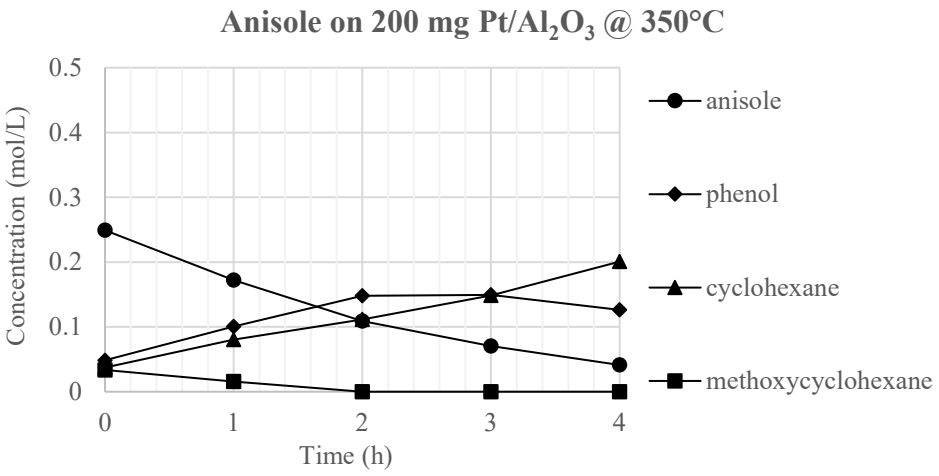

Figure 4-6. Anisole on 200 mg Pt/Al_2O_3 results – Concentration vs. Time at 350°C

To examine the role of mass transfer in the system, the inverse reaction rate was graphed versus the inverse catalyst mass, as shown in Equation 4-1 and Figure 4-7. In Equation

4-1, C_{H2} is the concentration of hydrogen in the system, which was constant throughout the experiments, r_A is the rate of reaction for anisole, $k_{H2}a_{H2}$ is the mass transfer resistance term for hydrogen across the gas-liquid interface, k_ca_c is the mass transfer resistance term for the catalyst surface, and $m_{catalyst}$ is the mass of the catalyst in the system. In Figure 4-7, the slope of the line is the inverse of k_ca_c, and the intercept is the inverse of $k_{H2}a_{H2}$. Although only two catalyst dosages were used, a clear trend can be observed at the higher temperatures. If reaction rate is proportional to catalyst mass, the intercept of this plot should be zero, but since it is not, this is indicative of external mass transfer limitations. Based on the graph, however, the mass transfer limitation from the catalyst surface is significantly larger than the hydrogen mass transfer limitation.

$$\frac{C_{H2}}{-r_A} = \frac{1}{k_{H2}a_{H2}} + \left(\frac{1}{k_ca_c}\right)\frac{1}{m_{catalyst}}$$ Equation 4-1

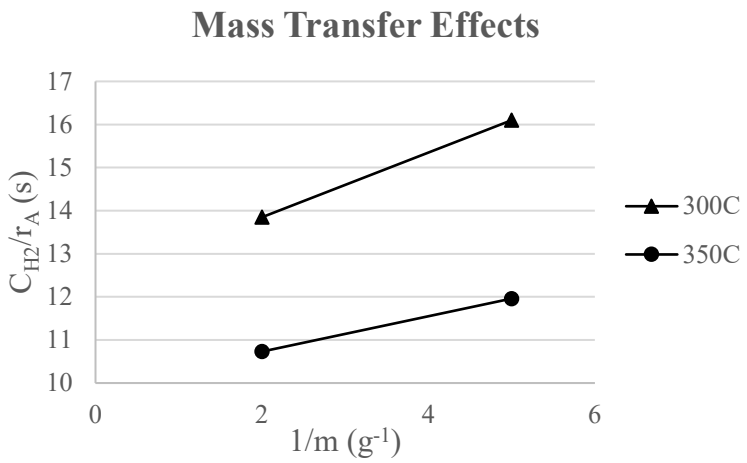

Figure 4-7. Mass transfer effects between 200 and 500 mg of Pt/Al_2O_3 for anisole at 350°C

4.3.3. Pd/C Catalyst Experiments

Pd/C is another common catalyst studied in the literature. Here, the noble metal catalyst provides a saturation functionality, without the cracking ability of the acidic alumina support. The Pd/C catalyzed reaction exhibited an initial saturation to methoxycyclohexane with subsequent methanol abstraction to cyclohexane. In comparison, Pt/Al_2O_3 has either an initial saturation step or an initial demethylation step. At 250°C, cyclohexane decreases with time and methoxycyclohexane is the primary product; this may indicate a reattachment of the methoxyl group to the cyclohexane ring in the lower temperature environment. At 350°C, there is a more rapid decline of anisole and the methoxycyclohexane intermediate than at 300°C. There is a 70% conversion of anisole at 300°C and nearly 100% conversion at 350°C. Some methoxycyclohexane is produced during the first hour of the process at 300°C; however, at 350°C, as shown in Figure 4-8, cyclohexane production dominates the entire four hour reaction period.

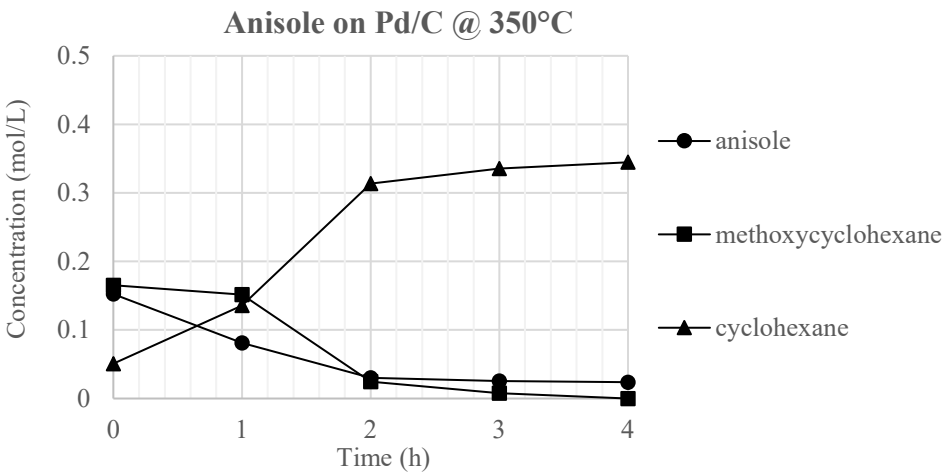

Figure 4-8. Anisole on Pd/C results – Concentration vs. Time at 350°C

4.3.4. Blended Model Compound Experiments

With the 50 mole percent anisole and 50 mole percent m-cresol mixture, at 250°C, demethylation appears to be the primary initial reaction. Since both anisole and m-cresol are converted to phenol this way, it is the primary product formed for the first two hours. Methylcyclohexane concentration decreases during this period, and then both methylcyclohexane and methoxycyclohexane production increase. Although anisole concentration drops from 50% to roughly 15% by the end of the pre-heating period, it remains relatively constant throughout the sampling period, reaching roughly 10% by the end of four hours. This behavior is not seen at higher temperatures. At 300°C, both anisole and m-cresol concentrations decrease steadily with time. The phenol intermediate also declines, while the methylcyclohexane concentration increases rapidly until the last hour, when phenol production increases again. Methoxycyclohexane persists at low levels (3-6%) throughout the four hours. As seen in Figure 4-9, at 350°C,

there is rapid production of methoxycyclohexane and methylcyclohexane, with decreasing anisole, m-cresol, and phenol concentrations. Conversion is nearly complete after three hours, while at the other temperatures, there are still secondary reactions in the last hour.

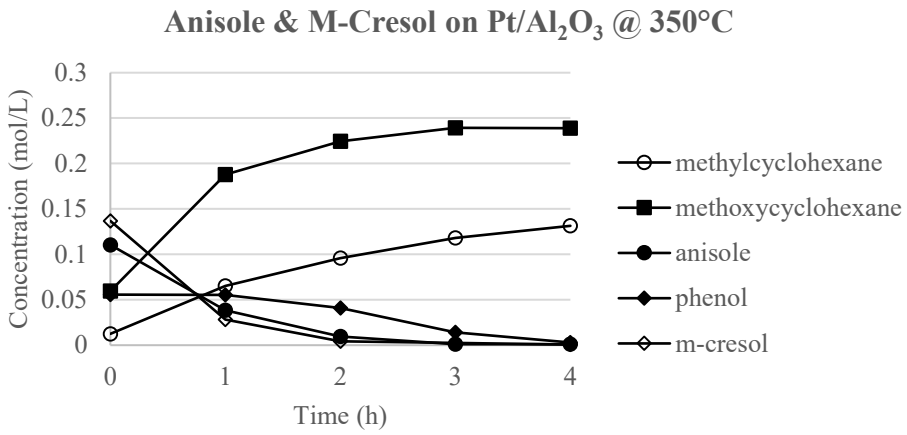

Figure 4-9. Anisole & M-Cresol Blend on Pt/Al_2O_3 results – Concentration vs. Time at 350°C

With the 50 mole percent anisole and 50 mole percent phenol blend, the presence of phenol seems to suppress the production of methoxycyclohexane and create another pathway via ring saturation to cyclohexanol. At 250°C, cyclohexanol production is the predominant reaction throughout the four hours, and appears to consume any phenol formed in the process; it is only after the anisole concentration has dropped below 30% that cyclohexane and methoxycyclohexane production increases. At 300°C, cyclohexanol and anisole concentrations decrease rapidly, methoxycyclohexane peaks

and then drops off quickly, and cyclohexane production dominates the process. As shown in Figure 4-10, at 350°C, there is no cyclohexanol detected during the four hour sampling period; indicating that it may have been consumed during the pre-heating period, that the higher temperature suppresses cyclohexanol production, or that the higher temperature greatly increases the conversion rate of cyclohexanol. Anisole, phenol, and methoxycyclohexane all decline quickly during the sampling period, and conversion to cyclohexane is complete by the end of the four hour sampling period.

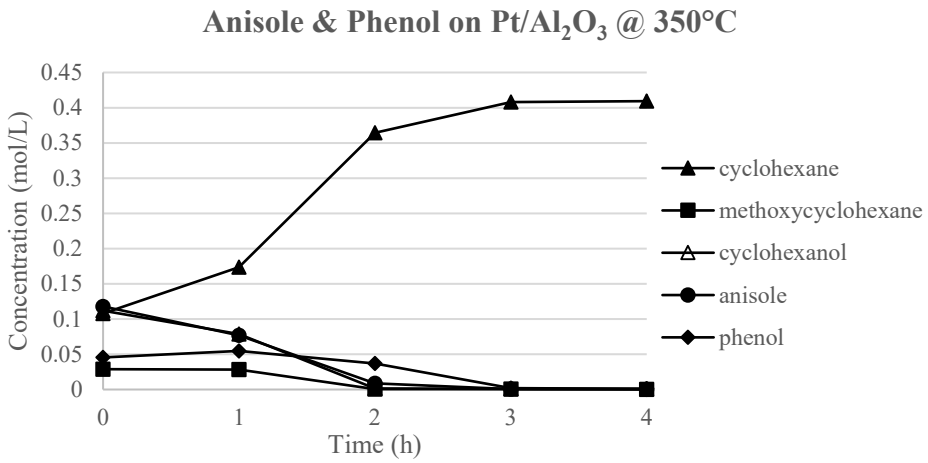

Figure 4-10. Anisole & Phenol Blend on Pt/Al_2O_3 results – Concentration vs. Time at 350°C

4.3.5. Lumped Parameter Reaction Network

Based on the results, a simple reaction network may be proposed for the HDT of the paradigm compounds over Pt/Al_2O_3 under an excess of hydrogen (Figure 4-11). This network is based only on the observed species, without any hypothetical reaction

intermediates included. A lumped parameter approach was taken, instead of considering each compound and reaction separately. For example, the ring saturation rate constants for the reactions of toluene, anisole, and phenol are assumed to be the same. This is reflected in the reaction network and later in the modeling section of this paper.

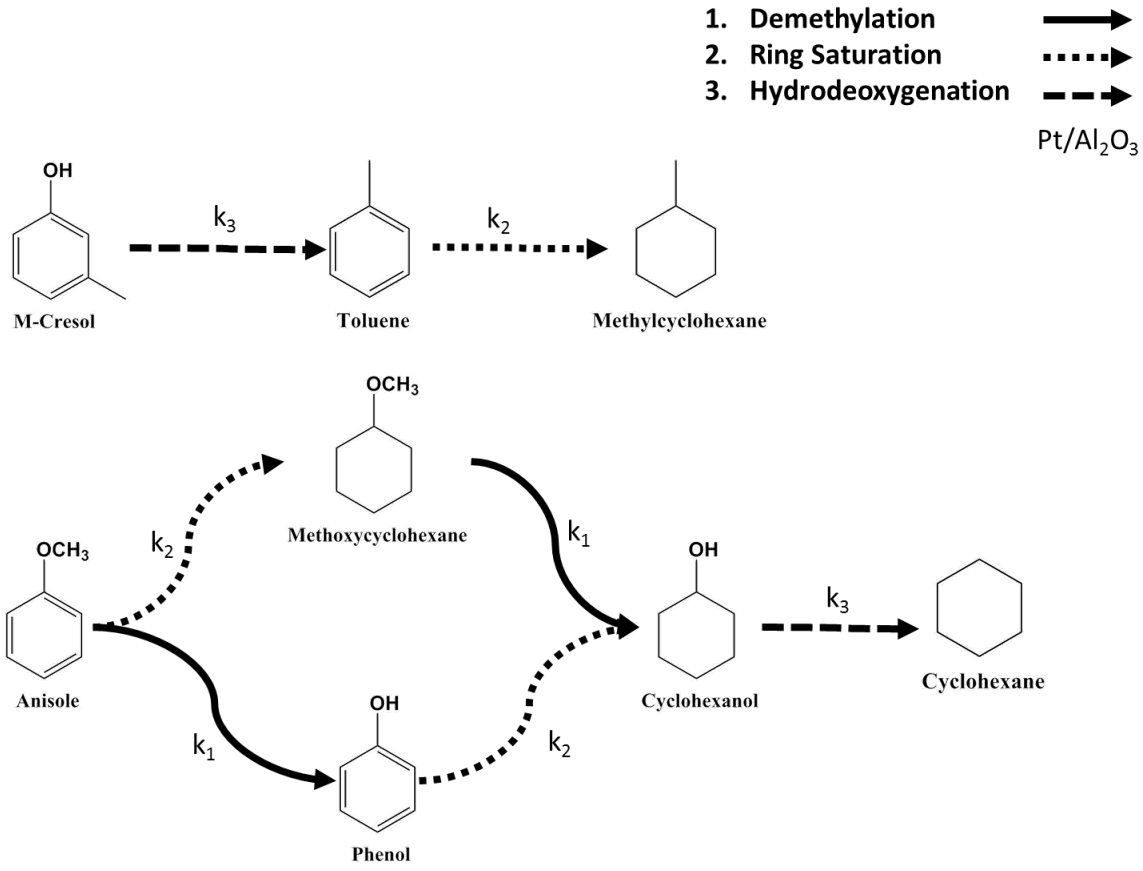

Figure 4-11. Proposed reaction pathways for hydrotreatment of anisole

4.4 Reaction Kinetics & Model

There are two distinct model types in literature for pyrolysis oil hydrotreatment: pseudo-first order and surface adsorption models. While pseudo-first order models are more simplistic, they are typically used to model flow reactors at atmospheric or low pressures.[19, 20] Surface adsorption models are typically used to model batch systems at elevated pressures.[21, 22] However, it should be noted that papers with kinetic models and parameter calculations are extremely limited. The objective of the work here is therefore to test both models for a higher pressure system.

4.4.1. Power Law Model

Using this reaction network, a simple second order surface reaction model was initially proposed. Due to the small particle size of the catalyst (less than 1 micron) and high mixing rates inside the reactor, the catalyst was assumed to be well-dispersed without liquid-to-catalyst surface mass transfer limitations. The correlations for mass transfer across the liquid-to-gas interface in a slurry reactor were taken from Fogler.[23] We also assumed no pore diffusion within the catalyst, $\eta = 1$, with all reactions occurring at the surface. Isothermal and isobaric operation were assumed, since the reactor had a heating jacket and was re-pressurized to compensate for any pressure losses during sampling. Based on these assumptions, transient material balances were developed for each species and in each phase. Samples of these material balances are shown in Equations 2 through 7, with nomenclature outlined in Table 4-1.

$$-\frac{dC_{H2,G}}{dt} - \{k_{La}\}_{H2}\left(H_{H2}C_{H2,G} - C_{H2,L}\right) = 0 \qquad \text{Equation 4-2}$$

$$-\frac{dC_{oil,G}}{dt} + \{k_{La}\}_{oil}\left(C_{H2,L} - H_{oil}C_{oil,G}\right) = 0 \qquad \text{Equation 4-3}$$

$$-\frac{dC_{H2,L}}{dt} + \{k_{La}\}_{H2}\left(H_{H2}C_{H2,G} - C_{H2,L}\right) - \{k_{Sa}\}_{H2}\left(C_{H2,L} - C_{H2,S}\right) = 0 \qquad \text{Equation 4-4}$$

$$-\frac{dC_{oil,L}}{dt} - \{k_{La}\}_{oil}\left(C_{oil,L} - H_{oil}C_{oil,G}\right) - \{k_{Sa}\}_{oil}\left(C_{oil,L} - C_{oil,S}\right) = 0 \qquad \text{Equation 4-5}$$

$$-\frac{dC_{H2,S}}{dt} = \{k_{Sa}\}_{H2}\left(C_{H2,L} - C_{H2,S}\right) - \sum_i \eta k_i C_{H2,S}^{m} C_{oil,S}^{n} \qquad \text{Equation 4-6}$$

$$-\frac{dC_{oil,S}}{dt} = \{k_{Sa}\}_{oil}\left(C_{oil,L} - C_{oil,S}\right) - \sum_i \eta k_i C_{H2,S}^{m} C_{oil,S}^{n} \qquad \text{Equation 4-7}$$

Table 4-1. Nomenclature for Equations 4-2 through 4-7

Nomenclature:

$\{k_La\}_i$	Mass transfer coefficient for gas-liquid (time^{-1})
$\{k_ca\}_i$	Mass transfer coefficient for liquid-surface of the catalyst (time^{-1})
$C_{H2,G}$	Concentration of hydrogen in the gas phase (gmols/volume)
$C_{H2,L}$	Concentration of hydrogen in the liquid phase (gmols/volume)
$C_{H2,S}$	Concentration of hydrogen in the solid phase (gmols/volume)
$C_{oil,L}$	Concentration of bio-oil in the liquid phase (gmols/volume)
$C_{oil,S}$	Concentration of bio-oil in the solid phase (gmols/volume)
H_C	Henry's Law constant, $C^* = C_g / H$ (mole/mole)
k_i	Reaction rate constant (time^{-1})
z	Length of the reactor (length)
m, n	Order of reaction
Q_G	Gas volumetric flow rate (volume/time)

Q_L	Liquid volumetric flow rate (volume/time)
A_c	Column cross sectional area (area)
η	Catalyst effectiveness factor

The reaction network was computationally fitted to the experimental data, and pseudo-first order rate constants (constant H_2 concentration) were generated for each reaction, temperature, and catalyst. These rate constants were graphed as Arrhenius plots, with activation energies and pre-exponential factors calculated for each reaction in the system. The power law model was compared to the data; an example of which is shown in Figure 4-12. While the trends are similar, the statistical fit of the curves was far from satisfactory, with correlation coefficients of only 0.44 to 0.89, and a more realistic model, such as a Langmuir-Hinshelwood model, including competitive adsorption effects might be preferable.

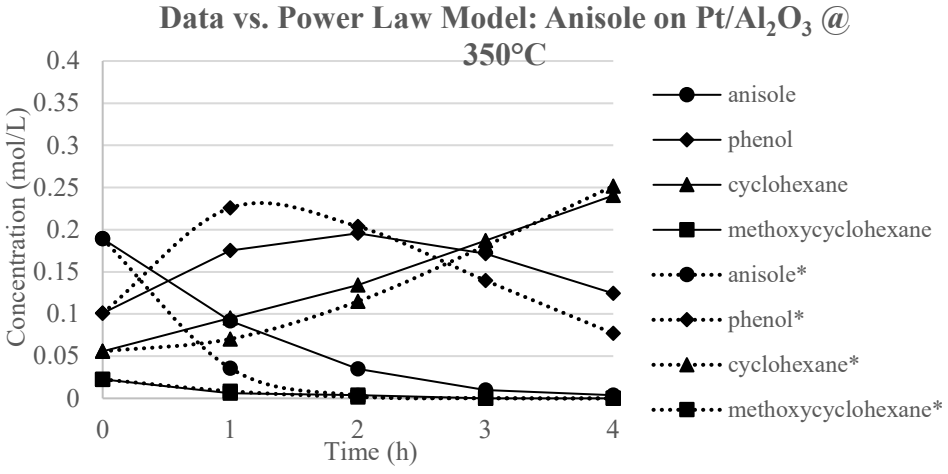

Figure 4-12. Anisole on Pt/Al_2O_3 model (dashed) vs. data (solid) comparison at 350°C for power law kinetic model

4.4.2. Surface Adsorption Kinetic Model

Further data analysis indicated that the data could not be modeled using a simple integral order reaction model, and therefore, a simple Langmuir-Hinshelwood model was created. Retaining the other assumptions from the previous model, a surface adsorption term (K_C for the hydrocarbons was added to account for competition for available surface sites. Material balances were accordingly modified to a Langmuir-Hinshelwood form, as shown in Equation 4-8. It is important to note that the hydrogen concentration is implicitly included in the rate constants, k_i. Since hydrogen was maintained in a large excess in the system and pressure was constant throughout the reaction period, hydrogen concentration is considered constant and can be lumped into the rate constants.

$$-\frac{dC_{oil,S}}{dt} = \{k_{Sa}\}_{oil}\left(C_{oil,L} - C_{oil,S}\right) - \frac{\sum_i \eta k_i C_{H2,S}^m C_{oil,S}^n}{1+\sum K_C C_{oil,S}^n} \qquad \text{Equation 4-8}$$

4.4.3. Coking Analysis

Elemental analysis was performed on three spent Pt/Al_2O_3 catalyst samples from tests run at 350°C, with results shown in Table 4-2. Only small amounts of coke were observed for all of the model compounds; moreover similar amounts were found for the three model compounds. Although some differences were found between the samples,

where phenol had the highest amount present as well as the highest C/H ratio. Based on these results, coking was neglected in the modelling of this system; however, a coking term could be included if necessary.

Table 4-2. Elemental analysis of spent catalyst on three samples from 350°C tests

Spent Catalyst	Carbon (mass %)	Hydrogen (mass %)	C/H ratio
Anisole	1.38	0.36	3.83
m-Cresol	1.48	0.37	4.00
Phenol	1.53	0.36	4.25

4.4.4. Parameter Fitting

This new Langmuir-Hinshelwood model was fitted to the experimental data, and pseudo-first order surface rate constants were calculated and fitted to an Arrhenius plot, with the pre-exponential factors and activation energies determined for each reaction. An Arrhenius plot for anisole over Pt/Al_2O_3 is shown in Figure 4-13, with a summary of the Arrhenius parameters shown in Table 4-3.

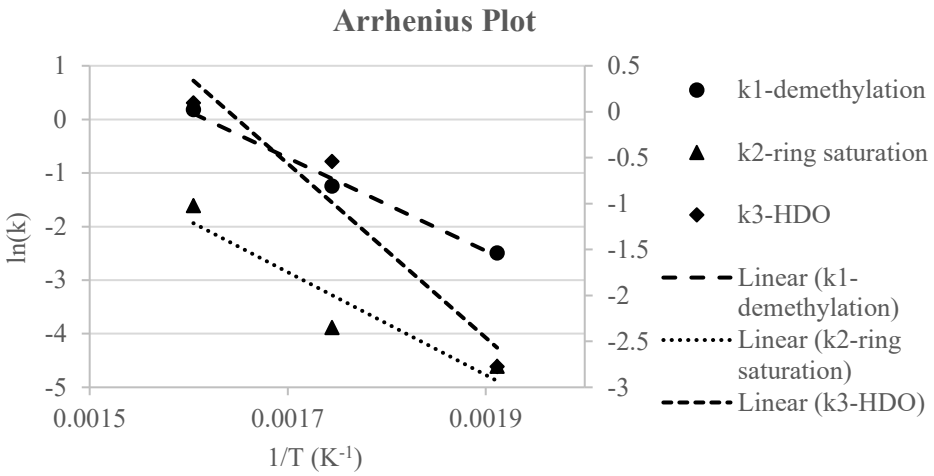

Figure 4-13. Arrhenius plot example for anisole on Pt/Al_2O_3

Table 4-3. Activation energies and pre-exponential factors for hydrotreatment rate constants, k_i

Model Compound	Catalyst	Reaction	Activation Energy (E_A, kJ/mol)	Pre-Exponential Factor (A_0)
Anisole	Pt/Al_2O_3	Demethylation (k_1)	72.14	$1.24x10^6$
Anisole	Pt/Al_2O_3	Ring Saturation (k_2)	79.77	$7.01x10^5$
Anisole	Pt/Al_2O_3	HDO (k_3)	78.79	$5.64x10^6$
M-Cresol	Pt/Al_2O_3	Ring Saturation (k_2)	76.32	$6.9x10^7$
M-Cresol	Pt/Al_2O_3	HDO (k_3)	65.01	$6.07x10^5$
Phenol	Pt/Al_2O_3	Ring Saturation + HDO (k_4)	59.51	$8.58x10^5$

4.4.5. Model Fitting

The model as compared to the experimental data yielded a statistically better fit than the simple power law model, although there are still some deviations at the longest time of four hours. The statistical fit of this model was significantly better than the power law model, with correlation coefficients from 0.80 to 0.98 for every temperature and every model compound. An example of this Langmuir-Hinshelwood model is shown in Equations 4-9 through 4-12 and Figure 4-14 for anisole on Pt/Al_2O_3 at 350°C.

Equation 4-9 (Anisole Concentration over Time)

$$\frac{d}{dt}A(t) = \frac{-(k_1 + k_2)A(t)H(t)}{1 + K_C A(t)}$$

Equation 4-10 (Phenol Concentration over Time)

$$\frac{d}{dt}P(t) = \frac{k_1 A(t)H(t) - k_4 P(t)H(t)}{1 + K_C A(t)}$$

Equation 4-11 (Methoxycyclohexane Concentration over Time)

$$\frac{d}{dt}MOC(t) = \frac{k_2 A(t)H(t) + k_3 MOC(t)H(t)}{1 + K_C A(t)}$$

Equation 4-12 (Cyclohexane Concentration over Time)

$$\frac{d}{dt}C(t) = \frac{k_3 MOC(t)H(t) + k_4 P(t)H(t)}{1 + K_C A(t)}$$

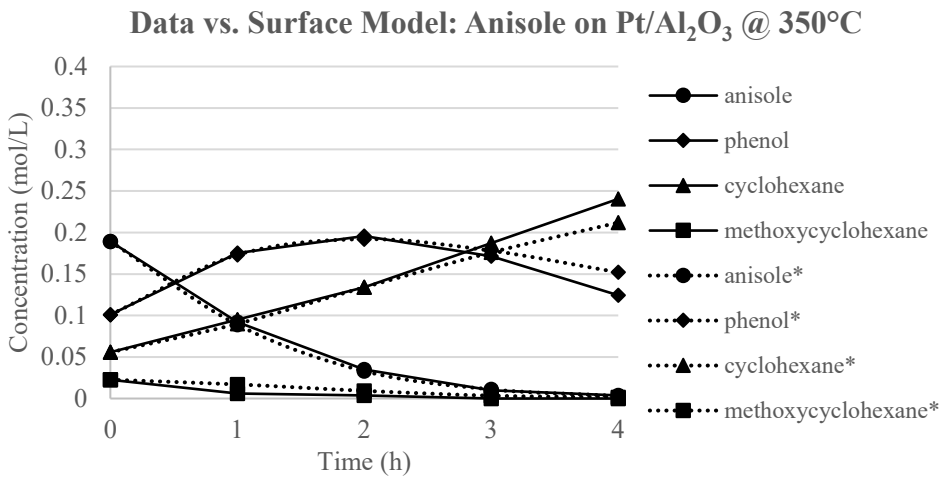

Figure 4-14. Anisole on Pt/Al_2O_3 model (dashed line with * in the legend) vs. data (solid line) comparison at 350°C for surface adsorption kinetic model

Figure 4-15 shows the same model at 300°C. Once again, the overall fit is excellent, but some deviation begins to occur towards the end of the residence time, possibly due to catalyst deactivation or coking of the active sites.

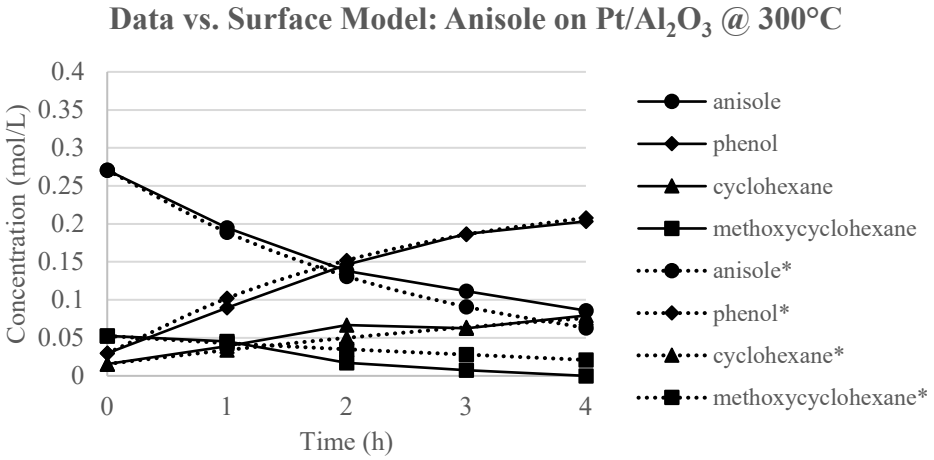

Figure 4-15. Anisole on Pt/Al_2O_3 model (dashed line with * in the legend) vs. data (solid line) comparison at 300°C for surface adsorption kinetic model

Figure 4-16 shows the model comparison to data for m-cresol at 350°C. Unfortunately, the overall fit for m-cresol is not as good as with anisole. The model seems unable to properly capture the initial delay in the reaction and instead smooths the curve for all temperatures with this model compound. However, the model seems able to predict the end behavior of the system, as the final composition at four hours is more accurate than with anisole.

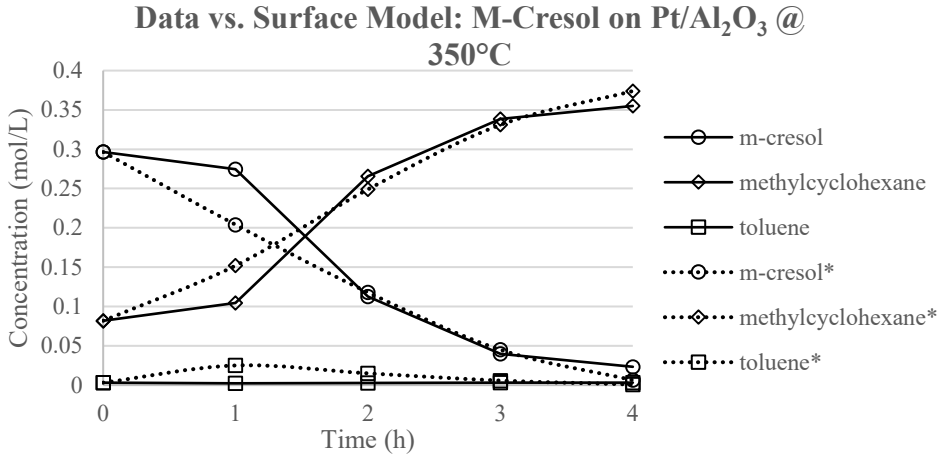

Figure 4-16. M-Cresol on Pt/Al_2O_3 model (dashed line with * in the legend) vs. data (solid line) comparison at 350°C for surface adsorption kinetic model

Figure 4-17 shows the model comparison to data for phenol. Again, there is less data available and the model still seems unable to predict one point of the reaction data, at

three hours in this case. Instead, it smooths the curve to reach a reasonably accurate final product composition.

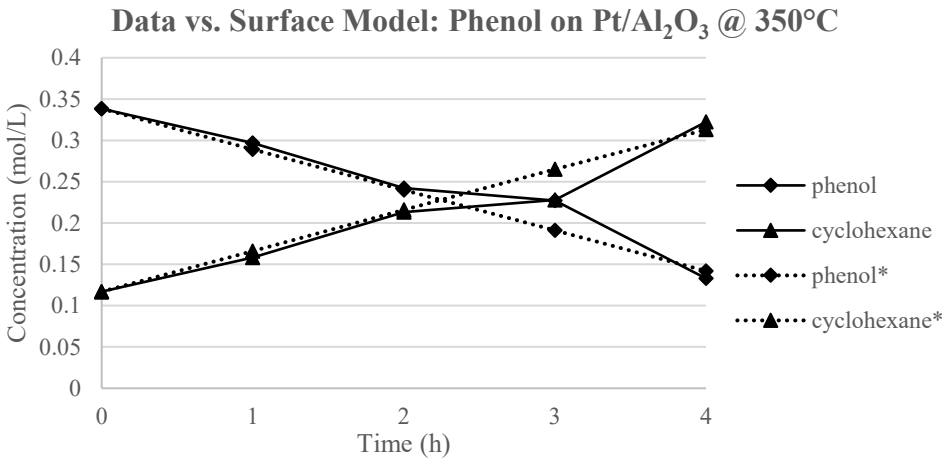

Figure 4-17. Phenol on Pt/Al_2O_3 model (dashed line with * in the legend) vs. data (solid line) comparison at 350°C for surface adsorption kinetic model

4.4.6. Model Validation

Figures 4-18, 4-19, and 4-20 show the same Langmuir-Hinshelwood model compared to separate experimental data sets run at 350°C. In Figure 4-18, the model is fit to another anisole data set. The overall fit at the beginning and the end of the residence time is excellent, except for some deviation at 2 hours. Figure 4-19 shows the model in comparison to m-cresol data from another data set. Once again, the fit is excellent, with slight deviation at the intermediate residence times of one and two hours. Figure 4-20 shows the model for phenol compared to data from another separate run. The model corresponds well with the data, with slight deviation at 1 and 2 hours residence time, but

an excellent fit for the final concentration. Any deviation is caused by the way the model smooths the concentration curve over the total residence time to achieve the final product composition.

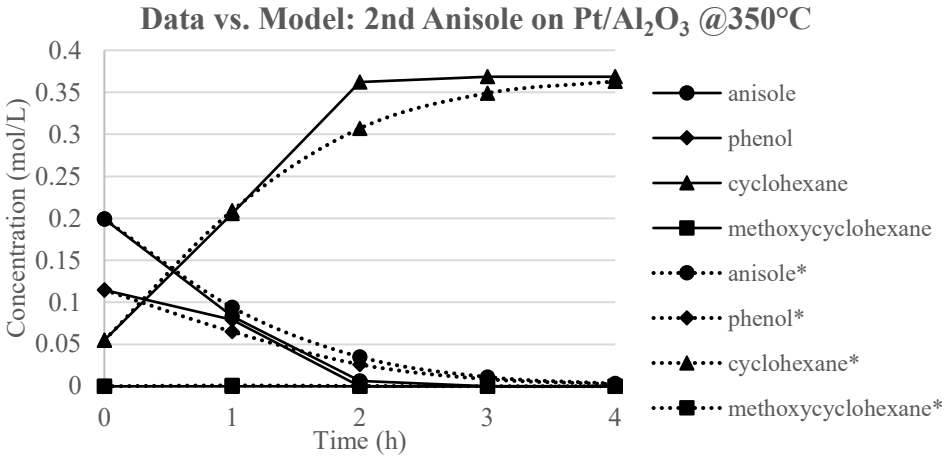

Figure 4-18. Anisole on Pt/Al_2O_3 model (dashed line with * in the legend) vs. data (solid line) comparison with new data set at 350°C for surface adsorption kinetic model

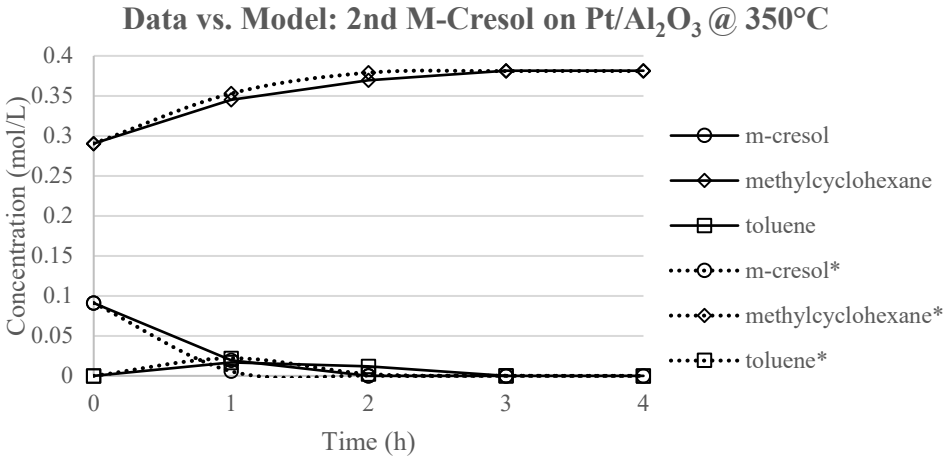

Figure 4-19. M-Cresol on Pt/Al_2O_3 model (dashed line with * in the legend) vs. data (solid line) comparison with new data set at 350°C for surface adsorption kinetic model

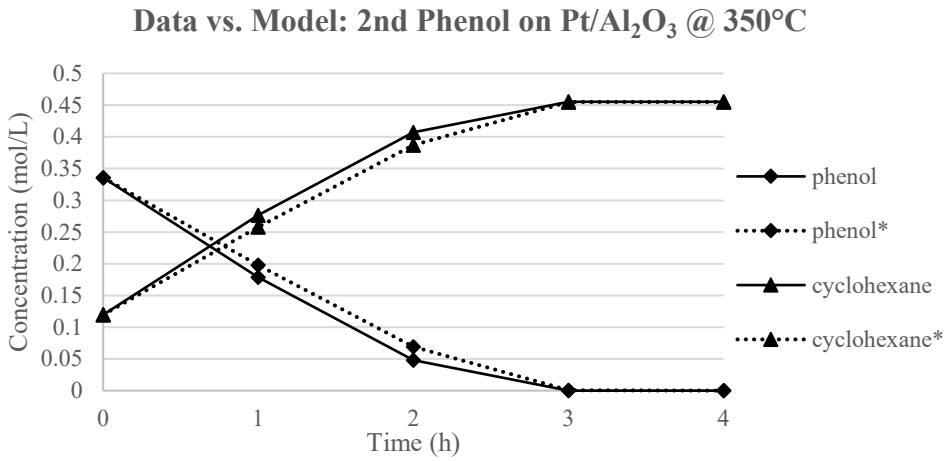

Figure 4-20. Phenol on Pt/Al_2O_3 model (dashed line with * in the legend) vs. data (solid line) comparison at 350°C for surface adsorption kinetic model

The model was also tested against the blended experimental data. The adsorption coefficients were combined into the model using Equation 4-13. Unfortunately, the model did not fit the data well. The correlation coefficients for the anisole and m-cresol blend were between 0.43 and 0.79. The correlation coefficients for the anisole and phenol blend were between 0.48 and 0.71. Clearly, there are other factors that need to be included in the model, such as coking or secondary reactions. The anisole and m-cresol blend, for example, only had methylcyclohexane in the product, even though there is demethylation observed in the reactor.

Equation 4-13 (Generic Equation for C_I)

$$\frac{dC_I}{dt} = \frac{k_1 C_{H2} C_I}{1 + K_I C_I + K_{II} C_{II}}$$

4.5 Conclusions

Pyrolysis oil model compounds were hydrotreated in a Parr batch reactor over Pt/Al_2O_3 and Pd/C catalysts. Three compounds with representative functional groups for the lignin-based fraction of pyrolysis oil were used: anisole, m-cresol, and phenol. Reactor temperatures (250-350°C) and a pressure (50 bar) similar to those in industrial processing were used. A residence time of 4 hours was sufficient to obtain high yields of deoxygenated products. The Pt/Al_2O_3 catalyst promoted two basic reactions: hydrogenation (ring saturation) and removal of the pendant groups. For anisole, the pathway shifted from a ring saturation reaction at the lowest temperature to demethylation at the highest temperatures, although the ultimate product was cyclohexane for both. For m-cresol, an initial hydrodeoxygenation reaction was followed almost immediately by ring saturation to methylcyclohexane. With phenol, cyclohexane is the principle product, indicating ring saturation and hydrodeoxygenation, possibly via a cyclohexanol intermediate (not observed). Tests with anisole conducted over less catalyst led to lower conversions. Analysis of the liquid-to-catalyst surface mass transfer indicated that it could affect the reaction rate, while the gas-to-liquid interface mass transfer was negligible. The mass transfer coefficients for gas-to-liquid and liquid-to-catalyst are included in the kinetic model. The Pd/C catalyst HDO tests with anisole

primarily showed ring saturation, with no deoxygenation occurring until after the aromatic ring was fully saturated. Two blends of the model compounds (anisole/m-cresol and anisole/phenol) were tested over Pt/Al_2O_3 to investigate competitive adsorption or other interactions. While no new reactions were observed, some competition for surface sites was reflected in the absorption term of the LH model. The weak interaction between model compounds provides evidence that the lumped parameter approach is appropriate for the pyrolysis oil hydrotreatment model.

The initial model applied a simple second order power law to the data, but the fit was unsatisfactory. It was determined that this was due to competitive surface adsorption effects on the reaction rate, therefore, a simple Langmuir-Hinshelwood model with adsorption terms for the hydrocarbons was used to more accurately represent the data. Arrhenius parameters and activation energies for the reaction rate constants and adsorption constants were fit to the data for each compound. The activation energies ranged from 50 to 80 kJ/mol for the HDO reactions. The model was subsequently validated using an independent data set and fit the data well, with correlation coefficients from 0.80 to 0.98 for all model compounds and all temperatures. This simple Langmuir-Hinshelwood model can represent the kinetics for hydrotreatment of pyrolysis model compounds over Pt/Al_2O_3 as a function of inlet composition and process conditions. The model's ability to predict shifts in the reaction pathway is crucial for optimizing process conditions for a desired product composition and for analyzing the associated energy and hydrogen consumption. The model can be used to assess processing conditions and

catalysts for scale-up, and to aid in life cycle assessment. An accurate techno-economic assessment for a given pyrolysis oil feedstock to produce a desired reactor product composition requires a process-level reactor model of the type developed here.

4.6 References

[1] Bridgwater and G. Peacocke, "Fast pyrolysis processes for biomass," Renewable and Sustainable Energy Reviews, vol. 4, pp. 1-73, 2000.

[2] G. W. Huber, S. Iborra, and A. Corma, "Synthesis of transportation fuels from biomass: chemistry, catalysts, and engineering," Chemical Reviews, vol. 106, pp. 4044-4098, 2006.

[3] Bridgwater, Anthony V. "Review of fast pyrolysis of biomass and product upgrading." Biomass and bioenergy 38 (2012): 68-94.

[4] E. Furimsky, "Hydroprocessing challenges in biofuels production," Catalysis Today, 2013.

[5] J. Adjaye and N. Bakhshi, "Catalytic conversion of a biomass-derived oil to fuels and chemicals I: model compound studies and reaction pathways," Biomass and Bioenergy, vol. 8, pp. 131-149, 1995.

[6] Evans, R. J. and T. A. Milne (1987). "Molecular characterization of the pyrolysis of biomass." Energy & Fuels 1(2): 123-137.

[7] Zhang, Qi, et al. "Review of biomass pyrolysis oil properties and upgrading research." Energy conversion and management 48.1 (2007): 87-92.

[8] Elliott, D. C. (2007). "Historical developments in hydroprocessing bio-oils." Energy & Fuels 21(3): 1792-1815.

[9] Asphaug, S., Catalytic Hydrodeoxygenation of Bio-oils with Supported MoP-Catalysts. 2013.

[10]

[11] Furimsky, E. (2000). "Catalytic hydrodeoxygenation." Applied Catalysis A: General 199(2): 147-190.

[12] Kalnes, T., T. Marker, and D.R. Shonnard, Green diesel: a second generation biofuel. International Journal of Chemical Reactor Engineering, 2007. 5(1).

[13] Mortensen, P. M., et al. (2011). "A review of catalytic upgrading of bio-oil to engine fuels." Applied Catalysis A: General 407(1–2): 1-19.

[14] L. Funkenbusch and M. Mullins, "Modeling Differential Catalytic Hydrotreatment of Surrogate Compounds for Pyrolysis Oil (2016 Annual Meeting)," in American Institute of Chemical Engineers, 2016. [Online]. Available: https://aiche.confex.com/aiche/2016/webprogram/Paper460758.html.

[15] Yang, H., et al. (2007). "Characteristics of hemicellulose, cellulose and lignin pyrolysis." Fuel 86(12): 1781-1788.

[16] S. J. Hurff and M. T. Klein, "Reaction pathway analysis of thermal and catalytic lignin fragmentation by use of model compounds," Industrial & engineering chemistry fundamentals, vol. 22, pp. 426-430, 1983.

[17] Schildhauer, T., E. Newson, and S. Müller, The equilibrium constant for the methylcyclohexane–toluene system. Journal of Catalysis, 2001. 198(2): p. 355-358.

[18] Y. Yang, H. a. Luo, G. Tong, K. J. Smith, and C. T. Tye, "Hydrodeoxygenation of Phenolic Model Compounds over MoS_2 Catalysts with

Different Structures," Chinese Journal of Chemical Engineering, vol. 16, pp. 733-739, 2008.

[19] E.-M. Ryymin, M. L. Honkela, T.-R. Viljava, and A. O. I. Krause, "Competitive reactions and mechanisms in the simultaneous HDO of phenol and methyl heptanoate over sulphided NiMo/γ-Al_2O_3," Applied Catalysis A: General, vol. 389, pp. 114-121, 2010.

[20] T. Nimmanwudipong, R. C. Runnebaum, S. E. Ebeler, D. E. Block, and B. C. Gates, "Upgrading of Lignin-Derived Compounds: Reactions of Eugenol Catalyzed by HY Zeolite and by Pt/γ-Al2O3," Catalysis letters, vol. 142, pp. 151-160, 2012.

[21] R. C. Runnebaum, R. J. Lobo-Lapidus, T. Nimmanwudipong, D. E. Block, and B. C. Gates, "Conversion of anisole catalyzed by platinum supported on alumina: The reaction network," Energy & fuels, vol. 25, pp. 4776-4785, 2011.

[22] Centeno, E. Laurent, and B. Delmon, "Influence of the Support of CoMo Sulfide Catalysts and of the Addition of Potassium and Platinum on the Catalytic Performances for the Hydrodeoxygenation of Carbonyl, Carboxyl, and Guaiacol-Type Molecules," Journal of Catalysis, vol. 154, pp. 288-298, 7// 1995.

[23] Gevert, J. Otterstedt, and F. Massoth, "Kinetics of the HDO of methyl-substituted phenols," Applied catalysis, vol. 31, pp. 119-131, 1987.

[24] Fogler, H.S., Elements of Chemical Reaction Engineering. 1992: Prentice-Hall.

5. Catalytic Hydrotreatment of Pyrolysis Oil Model Compounds over Pt/Al_2O_3 and Pd/C Part II: Continuous Reactors[3]

5.1 Introduction

Recently, substantial effort has been dedicated to biomass conversion research.[1] Biomass is an appealing alternative source for petroleum-based fuels and products, since it can be grown on a renewable time scale and is theoretically carbon-neutral. Pyrolysis oil, generated from woody biomass, is a complex mixture of oxygenated hydrocarbons.[2] Composition can vary, depending on source and processing methods, however, pyrolysis oil is generally composed of water, furans, phenolics, and other organic compounds.[3] Due to the high level of oxygenation (up to 40%) and high water content, crude pyrolysis oil tends to be highly corrosive, has low heating values when compared to traditional petroleum-based fuels, and is incompatible with existing infrastructure.[4,5,6,7] The petroleum industry experiences comparable contamination issues with crude oil, which can contain heavy metals, sulfur, nitrogen, and even some oxygen. Petroleum refineries catalytically hydrotreat their crude feed, typically using sulfided nickel/molybdenum (NiMo) or cobalt/molybdenum (CoMo) catalysts.[8] Catalytic hydrotreatment can also be used to treat pyrolysis oil and produce a

[3] This article is in preparation for submission to Industrial & Engineering Chemistry Research.

hydrocarbon mixture similar to gasoline that can be used as “drop-in” transportation fuel.[9]

Although the hydrotreatment step is the most costly, it is also the most poorly understood, in terms of its environmental and economic impacts.[10] Based on the literature, there is little data available on reaction kinetics of this process that would permit proper life cycle assessment (LCA) or techno-economic assessment (TEA).[11,12] Instead, such assessments must rely on proprietary data from industry sources or make broad, stoichiometric assumptions without considering specific process conditions and resulting pathway selectivities. However, once suitable experimental data has been collected and the reaction kinetics are properly understood, a kinetic model that can generate process-level details for simpler assessment and scaling of the process.

In this study, a lumped parameter model is used, which combines reaction pathways and/or reactants together. This approach has also been taken by the petroleum industry, where crude oil composition can include hundreds of components and vary drastically based on its source. Generating reaction data for each possible compound and accounting for all of their interactions is impractical, and the lumped parameter approach can streamline modeling to a more reasonable number of parameters. By focusing only on observed products and not hypothetical intermediates, the modeling can be further simplified, and experimental data can be collected to properly construct a reaction network and kinetic model. In this study, reaction pathways for pyrolysis oil model

compounds were studied in a continuous packed bed reactor over both Pd/C and Pt/Al_2O_3. Reactor temperature, catalyst, and residence time were varied, and kinetic rate constants were determined for each lumped reaction. This model is able to take a given feed composition and reactor conditions and accurately predict final product composition, yields and selectivities, optimal catalyst for a particular feed or product, and energy/hydrogen input required for input into an LCA or TEA.

5.2 Materials & Methods

The commercial catalysts, all model compounds, and analytical standards were obtained from Alfa Aesar or Sigma Aldrich. The differential reactor was a packed bed continuous reactor, constructed using a custom HPLC pump (Supercritical Fluid Technologies), two mass flow controllers (Omega), a tube furnace (Thermolyne), a coil condenser with a cold water shell constructed by the department machinist, and a back-pressure regulator (Novaspect). The reactor bed was ½" O.D. stainless steel. The tubing throughout the rest of the system was ¼" O.D. stainless steel. A simplified diagram is shown in Figure 5-1.

Prior to each test, 5% molar solutions of the model compound in dodecane were measured out. Anisole, guaiacol, m-cresol, and phenol were selected as model compounds for the lignin fraction of pyrolysis oil. They offer a range of functional groups commonly found in pyrolysis oil, and have the aromatic ring structure that is common among lignin-based compounds, as discussed in the previous part of this study. Guaiacol was chosen to supplement the suite of compounds for the second part of this

study for its dual oxygenated groups. Dodecane was used as a fully saturated, inert solvent to maintain control of the reactions. Two noble metal catalysts were tested: palladium on carbon (Pd/C) and platinum on alumina (Pt/Al_2O_3), both with 5% metal loading and 1 micron particle diameter. 500 mg of catalyst was loaded into the reactor with plugs of glass wool to hold the catalyst bed in place. The reactor was maintained at 100 psi (6.7 bar), with 5% hydrogen in argon gas at 0.5 L/min, and 250, 300 or 350°C. Once the system reached steady state, the liquid feed was pumped into the system at 0.5 mL/min. This resulted in a liquid contact time of 10 seconds for the bench-scale reactor. The liquid product was collected at the end, while any excess gas and gaseous byproducts were vented through the hood. Liquid samples were analyzed using a GC/MS (Thermo Scientific) and a GC/FID (HP).

The pilot reactor bed was 1" O.D. (0.8" I.D.) Inconel alloy. A diagram of both reactors can be seen in Figure 1. For the pilot tests, a catalyst bed made from stainless steel tubing and mesh was inserted into the reactor and held 4.65 g of the synthesized catalyst. A liquid contact time of 30 seconds was established for the pilot-scale reactor. The materials for catalyst synthesis were also acquired from Sigma. The synthesized catalyst was generated using the incipient wetness impregnation method, where hexachloroplatinic acid in water was dripped into a bed of activated alumina pellets (Alcoa, 10-25 mesh). The catalyst was dried in a muffle furnace at 95°C for 12 hours before being calcined at 550°C for 2 hours. The catalyst was then cooled, and the process repeated until the catalyst stopped absorbing platinum solution. The resulting

catalyst was then reduced in the reactor catalyst bed for 6 hours at 500°C under hydrogen. This process yielded a granular Pt/Al_2O_3 catalyst with a metal loading of 4.95%

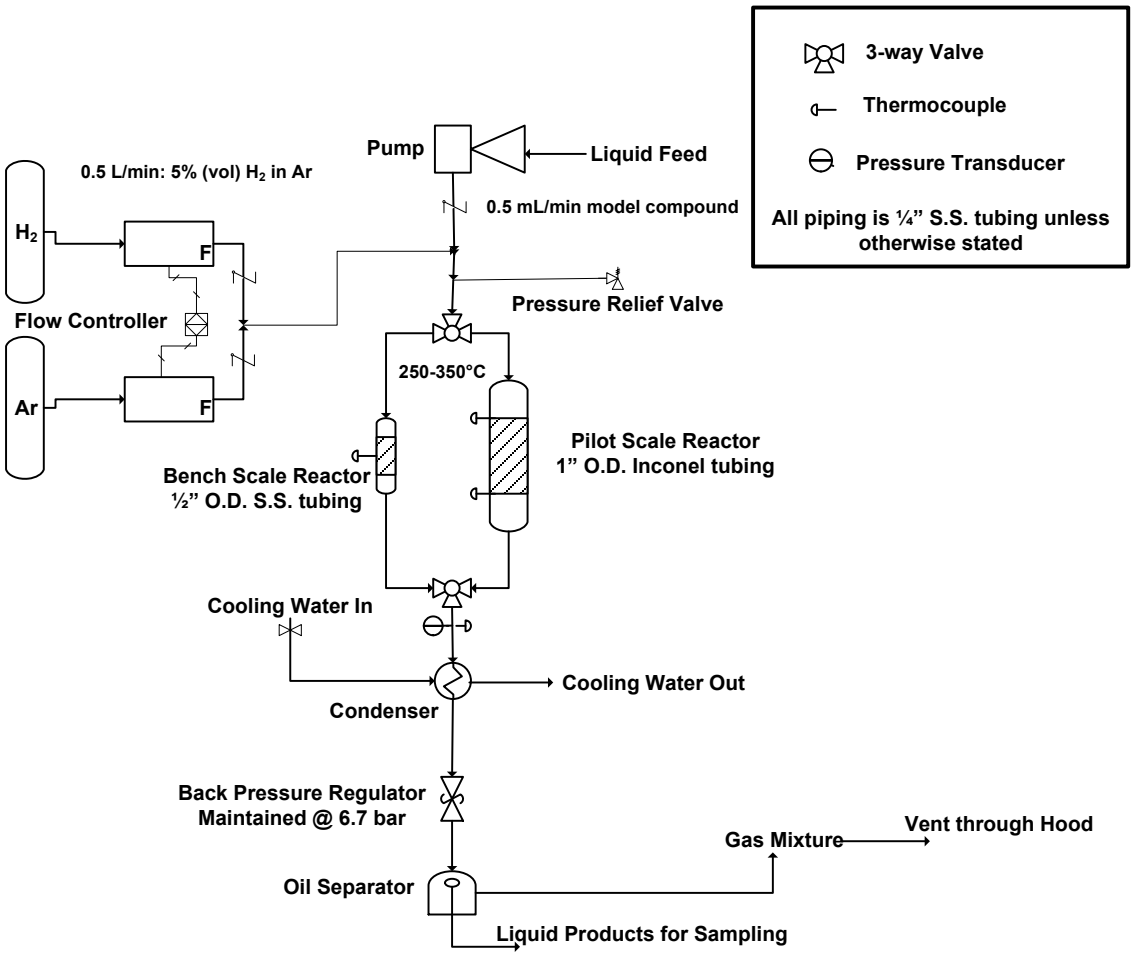

Figure 5-1. Differential Reactor and Pilot-Scale Packed Bed Reactor Diagram

5.3 Results

5.3.1. Differential Reactor Experiments

For the anisole differential reactor tests with Pd/C, conversion of anisole rose with increasing temperature, from 34% at 250°C to 61% at 350°C. Due to the short residence time, however, only an initial ring saturation reaction of anisole to methoxycyclohexane was observed. With Pt/Al_2O_3, overall conversion of anisole was significantly lower, ranging from 3% at 250°C up to 7% at 350°C. However, the reaction pathway was the same, with a ring saturation reaction to methoxycyclohexane.

With guaiacol in the bench-scale reactor, conversion over Pd/C went from 12% at 250°C to 56% at 350°C. Again, deoxygenation was not complete by the end; only partial deoxygenation of guaiacol to phenol was observed. However, it should be noted that, unlike with the other model compounds, guaiacol has two oxygenated groups attached to the ring. This seems to cause guaiacol to lose its methoxyl group, instead of undergoing a ring saturation reaction like the other model compounds with only one oxygenated group attached to the ring. For the experiments run over Pt/Al_2O_3, conversion was only slightly lower than with the Pd/C tests, ranging from 6% at 250°C up to 48% at 350°C. The same reaction pathway leading to phenol was observed.

As with anisole, the Pd/C bench-scale reactor tests with m-cresol yielded only the ring saturation reaction to convert m-cresol to methylcyclohexanol. At 250°C, conversion of m-cresol was 29%; at 350°C, it reached 59%. For Pt/Al_2O_3, a different reaction pathway was observed - a demethylation reaction to phenol, rather than a ring saturation to

methylcyclohexanol. However, the reaction seemed to be suppressed until 350°C. Conversion jumped from 3% at 250°C to 46% at 350°C.

The Pd/C bench-scale reactor tests using phenol yielded ring saturation reactions to cyclohexanol. Conversions for phenol were much lower than for the other model compounds, ranging from 10% at 250°C up to 30% at 350°C. With Pt/Al_2O_3, once again, phenol conversion was lower than other model compounds, and lower than with Pd/C. The same ring saturation reaction pathway was observed, however. Conversion to cyclohexanol ranged from 2% at 250°C up to 7% at 350°C.

Using the bench-scale experimental results, a preliminary reaction network was hypothesized. The only difference seen between the two catalysts was with m-cresol, all other model compounds yielded the same pathway for both catalysts. This network is only based on observed compounds, with no hypothetical intermediates included, and takes a lumped parameter approach.

5.3.2. Pilot-Scale Experiments

Based on the bench-scale reactor results discussed earlier, only Pt/Al_2O_3 was selected for synthesis and further testing in the pilot-scale reactor. The extra cracking functionality is desirable for deoxygenating phenolic compounds. A Pt/Al_2O_3 catalyst with 5% metal loading was synthesized, as discussed earlier. These results will be used to test the kinetic model and rate constants generated from the differential reactor tests.

Anisole initially reacted to form phenol via a demethylation reaction, followed by a ring saturation and hydrodeoxygenation reaction to cyclohexane. Cyclohexanol or any other intermediates were not observed. Conversion started at 74% at 250°C and increased to 97% at 350°C. It is interesting, however, to see that there was no methoxycyclohexane observed, indicating a different reaction pathway. This may be a function of the longer residence time in the reactor.

For guaiacol, conversion is quite low, perhaps due to the double oxygenated group, ranging from 17% at 250°C to 28% at 350°C. Guaiacol follows the route seen with the bench-scale reactor, with an initial methanol abstraction reaction to phenol, and a subsequent ring saturation and hydrodeoxygenation reaction to cyclohexane. Again, no cyclohexanol or other intermediate is seen between phenol and cyclohexane.

With m-cresol in the pilot reactor, conversion was high, ranging from 30% at 250°C to 94.5% at 350°C. The same reaction pathway was seen as with the Pt/Al_2O_3 differential reactor experiments with an initial demethylation reaction to phenol. However, in the pilot reactor, the reaction pathway achieved full deoxygenation with conversion of phenol to cyclohexane. Once again, no intermediates between phenol and cyclohexane were seen.

Based on the results for guaiacol and m-cresol, compounds with two pendant groups do not undergo ring saturation until one of the pendant groups has been removed with a Pt/Al_2O_3 catalysts. The Pd/C in the differential reactor, however, exhibited a ring saturation functionality for m-cresol. This indicates that the forced removal of a pendant group prior to ring saturation is due to the alumina functionality.

For phenol, conversion remained at roughly 50% across all temperatures, ranging from 49% at 250°C to 52% at 350°C. Phenol converts directly to cyclohexane, with no observed intermediates. As with the bench-scale tests, phenol has a lower conversion than the other model compounds. All of the model compounds seem to follow the same pathway through phenol as a reaction intermediate in the pilot scale reactor, followed by ring saturation and hydrodeoyxgenation to cyclohexane.

Based on only observed compounds in the data from both sets of experiments, a reaction network was hypothesized, as shown in Figure 5-2. Compounds noted with an asterisk are intermediates observed in the differential reactor but not the pilot reactor.

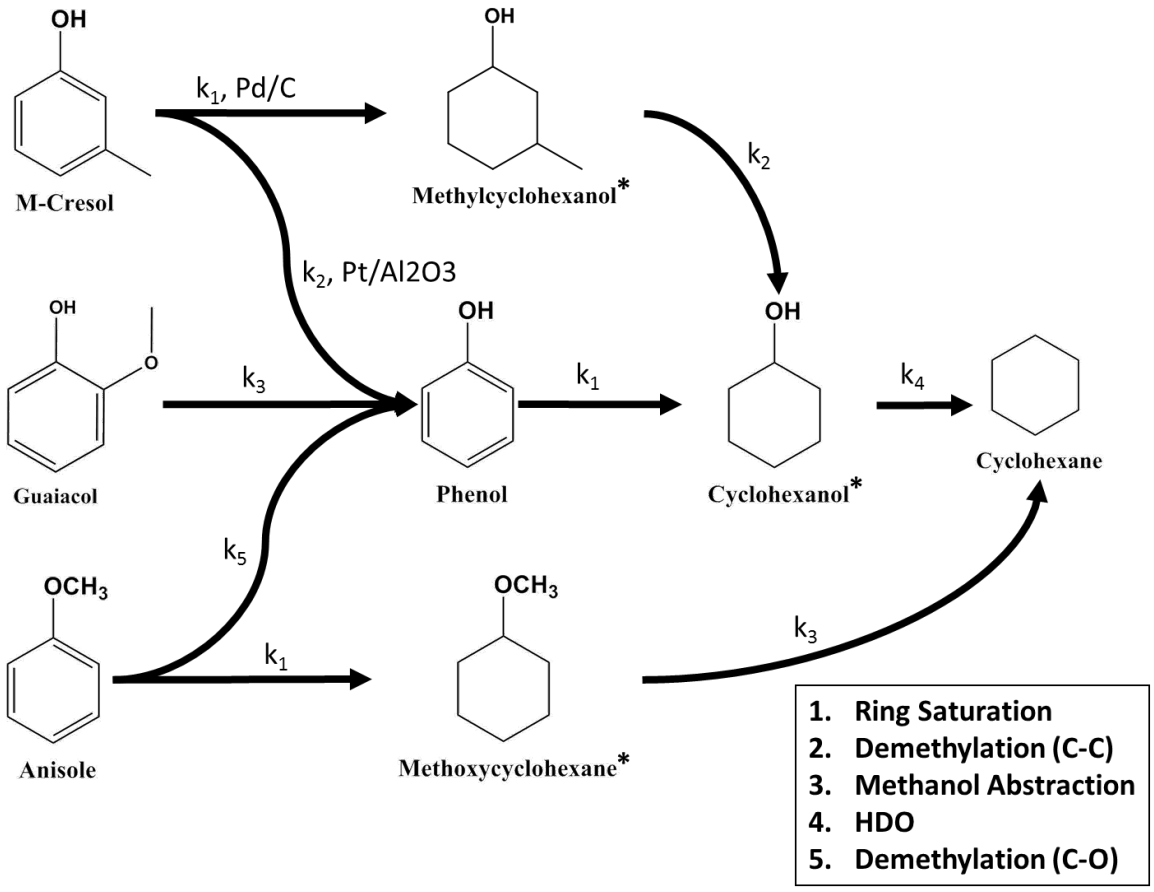

Figure 5-2. Lumped Reaction Network

5.4 Reaction Kinetics & Model

5.4.1. Model Assumptions

Based on the reaction network shown in Figure 5-2, the Langmuir-Hinshelwood kinetic model developed in the previous part of this study was adapted for this system.[13] The catalyst was assumed to be uniformly coated. Liquid-gas interface mass transfer correlations and internal pore diffusion factors were adapted from Fogler and Kindt.[14,15] Isothermal and isobaric operation were assumed inside the reactor bed. Differential

material balances were performed on each of the species, as shown in Equations 5-1 through 5-6. Nomenclature is shown in Table 5-1.

$$-\frac{dC_{H2,G}}{d\tau} - \{k_{La}\}_{H2}\left(H_{H2}C_{H2,G} - C_{H2,L}\right) = 0 \qquad \text{Equation 5-1}$$

$$-\frac{dC_{oil,G}}{d\tau} + \{k_{La}\}_{oil}\left(C_{H2,L} - H_{oil}C_{oil,G}\right) = 0 \qquad \text{Equation 5-2}$$

$$-\frac{dC_{H2,L}}{d\tau} + \{k_{La}\}_{H2}\left(H_{H2}C_{H2,G} - C_{H2,L}\right) - \{k_{Sa}\}_{H2}\left(C_{H2,L} - C_{H2,S}\right) = 0 \qquad \text{Equation 5-3}$$

$$-\frac{dC_{oil,L}}{d\tau} - \{k_{La}\}_{oil}\left(C_{oil,L} - H_{oil}C_{oil,G}\right) - \{k_{Sa}\}_{oil}\left(C_{oil,L} - C_{oil,S}\right) = 0 \qquad \text{Equation 5-4}$$

$$-\frac{dC_{H2,S}}{d\tau} = \{k_{Sa}\}_{H2}\left(C_{H2,L} - C_{H2,S}\right) - \frac{\sum_i \eta k_i C_{H2,S}^m C_{oil,S}^n}{1+\sum K_C C_{oil,S}^n} \qquad \text{Equation 5-5}$$

$$-\frac{dC_{oil,S}}{d\tau} = \{k_{Sa}\}_{oil}\left(C_{oil,L} - C_{oil,S}\right) - \frac{\sum_i \eta k_i C_{H2,S}^m C_{oil,S}^n}{1+\sum K_C C_{oil,S}^n} \qquad \text{Equation 5-6}$$

Table 5-1. Nomenclature for Equations 5-1 through 5-6

Nomenclature:

$\{k_La\}_i$	Mass transfer coefficient for gas-liquid interface (time^{-1})
$\{k_ca\}_i$	Mass transfer coefficient for liquid-surface of the catalyst (time^{-1})
$C_{H2,G}$	Concentration of hydrogen in the gas phase (gmols/volume)
$C_{H2,L}$	Concentration of hydrogen in the liquid phase (gmols/volume)
$C_{H2,S}$	Concentration of hydrogen in the solid phase (gmols/volume)
$C_{oil,L}$	Concentration of bio-oil in the liquid phase (gmols/volume)

$C_{oil,S}$	Concentration of bio-oil in the solid phase (gmols/volume)
H_C	Henry's Law constant, $C^* = C_g / H$ (mole/mole)
k_i	Reaction rate constant ($time^{-1}$)
K_C	Surface adsorption constant
τ	Residence time (time)
m, n	Order of reaction
Q_G	Gas volumetric flow rate (volume/time)
Q_L	Liquid volumetric flow rate (volume/time)
A_c	Column cross sectional area (area)
η	Catalyst effectiveness factor

5.4.2. Rate Kinetics

Because different catalysts were used, kinetic rate data for each reactor needed to be fit to the model. For the differential reactor, intrinsic activation energies and pre-exponential factors were calculated and are shown in Table 5-2. For the pilot-scale reactor, apparent activation energies and pre-exponential factors were found and are shown in Table 5-3. Because two different catalysts were used, some differences in their functionality and activity was expected. While both are bifunctional catalysts, the pilot-scale reactor had a more active alumina substrate, whereas the differential reactor was more strongly affected by the platinum loading. The alumina support of the pilot-scale catalyst is highly activated alumina, and this causes a change in the dominant functionality which can be seen in the spontaneous shift from phenol to cyclohexane, with no intermediates observed. The activated nature of the support may also lower the activation energies of certain reactions in the pilot-scale reactor. The size of the catalyst

(powder vs. pellet) also affects mass transfer within the reactor bed, and can affect reaction rates. The powdered catalyst used in the differential reactor was chosen to eliminate internal mass transfer limitations and minimize external mass transfer limitations. This, along with the low conversions targeted by tuning the residence time, allowed the determination of intrinsic reaction rates and intrinsic activation energies. The small particle size also presented the platinum hydrogenation as the dominant functionality. On the other hand, the pellet catalyst used in the pilot scale reactor presents both internal and external mass transfer limitations. As a result, only apparent activation energies can be calculated, which are lower than the intrinsic activation energies.

Table 5-2. Intrinsic activation energies and pre-exponential factors for hydrotreatment in the differential reactor

Catalyst	Reaction	Activation Energy (E_A)	Pre-exponential factor (A_0)
Pt/Al_2O_3	Ring Saturation	37.1 kJ/mol	8.5×10^1
Pt/Al_2O_3	Methanol Abstraction	71.7 kJ/mol	7.8×10^5
Pt/Al_2O_3	Demethylation	91.7 kJ/mol	4.6×10^7

Table 5-3. Apparent activation energies and pre-exponential factors for hydrotreatment in the pilot-scale reactor

Catalyst	Reaction	Activation Energy (E_A)	Pre-exponential factor (A_0)
Pt/Al_2O_3	Demethylation	64.9 kJ/mol	4.2×10^4
Pt/Al_2O_3	Ring Sat. & HDO	43.4 kJ/mol	3.2×10^5
Pt/Al_2O_3	Methanol Abstraction	51.9 kJ/mol	8.3×10^1

5.4.3. Model Comparison to Results

The differential reactor kinetics were used to model the differential reactor, and the pilot reactor kinetics were used to model the pilot-scale reactor. The differential reactor model results are shown in Table 5-4 and the pilot-scale model results are shown in Table 5-5, and all conversions are matched within 1% accuracy. This indicates that the process-level, LH model discussed in the previous study and this study are valid, when using the kinetic data for the relevant catalyst and reactor conditions.

Table 5-4. Data vs. Model Comparison for Conversion of Anisole on Pt/Al_2O_3 in Differential Reactor

Temperature	Data	Model
250°C	3.2%	3.8%
300°C	4.8%	5.3%
350°C	6.7%	7.1%

Table 5-5. Data vs. Model Comparison for Conversion of Anisole on Pt/Al_2O_3 in Pilot Reactor

Temperature	Data	Model
250°C	74.2%	75.1%
300°C	91.1%	91.6%
350°C	96.9%	96.8%

5.5 Conclusions

In the previous part of this study, a batch reactor was used to hydrotreat pyrolysis oil model compounds. Here, a continuous packed bed reactor was designed to model a reactor similar to what is used in industry. Initially, a differential reactor was constructed to investigate the intrinsic reaction kinetics of the system; this reactor was deliberately designed to achieve low conversions. Four model compounds were used in this study: anisole, m-cresol, phenol, and guaiacol. Guaiacol was added to the previous batch reactor set to explore the effects of two oxygenated groups on the aromatic ring. Two different catalysts were tested over three different temperatures: Pd/C, a simple noble metal catalyst, and Pt/Al_2O_3, a noble metal catalyst with an acidic support. The reactor bed was scaled up to pilot scale, with high conversions and catalyst with a pellet support instead of a powdered substrate, and a similar suite of experiments were run to generate kinetic data for a different catalyst and set of reactor conditions. The pilot-scale reactor targeted higher conversions using the same process conditions as the differential reactor in a larger reactor bed and with more catalyst. Each set of experiments were fit to the LH model developed in the previous study, and then the models were compared to the pertinent reactor.[13] The model provided an excellent fit (within 1%) to the data for both reactors. However, in order to use this process-level model, appropriate rate information must be taken for the specific catalyst and reactor conditions. The model can then be used to estimate final product composition, hydrogen consumption, and heating/cooling requirements for the reactor given an initial feedstock and a small number of preliminary tests with the catalyst and reactor conditions. This type of model is useful in rapidly assessing processing conditions and catalysts prior to an expensive scale-up and to aid in

life cycle and techno-economic assessments, which require process-level models in order to properly analyze a given feedstock or process.

5.6 References

[1] A. Bridgwater and G. Peacocke, "Fast pyrolysis processes for biomass," Renewable and Sustainable Energy Reviews, vol. 4, pp. 1-73, 2000.

[2] J. Adjaye and N. Bakhshi, "Catalytic conversion of a biomass-derived oil to fuels and chemicals I: model compound studies and reaction pathways," Biomass and Bioenergy, vol. 8, pp. 131-149, 1995.

[3] R. J. Evans and T. A. Milne, "Molecular characterization of the pyrolysis of biomass," Energy & Fuels, vol. 1, pp. 123-137, 1987/03/01 1987.

[4] G. W. Huber, S. Iborra, and A. Corma, "Synthesis of transportation fuels from biomass: chemistry, catalysts, and engineering," Chemical Reviews, vol. 106, pp. 4044-4098, 2006.

[5] A. Bridgwater, "Review of fast pyrolysis of biomass and product upgrading," Biomass and Bioenergy, vol. 38, pp. 68-94, 2012.

[6] Q. Zhang, J. Chang, T. Wang, and Y. Xu, "Review of biomass pyrolysis oil properties and upgrading research," Energy Conversion and Management, vol. 48, pp. 87-92, 2007.

[7] E. Furimsky, "Hydroprocessing challenges in biofuels production," Catalysis Today, 2013.

[8] D. C. Elliott, "Historical developments in hydroprocessing bio-oils," Energy & Fuels, vol. 21, pp. 1792-1815, 2007.

[9] S. Asphaug, "Catalytic Hydrodeoxygenation of Bio-oils with Supported MoP-Catalysts," 2013.

[10] E. Furimsky, "Catalytic hydrodeoxygenation," Applied Catalysis A: General, vol. 199, pp. 147-190, 2000.

[11] T. Kalnes, T. Marker, and D. R. Shonnard, "Green diesel: a second generation biofuel," International Journal of Chemical Reactor Engineering, vol. 5, 2007.

[12] P. M. Mortensen, J. D. Grunwaldt, P. A. Jensen, K. G. Knudsen, and A. D. Jensen, "A review of catalytic upgrading of bio-oil to engine fuels," Applied Catalysis A: General, vol. 407, pp. 1-19, 11/4/ 2011.

[13] Funkenbusch, L.T., Mullins, M.E., Salam, M.A., Olsson, L., Hydrotreatment of Pyrolysis Oil Model Compounds over Pt/Al_2O_3 and Pd/C Catalysts: Part I: Batch Reactors, Industrial & Engineering Chemistry Research, submitted August 2017.

[14] H. S. Fogler, "Elements of chemical reaction engineering," 1999.

[15] L. M. Kindt, M. E. Mullins, D. W. Hand, A. A. Kline, D. L. Carter, and J. D. Garr, "Catalytic oxidation model development of the volatile reactor assembly unit of the international space station water processor," SAE Technical Paper 0148-7191, 1995.

6. Assessment of Hydrothermal Liquefaction Oil with Catalytic Upgrading for Renewable Fuel and Chemical Production[4]

6.1 Introduction

Since the early 1900's, researchers have shown that renewable petroleum substitutes could be derived from pulp and paper biomass. Early "recipes" for hydrothermal liquefaction and processing of wood and lignin wastes are found as early as 1902.[1] In 1934, Ernst Berl discussed the dissolution of agricultural wastes in water with alkali salts at elevated temperatures to produce a crude bio-oil with a high heating value, and yields as high as 60 wt%.[2] Since then, perhaps thousands of papers and reviews have been published on the topic.[3,4] The majority of experimental papers are batch studies based on mixing various ingredients in a pressurized vessel and "cooking" until done. Continuous catalytic near-critical water (NCW) processes were developed over two decades ago by Kjeld Andersen in Germany and by Erik Sogaard at Aalborg University in Denmark for processing anaerobic digested sewage sludge and agricultural wastes.[5] These processes share similarities to other hydrothermal processes but have the potential to create lower oxygen oils, especially with the use of proton donors such as hydrogen or alcohols in solution. Further development of the catalytic NCW process for biomass

[4] This article is an invited submission to WIREs Energy & Environment for November 2017, and is a collaboration with Dr. Lennart Vamling, Tallal Belkheiri, Nattapol Srettiwat, Dr. Olumide Winjobi, Dr. David R. Shonnard, and Dr. Tony N. Rogers.

feedstocks has been carried out by a Danish company, CatLiq®, which was recently purchased by a Turkish company in 2010.[6] The research at Chalmers is characterized by its emphasis on using lignin as a feedstock and a close relationship with Valmet, the leading supplier of process technology to the pulp and paper industry. Compared to most biomass, lignin has a low hydrogen and high phenolic content, making its depolymerization chemistry significantly different from other mixed biomass, agricultural, or cellulosic feedstocks.

Previous studies have performed a TEA for the upgrading of fast pyrolysis oil of corn stover to transportation fuels.[7] The proposed basis for this study is the conversion of lignin or black liquor from wood pulping mills to bio-oil, since these are often considered wastes or byproducts in pulp making. Lignin availability has greatly increased due to energy efficiency measures in Kraft pulp mills, which allows separation of 25 to 40 wt% of the lignin in black liquor without disturbing pulp production.[8] Removing the lignin in the black liquor can reduce recovery boiler bottlenecks and can be converted to bio-oil while increasing the pulp mill capacity. The recovered lignin has a very low ash content (<1 wt%), and the resulting oil has few solids from this source. The lignin sulfur content is also low (<3 wt%), and the corresponding NCW bio-oil product has <0.5 wt% sulfur; the difference is sequestered to the aqueous phase as sulfates. However, lignin has a lower hydrogen content than other cellulose-based feeds, making it difficult to obtain high oil yields. Therefore, the addition of hydrogen donor compounds to the process may be beneficial. Using lignin/black liquor as a bio-oil

source does not increase production demand for woody feedstocks or compete with food production, and the infrastructure already exists for collection and recovery of a large feedstock supply.

Supercritical water is an excellent processing fluid for lignin. Due to its strong solvating properties, low dielectric constant, weaker hydrogen bonds, and high isothermal compressibility, it is a suitable medium for biomass dissolution and degradation reactions. A potential drawback is that, at supercritical conditions, alkali salt catalysts have very low solubility in water. Therefore, NCW is preferable, since the catalyst salts are soluble and the water retains properties close to those of supercritical water. NCW has been shown to promote the degradation of lignin material into phenolic compounds.[9] NCW acts as an effective solvent for biomass dissolution.[10,11,12] Other authors have demonstrated the conversion of lignin without catalysts in super-critical water (400–600°C), but reported that the yield of phenolic compounds is low.[13,14,15] Pińkowska et al. and Yong et al. have demonstrated lignin depolymerization in both sub- and supercritical water for a range of temperatures from 473K to 663K.[16,17] Many other authors have used strong bases as a catalyst to degrade lignin in NCW, but high yields of heavy fractions and char were still obtained.[18,19,20,21] Most of these lignin depolymerization studies had low liquid product yields and significant carbon char residues due to re-polymerization reactions of the decomposed fragments.[22,23] Research on the influence of solvent, catalyst and operating parameters has been done to optimize

the yield of liquid products, but further study of the chemical mechanisms for oxygen removal and char formation are needed.[17,18,24]

6.1.1 Process Chemistry

Lignin is a complex high molecular weight compound with a random structure consisting of several monomeric compounds. Some of the most common monomers are alkyl phenolic compounds which are well suited for upgrading to alkyl benzenes, as shown in Figure 6-1.

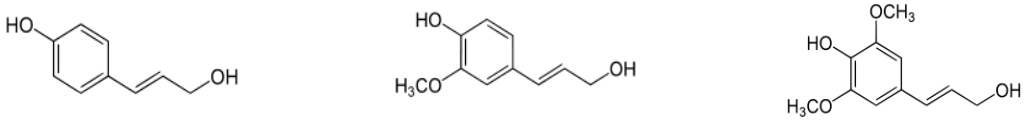

Paracoumaryl alcohol Coniferyl alcohol Sinapyl alcohol

Figure 6-1. Alkyl phenolic compounds

An example lignin fragment is shown in Figure 6-2. The chemical mechanisms in the NCW liquefaction of lignin to yield phenolics include hydrolysis and cleavage of the β-O-4 ether bond and C_α–C_β aliphatic bonds, which are shown in Figure 6-2, as well as demethoxylation (DMO) and decarboxylation (DCO) of the pendant groups. Alkylation and condensation reactions may also occur in competition with these main reactions. The aromatic rings of lignin are not very reactive during the hydrothermal reactions, evidenced by the fact that phenolic monomers and dimers are obtained via cleavage of the ether and aliphatic carbon bonds at relatively low temperatures and short reaction

times. Higher temperatures favor DMO/DCO and alkylation of phenolic compounds, producing various alkyl phenols including guaiacol. These aliphatic side chains are very reactive and undergo condensation reactions with each other forming char, tar, and suspended solid products. To moderate these condensation reactions, end-capping agents or hydrogen donors may be added, including phenol, methanol, ethanol, or tetralin, and have proven effective in reducing solids formation.[25] This is an indication that additives may affect reactive sites, thus effectively terminating re-polymerization.

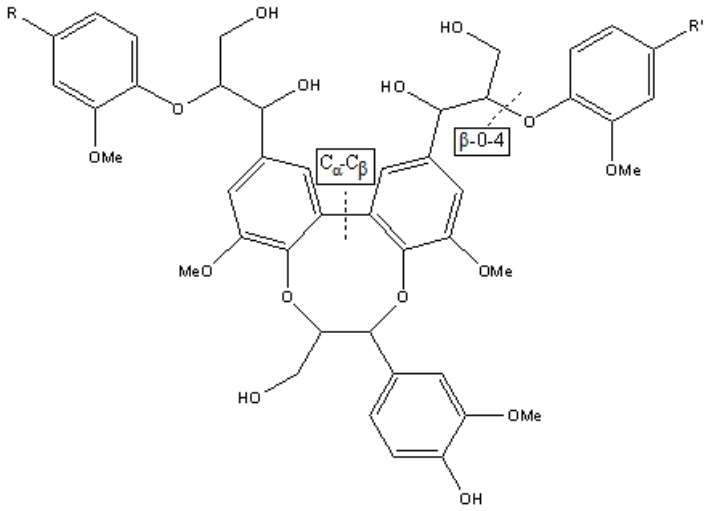

Figure 6-2. Example of lignin structure and bond cleavage

Oxygen heteroatom removal occurs most readily by dehydration or by decarboxylation. In some cases, this may also be achieved via demethoxylation. Even with an excess of water, dehydration reactions may occur at elevated temperatures and pressures over the certain catalyst.[26] Promotion of the DCO reactions are attractive since they decrease the

oxygen content of the feedstock, while increasing the H:C ratio. However, removal of carbon via these reactions lowers the final fuel product energy content. Fatty acids contain both hydroxyl and carboxylic acid groups, and a decarbonylation pathway can also occur.[27] Supplementing the HTL reaction with a hydrogen source and removing oxygen as H_2O yields more bio-oil per biomass input, with some of the fuel's energy content coming from the additional hydrogen. The DCO and DMO reactions in hydrothermal processing can be suppressed or enhanced by selection of an appropriate catalyst. Goudriaan (1990) as well as Boocock (1985) have shown that under liquefaction conditions (300°C to 350°C in NCW), most of the oxygen in lignin is removed as carbon dioxide, and the balance remaining organically bound in the liquid phase.[28,29] Although the mechanism of this process is unclear, it most probably occurs via formation of oxalate or formate intermediates. There is continuing research on the influence of solvent, catalyst and operating parameters to optimize the yields and composition of the liquid products; but elucidation of the chemical mechanisms would greatly enhance this process.

In a typical NCW process, dry lignin recovered via evaporation is mixed with water at a high pH (using K_2CO_3 or KOH) to facilitate the depolymerization. The depolymerization involves several chemical mechanisms which depend upon the solution, hydrogen donor compounds present, or the alkali salt catalyst used. The depolymerization is often supported by a heterogeneous catalyst compatible with water under high pressure and at high pH such as ZrO_2. Depolymerization reactions are fast, but to prevent re-

polymerization, an end-capping agent can be added to the feed. Since phenol and phenol-like compounds are depolymerization products, some of this demand may be met via recovery and recirculation of the process water containing these compounds.

6.1.2 Homogeneous alkali catalysts

*S*trong alkali salts are commonly used both as Kraft pulping agents and as HTL catalysts. The consensus of HTL catalyst reviews indicate that the reactivity of the alkalis may be generally ranked as $K_2CO_3 > Na_2CO_3 > KOH > NaOH$. Strong bases, such as KOH and NaOH, are often used for lignin fragmentation; however, potassium carbonate can promote similar reactions at more moderate pH's (8 to 9.5). The product water stream maintains a pH about one unit lower than the feed. The HTL product composition is quite sensitive to the concentration of salts used. Belkheiri et al. found that with K_2CO_3 of 3 to 4 wt%, excellent depolymerization is obtained, but further increasing the salt concentration to 6 and 10 wt%, enhanced condensation and re-polymerization.[30] As a side benefit, carbon dioxide produced via decarboxylation is rapidly converted to carbonates during the process, generating little or no greenhouse gases.

6.1.3 Heterogeneous HTL catalysts

The heterogeneous catalysts for lignin and lignocellulose depolymerization fall into two groups: supported transitional metal catalysts and metal oxide/mixed metal oxide catalysts. The mechanisms by which these work are quite different. Supported transition metals promote hydrolysis and hydrogenolysis, and at higher temperatures and

pressures, reforming reactions may occur. The solid catalysts must be compatible with alkali ions (Na^+, K^+) or they may negatively affect performance. Lignin obtained from Kraft pulping has a significant sulfur content, which will poison transition metal catalysts. The proper catalyst should be stable in a high temperature alkali solution, be sulfur resistant, and have low coking potential. Considerations for heterogeneous HTL catalyst selection include:

Metal oxide catalysts which promote oxygen removal via dehydration, DCO, and DMO reactions have been used for lignin and lignocellulosic depolymerization. The metal oxide that meet this requirement are period 4 and 5 transition metal oxides. Among the most active reported in the literature are oxides of chromium (CrO), manganese dioxide (MnO_2), Fe_2O_3, Y_2O_3, zirconia (ZrO_2), which are all mild Lewis acids. Studies are also reported with molybdenum oxides, vanadium oxides, and zinc oxide with limited success. Reports of mixed metal oxides (e.g. CrO/ZrO_2, MnO_2/Al_2O_3, and yttria-stabilized ZrO_2) used to promote the desired reactions are also found.[31]

Transition metal catalysts, alone or on a support, have been tested for lignin and lignocellulosic depolymerization. Heterogeneous catalysts to aid in the depolymerization have been extensively reviewed.[32] Yan et. al. found that Pd/C catalyst cleave the C–O bonds without disrupting the C–C yielding guaiacyl propane, syringyl propane, guaiacyl propanol, and syringyl propanol.[33] Ideally, an HTL catalyst would cleave the bond between the lignin's phenolic structural units without damaging the benzene ring or the

pendant alkyl group, while also inhibiting condensation, but no such catalyst has been demonstrated. Work on catalytic HTL in NCW by Elliott and co-workers, have employed numerous catalysts including ruthenium, rhodium, and nickel on stable supports such as zirconia, titania, γ-alumina, and carbon.[34]

Interaction of the catalysts with end-capping agents and hydrogen donor compounds is important in preventing repolymerization. In their absence, heterogeneous catalysts may be heavily coked in less than an hour of operation, rendering them ineffective in the depolymerization process. Hydrogen donor solvents have been investigated for the conversion of lignin. Belkheiri et al. examined the effect of methanol and phenol together with K_2CO_3 and zirconia on the conversion of Kraft lignin into bio-oil in NCW.[35] Those results showed that while methanol may serve as a hydrogen donor, phenol had a much greater effect in improving oil yields. Since phenol and phenol-like compounds are products of the depolymerization, some demand could be met via recovery and recirculation of phenol. Addition of 1 wt% of phenol reduced solids production by over 50%, and a combined addition of methanol plus phenol by over 70%.

Cellulose or hemicellulose derivatives may also prevent char formation. Zhu et al. found that addition of xylan/xylose to lignin reduced char formation in HTL studies, and the bio-oil composition is enhanced.[36] Although, these may add more oxygen to the final oil, it may also reduce the total char and tar formed in the process, and raise oil yields.

The direct use of black liquor, which contains hemicellulose and some residual cellulose compounds, might have similar benefits in the depolymerization process.

6.2 Materials & Methods

For our analysis of the viability of the lignin HTL to fuel/BTEX system, we focus on three key unit operations which have the greatest degree of technical uncertainty. We have used empirically-derived, process-level models for the reactor stages which have the greatest impact and the highest uncertainty in ASPEN simulations. For these two processes (the HTL reactor and the hydrotreatment reactors), we use these experimentally-based models to derive the material and energy balances, and integrate the resulting inputs and outputs into an overall process simulation using ASPEN; for the phenolics separation and extraction, we use only an ASPEN model with the process inputs defined by experiments on the HTL pilot plant and the UNIFAC LLE model to estimate the outlet steam composition, which is shown in red in the simplified block diagram in Figure 6-3. We describe in detail these three key units below.

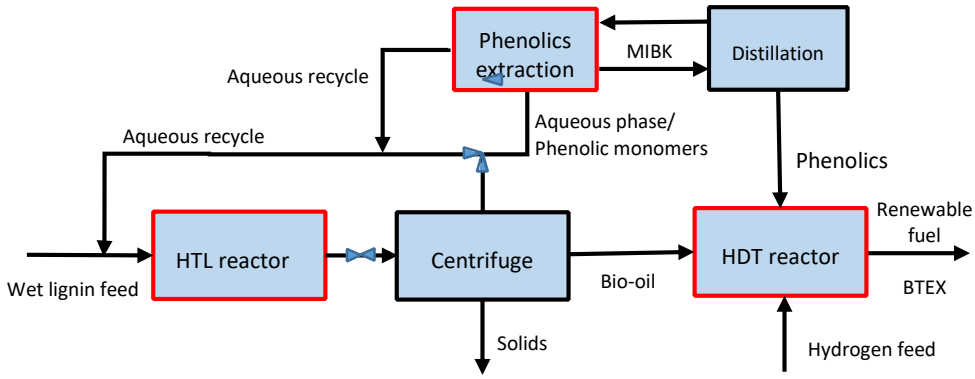

Figure 6-3. Simplified Block Diagram

6.2.1 HTL reactor design and operation

Catalytic NCW depolymerization can convert lignin into a low oxygen content crude bio-oil with a high stability product which is easy to store and transport. The underlying principle is to use the solvating power of NCW along with alkali salt catalysts to depolymerize the larger molecules associated with biomass and produce a bio-oil product, which may be further processed to produce transportation fuels. Unlike pyrolysis or gasification, the production of gaseous byproducts is minimal (<2 wt%), and the NCW process has higher liquid yields and lower oxygen content (<15 wt%) than pyrolysis oil (>30 wt%). The homogeneous alkali catalysts and most of the monomeric phenolic compounds remain in the aqueous phase and may be recovered or recycled. The heterogeneous catalyst performance eventually decreases due to char formation, but the energy content of the char may be recovered during regeneration in steam or air and reused for process heat. Unlike gasification or pyrolysis technologies, which work best

with dry feeds, the NCW process works well with raw, high moisture content feeds, making it ideal for recovered lignin or black liquor from a pulping process. If the oxygen content of the bio-oil is low enough (<10 wt%), it may be co-processed in the hydrotreatment reactor at existing refineries to produce a gasoline or diesel fuel blends.[37]

Although the design and equipment for the HTL process is fairly advanced, a clearer understanding of the chemistry is needed. Since the NCW process is intended for bulk production, only continuous reactors have a clear advantage for up-scaling. In our NCW process, a solid catalyst is used, which is most easily handled in a Plug Flow Reactor (PFR). Chalmers uses a hybrid reactor which is a PFR with internal recirculation, meaning that a pump is used instead of the stirrer in a CSTR.[25] This adds additional flexibility, since different recirculation ratios (RR) can be used, and the PFR/recycle design is best for maximizing targeted intermediate reaction products by finding an optimal RR.[38] For lignin, a RR of 4 to 5 reduced char and solids formation by more than 50% over lower (<2) or higher ratios (>10); in addition, 27% higher oil yields, and a lower average MW distribution (5 kDa vs 9 kDa) were obtained. An equally important design parameter is the average residence time, and recent findings indicate that it should be possible to decrease this further, increasing the process thoroughput.

6.2.2 Product separation and extraction

One of the major aspects of HTL processing of biomass is that a significant percentage of the organics produced are water soluble, and could be recovered and hydrotreated to improve the process efficiency and economics. The HTL reactor effluent yields a two-phase bio-oil/water mixture with some char and solid particles. Separation of the oil/water/solids is readily accomplished using existing technology (e.g. Alfa Laval 3-phase centrifuges), yielding an oil product with <1% water and solids.[39] The water-rich phase contains 10 to 30 wt% soluble monomers depending upon the process conditions.[25] A portion of this stream may be recycled to the reactor providing capping compounds to the process, or it can be extracted using liquid-liquid extraction (LLE) to recover the phenolic monomers for further processing. Standard LLE equipment can be used, but sizing and staging the LLE equipment required is problematic due to a lack of the appropriate thermodynamic partitioning data. ASPEN can calculate the component activity coefficients, but some of the appropriate chemical groups for UNIFAC calculations are not available.

6.2.3 Hydrotreatment/hydrodeoxygenation of products

The NCW bio-oil has a greatly reduced oxygen content and thus may require less hydrogen for catalytic upgrading than pyrolysis oil or similar potential feedstocks. The Swedish refiner Preem has suggested that a product oil containing less than 10% oxygen could be blended with crude oil and directly added to their renewables HDT unit, allowing integration into existing production and distribution systems.[37] Using both the phenolic monomers, the HDT reaction kinetics and products yield/selectivity have been

determined as a function of process variables including reactant concentration, temperature, hydrogen pressure, residence time, feedstock type, and catalyst type. The viability of producing BTEX products from the recovered phenolic monomers using an HDO processes has been evaluated in the Michigan Tech pilot unit, and necessary modifications to the production process identified. These experimental and modeling results have been used in a process-level model for the design of larger scale reactors, and incorporated into ASPEN simulations to facilitate the integrated process assessment work.[40,41]

6.2.4 Model synthesis

A process-level, experimentally-based model for the catalytic NCW reactor, including the feedstock, products, process conditions and operation has been developed by Chalmers University. The LLE step has been modeled in ASPEN, and catalytic treatability studies of the bio-oil to fuel and the phenolic stream to BTEX compounds has been modeled via both data-based process-level models and ASPEN.[40,42,43] This forms the basis for a techno-economic analysis (TEA) of a lignin-to-fuel process with co-production of commodity chemicals using a model with a higher degree of certainty than possible by using a process simulator alone. To move realistically evaluated equipment size, hydrogen and energy usage, and obtain more accurate cost estimates, the kinetics of the key reactions and separation steps were included in the model.

6.2.5 Proposed route and feedstock selection

The goal of this study is to evaluate the technoeconomic aspects of the production of hydrocarbon products and transportation fuels via HTL of excess lignin available from modern pulp mills as the principal feedstock. Pilot scale facilities have demonstrated an impressive yield of bio-oil ranging from 69 to 88 wt% on a dry lignin basis, corresponding to between 140 and 175 gallons of bio-oil per ton of dry lignin.[44] Since the current value of excess lignin in the pulp mill is based upon its use as an auxiliary fuel or waste material, the cost of the feedstock per gallon of bio-oil is low compared to specifically cultivated biomass feedstocks. Since the aqueous phase from HTL is rich in phenolic compounds, production of chemical co-products, such as benzene, toluene, ethylbenzene, and xylenes (BTEX), also could provide additional revenues for the pulp and paper industry. We have performed economic estimates on this technology for energy usage, capital, and operating costs to produce drop-in transportation fuels and a BTEX co-product. Three different technology scenarios are examined: 1) A baseline case utilizing existing commercial-level process targets, 2) a second case, based upon the best proven laboratory-scale results for feedstock to oil conversion, and finally, 3) a target level of performance needed to reach the implementation level desired by industry.[37] Estimates of selling price per gasoline gallon equivalent (GGE) are made via TEA models. Target performance metrics also include reductions in greenhouse gas emissions compared to fossil gasoline, to qualify the fuel as an advanced biofuel according to U.S. EPA regulations. The performance relative to EU sustainability criteria (50% reduction by 2017 and 60% by 2018) are also included. The major assumptions in the analysis of these three scenarios include:

1. *Integration with pulp mill lignin feedstocks:* By using lignin or black liquor, a significant supply of biomass feedstocks becomes available. Materials that are now waste or byproducts in pulp and paper processing might be used for fuel or chemical production, enhancing the profitability of that industry. By integrating fuel production processes directly into the existing pulp mills for raw materials, major cost improvements can be achieved. The lignin raw material for the process is already being collected and pre-processed within the pulp mill, eliminating the logistics development for collection and processing required by other feedstocks. A typical Swedish pulp mill (e.g. Södra Cell Värö pulp mill in Sweden) produces ~125,000 metric tons of recoverable excess lignin per year, and this serves as the basis for our study.[8]

2. *Integration with existing refinery facilities:* To use crude bio-oil as a feedstock in the hydrotreatment reactor of a traditional refinery, the oxygen content must be low enough for use with existing catalysts and process conditions. Currently the lowest oxygen levels achieved in HTL are around 13 wt%. Although it is possible to use at those levels, refiners would prefer a feed with <10 wt% oxygen to reduce hydrogen usage and prevent catalyst coking.[37] During their NCW process development, the Chalmers team attained levels <15 wt% oxygen, very close to desired levels.[25] Under optimal conditions, oxygen levels as low as 10 wt% are stoichiometrically possible.[37] This is a key variable in the study, thus three scenarios for oxygen content are explored. A baseline case at 16 wt%

oxygen, the state-of-the-art research results (13 wt%), and a projected 2020 target technology goal of 10 wt% oxygen as desired by Preem.[37]

3. *Suppression of char and tar formation:* By optimizing the process conditions and additives, researchers have steadily reduced the char content (solids) from 15 wt% to 12 wt%. Although char may be separated and burned as an auxiliary fuel, it also reduces the yield of bio-oil and aqueous hydrocarbons, and fouls equipment and catalysts. The three scenarios also include levels of char formation, including the current pilot-scale level (15 wt%), the best current research results (12 wt%), and a 2020 target projection of 8 wt% char.

4. *Improved utilization of aqueous phenolic byproducts*: Since up to 30 wt% of the total organics (e.g. phenolics) produced in the HTL process remain dissolved in the aqueous phase, the co-production of significant quantities of BTEX solvents from this stream becomes attractive. A BTEX co-product significantly impacts process viability and production costs. Separation schemes for aqueous phenolics have been explored in other contexts, but no technology is proven for this application.[45] Distillation is energy intensive, and the phenolic recovery is poor. LLE is less energy intensive, and the extraction solvent may be recycled. Recycling of end-capping agents and phenolic monomers back to the HTL reactor to reduce solids and improve oil yields is also assumed. Therefore, the base technology for phenolic separations is liquid-liquid extraction with methyl isobutyl ketone (MIBK) or ethyl acetate (EA), and with partial phenolic recycle (recycle ratio of 4) back to the HTL reactor.

Figure 6-4 shows the proposed base process for converting excess lignin directly from a standard Kraft process pulp mill into transportation fuels and BTEX compounds. The wet lignin feed may be supplied from the excess black liquor or from a lignin separation process, such as the LignoBoost® process. The effluent from the NCW reactor is separated by an Alfa-Laval three-phase centrifuge into suspended solids, oil-rich, and water-rich phases. The bio-oil may be used directly as a co-feed to a refinery hydrotreatment unit for fuel production, while the water-rich stream is partially recycled or sent to a phenolics extraction unit to recover BTEX precursors. Monomeric phenolic compounds preferentially partition into water at high pH (>8), with over 90% being partitioned at pH's above 11. To effectively concentrate the aqueous phenolic stream, the pH must be lowered (~7) and extracted using standard LLE equipment.[45] Since MIBK is much more volatile than the phenolics, the extractant/phenolic stream can be readily separated via simple distillation. The concentrated phenolic stream may then be fed into a hydrodeoxygenation (HDO) reactor for conversion to BTEX compounds, or partially recycled as an end-capping agent to the HDT reactor. Further purification/separation via distillation may follow. In this study, the evaluation focuses on three unit operations (red) in the flow diagram. A process-level, experimentally-based model for the catalytic NCW reactor, including the feedstock, products, process conditions and operation has been developed by the Chalmers team. The LLE step has been modeled in ASPEN, and catalytic treatability studies of the bio-oil to fuel and the phenolic stream to BTEX

compounds has been modeled via both data-based process-level models and ASPEN.[40,42,43]

This study integrates laboratory data and models to develop more accurate process simulations and flowsheet analyses for a commercial-scale NCW lignin-based biofuels and BTEX production system. The flowsheet includes operations from lignin preprocessing through the final catalytic upgrading step. The primary objective is to translate research advances into economic performance metrics and life cycle environmental impacts throughout the project as formative and summative assessments. The process TEA explores fossil energy input requirements for process heat and power demands and in scenarios will investigate technological improvements in the HTL, separations and upgrading areas. Process stream compositions and yields are incorporated from the laboratory research conducted by the authors for each of the studied unit operations, replacing initial baseline default data with experimentally-validated data where possible. This was based on already-developed Aspen flowsheets for a full pyrolysis conversion process simulation as described in Winjobi et al..[40] The flowsheet analysis determines energy demands for all flowsheet unit operations using heat capacities, temperature changes in process streams, product and co-product yields, stream compositions, and heats of reaction calculated using heats of formation for components in process streams.

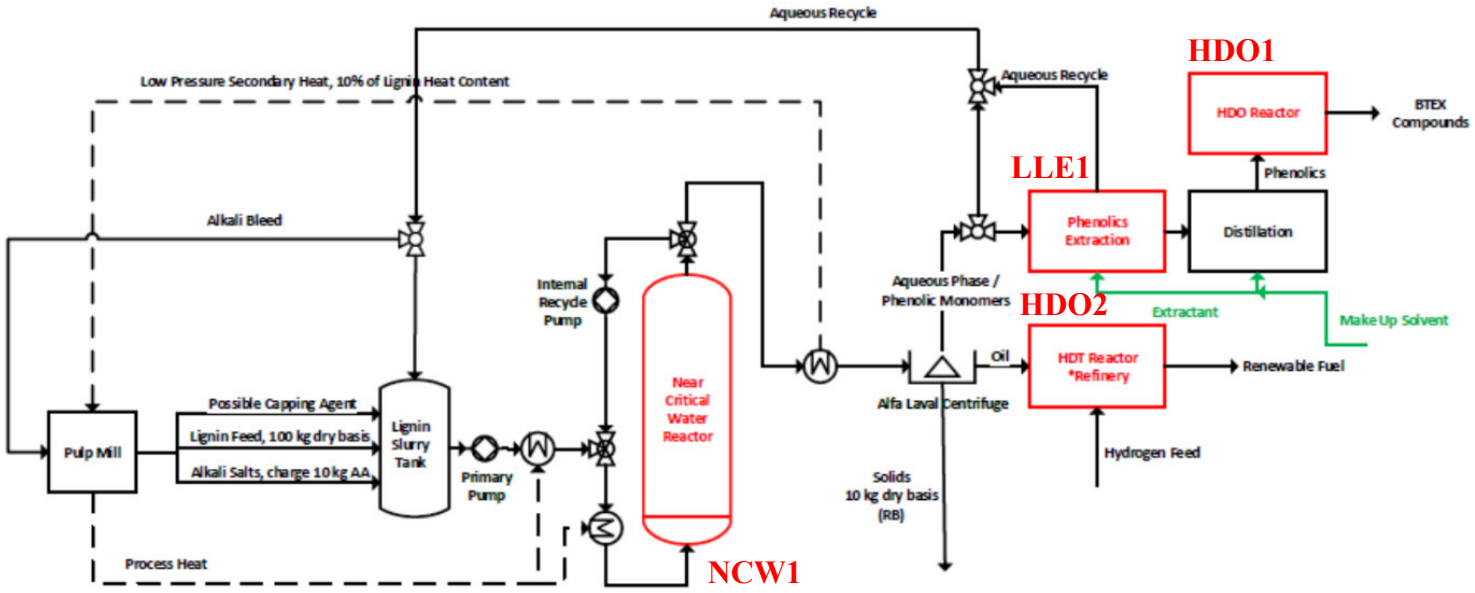

Figure 6-4. Integrated pulp mill to refinery process

6.2.6 Analysis for environmental impact

As the concentration of CO_2 in the atmosphere passes 400 ppm from a pre-industrial level of 285 ppm, low carbon energy technologies are urgently needed to bring climate change under control. Capping global GHG emissions at the current level for 50 years will ensure that CO_2 levels in the atmosphere remain below 550 ppm by 2060 and avoid the worst effects of manmade climate change. Renewable and sustainable biomass-based substitutes for liquid transportation fossil fuels, such as waste lignin from the pulp industry, will help achieve this goal. The proposed assessments in this project will provide important feedback to the research teams on techno-economic and environmental life cycle performance, and help guide research and inform decision makers in industry and government about the sustainability of the proposed fuels and chemicals produced.

6.3 Technoeconomic Assessments

The objective of this study was to conduct formative and summative TEAs on the conversion of lignin to two main products: drop-in fuel blends from NCW bio-oil and BTEX compounds from the aqueous phenolic stream. The minimum selling price of both products is determined using a discounted cash flow rate of return analysis by setting the net present value to zero as outlined in the study by Winjobi et al.[40] Updates were made to the baseline models using experimental data to define key scenarios for comparison within the NCW conversion platform. This TEA employs literature and

vendor quotes for equipment, and uses Peters and Timmerhaus investment, installation, and scale-up factors to estimate total project costs.[46] Equipment costs from previous years were escalated to base year 2016 using the Chemical Engineering Plant Cost Index (CEPCI), which is provided monthly by the journal *Chemical Engineering*.[47] Employee costs are estimated using data from Peters et al. and wage rates from the Bureau of Labor and Statistics for the U.S. analyses and comparable sources in Sweden.[46,48] These initial TEA modeling results illustrate preliminary estimates for key cost factors and can help guide future research with an eye towards reducing key cost factors where possible. The process model inputs for heat, power, and other process needs flow into the Aspen simulations where appropriate, and also inform our choices for the TEA modeling efforts.

6.3.1 Near-critical water hydrothermal liquefaction reactor

The success of this process is based mainly upon the NCW reactor and the assumptions made on the process. Table 6-1 displays the operating conditions of the NCW reactor. The reactor is run at 350°C and 25 MPa, with a recycle ratio of 3 – 6. The residence time decreases across the scenarios from 11 minutes in the first scenario to 3 minutes in the third scenario. A K_2CO_3 or KOH catalyst is used, with the amount of catalyst increasing from 0.5 kg catalyst in the first two scenarios to 1 kg catalyst in the third scenario, which contributes to the decreased residence time. The desired mass of product also increases from 88 wt% of the total product in the first scenario to 90 wt% in the last two scenarios. Table 6-2 shows the input from the pulp mill, which will be used for all three scenarios,

and the outputs from the process, based on the three different scenarios. The input stream is assumed to be the lignin feed from the pulp mill, water, added catalysts (alkali salts), and end-capping agents. The effluent compositions for the first and second scenarios have been verified via experimental studies at Chalmers.[30] The third scenario is an optimal case based on the minimum oxygen content, product distribution, and solids content targets proposed by refiners.[37] The primary differences are the oxygen and char content, which decrease with each improved scenario. The input stream has a carbon to oxygen ratio (C/O) of 3.4 and a carbon to hydrogen ratio (C/H) of 1.0. The output bio-oil stream has an increasing C/O ratio of 6.2 in the first scenario to 10.4 in the third scenario, and a decreasing C/H ratio of 1.0 in the first scenario to 0.7 in the third scenario. The increasing C/O ratio indicates increased oxygen removal across the three scenarios, while the decreasing C/H ratio indicates a higher percentage of desired products (alkylphenols). Oxygen removal is due to the formation of carbonates and small organics, such as acetic acid and lighter aldehydes, in the aqueous phase. The mechanism for this removal is unclear, although it is most likely through the oxalate cycle. The aqueous stream shows a decrease in phenol over the three scenarios, as well as an increase in alkylphenols. The other aromatic compounds remain relatively stable across the scenarios. The percentage of phenolic monomers in the organics of the aqueous phase increases across the three scenarios from 56% to 64%, which improves the economic viability of BTEX production.

The process economics for the near-critical water hydrothermal liquefaction reactor, including capital and operating costs, are based upon a methodology found in Knorr et al.[49] In the Knorr study, five reactor cases were investigated for a hydrothermal liquefaction reactor, and factored in heat integration, stream viscosities, and cost minimization. All cases utilized a feed rate of 2000 dry metric tons of wood chips per day, with critical or near-critical water as a solvent, which results in a 15 wt% dry solids feed entering the HTL reactor. For the reactors presented, no catalyst was used, which differs from the reactor studied at Chalmers, but an alkali carbonate reagent was used to maintain a pH of seven or larger. For this TEA, Knorr's Case A was chosen as a model, where the recycle stream is at the reactor temperature (350°C in this case) and is used to provide indirect heating to the feed stream, which enters the reactor at 250°C. Knorr et al. state that this design requires a large recycle ratio (77.5%) to maintain a feed temperature of 250°C, which also causes an increase in the overall residence time. The high solids content also requires recycle pumps capable of handling up to 15% wt% dry solids. Material balances and solubility limits were modeled using AspenPlus, with a key assumption that the thermal properties of the stream were best modeled using a thermodynamic package for water. [49]

Table 6-1. NCW reactor operating conditions[30]

Temperature	350°C		
Pressure	25 MPa		
Residence time	11 min	6 min	3 min

Recycle ratio	3 to 6		
Alkali salt catalysts	K_2CO_3 or KOH		
Amount of alkali catalyst required per amount of reactant	0.1 kg catalyst / kg lignin feed		
Solid catalyst substrate	0.5 kg catalyst		1 kg catalyst
Mass flow of feed/mass of catalyst	5 kg / hr / kg catalyst		
Mass of desired product/Mass of total product (wt%)	88%	90%	90%
Mass of reactant feed/total influent mass (wt %)	5.50%		

Table 6-2. NCW reactor inputs and outputs[30]

Unit Operation Material Streams In:					**Unit Operation Material Streams Out:**				
Influent mass flow rate of dry lignin feedstock	kg/hr	17k		Effluent mass flow rates (bio-oil)	kg/hr	10k	10.5k	10.8k
Elemental composition of lignin feed				Elemental composition of bio-oil output[44]				
Carbon	wt.%	65.6%		Carbon	wt.%	75.0%	76.0%	78.0%
Hydrogen	wt.%	5.7%		Hydrogen	wt.%	6.0%	8.0%	9.0%
Oxygen	wt.%	26.0%		Oxygen	wt.%	16.0%	13.0%	<10.0%
Sulfur	wt.%	1.9%		Sulfur	wt.%	0.5%	0.5%	0.5%
Inorganic	wt.%	0.8%		Inorganic	wt.%	2.5%	2.5%	2.5%
				*Phenolic groups shown in Table 6-5				
Component composition								
Lignin	wt.%	5.5%		Effluent mass flow rates (aq. organics)	kg/hr	4.7k	4.8k	5.0k
Potassium carbonate	wt.%	1.6%		Phenolic monomers in organics (aqueous phase)				
Potassium hydroxide	wt.%	0.4%		Anisoles	wt.%	3.7%	4.0%	4.0%
Phenol	wt.%	4.0%		Phenol	wt.%	32.1%	28.0%	24.0%
Water	wt.%	88.5%		Alkylphenols	wt.%	6.6%	12.0%	18.0%
				Guaiacols	wt.%	1.9%	1.5%	1.5%
				Catechols	wt.%	4.0%	5.0%	5.0%
				Cresols	wt.%	5.0%	6.0%	7.0%
				Other	wt.%	3.0%	4.0%	4.0%

6.3.2 Centrifuge

Alfa-Laval centrifuges are a well-developed technology that will be used, in this process, to separate the effluent from the NCW reactor. The three-phase centrifuge will separate the effluent into a bio-oil stream, which will be hydrodeoxygenated to produce fuel, an aqueous phase, which will first undergo liquid-liquid extraction, and then can either be recycled back into the NCW reactor or hydrodeoyxgenated to produce BTEX compounds, and a solids phase that will remove the char from the system. The char can be burned for heat somewhere else in the process. The separation efficiencies assumed here are found in the Alfa-Laval catalogue.[50]

6.3.3 LLE Separation Process

The feed to the LLE unit (LLE1) is the aqueous phase of the NCW effluent, described in Table 1, after being separated via Alfa-Laval centrifuge. In the NCW process, almost 90% of the feed is water, which needs to be recovered or recycled. Separating and recovering the organics in the aqueous phase, either to recycle back into the reactor or to generate BTEX compounds as a co-product, is a crucial part of the process. Table 6-3 depicts the inputs and outputs for the liquid-liquid extraction process. The input streams are the extractant (MIBK or ethyl acetate) and the aqueous phase of the NCW reactor, after separation by the Alfa-Laval centrifuge, across the three scenarios. The primary differences between the scenarios are the decreasing phenol content, the increasing alkylphenol content, and the total percentage of phenolics increases. For the effluent, the primary effect of the process is to remove the water. The water phase is recycled back

into the NCW reactor, with trace amounts of phenolics. Across the three scenarios, the effluent has decreasing oxygen content, starting with a C/O ratio of 6.8 in the first scenario and increasing to 8.8 in the third scenario. While the increase in specific compounds' concentrations is due to the removal of the water, the thermodynamics of the extraction are selective for some compounds. For example, guaiacols, actually decrease with the improving scenarios from 2.3% to 1.0%, indicating that they leave with the water upon extraction. These effluent compositions are based on work by Nattapol, and are modeled using ASPEN Plus.[42] The ASPEN Plus model designed for this process utilizes the Predictive Soave-Redlich-Kwong (PSRK) equation of state and the UNIFAC activity model. The PSRK equation of state is used for polar systems with no electrolyte components at high temperatures and pressures. Unfortunately, ASPEN Plus, does not include specific UNIFAC groups for phenolics, so the values for those groups were estimated.

Table 6-3. LLE inputs and outputs

Unit Operation Material Streams In:						**Unit Operation Material Streams Out:**				
Influent mass flowrate (Organics)		kg/hr	4.7k	4.8k	5.0k	Effluent mass flowrate (Phenolics)	kg/hr	2.6k	2.7k	2.8k
Aqueous organic phase from centrifuge (% of total organics)						Elemental composition of product stream				
	Anisole	wt.%	3.7%	4.0%	4.0%	Carbon	wt.%	76.0%	78.0%	79.0%
	Phenol	wt.%	32.1%	28.0%	24.0%	Hydrogen	wt.%	8.0%	8.0%	9.0%
	Alkylphenols	wt.%	6.6%	12.0%	18.0%	Oxygen	wt.%	15.0%	13.0%	12.0%
	Guaiacols	wt.%	1.9%	1.5%	1.5%	Sulfur	wt.%	0.0%	0.0%	0.0%
	Cresols	wt.%	5.0%	6.0%	7.0%	Inorganic	wt.%	1.0%	1.0%	1.0%
	Catechols	wt.%	4.0%	5.0%	5.0%					
	Other	wt.%	3.0%	4.0%	4.0%	Phenolics from LLE (wt%) [42]				
	Total phenolics	wt.%	56.0%	61.0%	64.0%	Anisole	wt.%	7.0%	7.0%	8.0%
						Phenol	wt.%	61.0%	52.0%	45.0%
						Alkylphenols	wt.%	12.5%	21.0%	28.0%
						Guaiacols	wt.%	2.3%	2.0%	1.0%
						Cresols	wt.%	9.0%	10.0%	10.0%
						Catechols	wt.%	7.0%	7.0%	7.0%
						Other	wt.%	1.0%	1.0%	1.0%
						Total phenolics	wt.%	100.0%	100.0%	100.0%

6.3.4 HDO1 Reactor

The HDO1 reactor input stream comes from the LLE unit, and is composed of phenolic compounds, diluted to 5% molar in dodecane, an inert solvent that will help in controlling the reactor. The reactor is operated at 300°C and 7 MPa over a noble metal catalyst, such as Pd/C or Pt/Al_2O_3, with a 3 minute residence time. The gas was 5% hydrogen mixed with an inert carrier gas. The inputs and outputs are shown in Table 6-4. The primary goal of this reactor is to hydrodeoxygenate the phenolics and convert them to BTEX or cyclic hydrocarbon compounds, and for this reactor, deoxygenation was complete by the end of the residence time. The HDO1 reactor is simulated using a process-level model and an ASPEN Plus simulation developed in previous work for a catalytic hydrodeoxygenation system for wood-based pyrolysis oil.[40,51] Across the three scenarios, the total BTEX in the products increased from 60% to 65%, with saturated cyclic hydrocarbon products decreasing from 16% to 11%. The water and other products remain constant, as they are not affected by any process improvements. With the assumptions in this study, the primary products were the BTEX compounds, but the process or reactor operating conditions could be altered to produce a biofuel blending stream instead, depending on market demand.

Table 6-4. HDO1 inputs and outputs

Unit Operation Material Streams In:						**Unit Operation Material Streams Out:**				
Influent mass flow rates		kg/hr	2.6k	2.7k	2.8k	Effluent mass flow rates	kg/hr	1.9k	2.0k	2.1k
Phenolics from LLE (wt%) [42]						Effluent composition from HDO2 unit (wt%) [40]				
	Anisole	wt.%	7.0%	7.0%	8.0%	Benzene	wt.%	62.5%	60.0%	60.0%
	Phenol	wt.%	61.0%	52.0%	45.0%	Cyclohexane	wt.%	16.25%	13.75%	11.25%
	Alkylphenols	wt.%	12.5%	21.0%	28.0%	Toluene	wt.%	11.25%	13.75%	15.0%
	Guaiacols	wt.%	2.3%	2.0%	1.0%	Methylcyclohexane	wt.%	2.5%	1.25%	1.250%
	Cresols	wt.%	9.0%	10.0%	10.0%	Ethylbenzene	wt.%	1.25%	5.0%	7.5%
	Catechols	wt.%	7.0%	7.0%	7%	Ethylcyclohexane	wt.%	1.25%	1.25%	1.25%
	Other	wt.%	1.0%	1.0%	1%	Other	wt.%	5.0%	5.0%	3.75%
						Total BTEX (wt%)	wt.%	75.0%	62.0%	82.50%
						Saturated products	wt.%	20.0%	14.0%	13.75%
						Other	wt.%	5.0%	5.0%	3.75%

6.3.5 HDO2 Reactor

The upgrade of the bio-oil to hydrocarbon biofuel is modeled in a two-step pathway, an initial stabilization step followed by a final hydrotreatment step.[51] The upgrade of the bio-oil to a hydrocarbon biofuel is modeled utilizing reaction pathways suggested in the literature for conversion of the representative compounds in the bio-oil to hydrocarbons.[51,52,53,54,55,56,57] In this study, aldehydes and ketones are modeled to be converted to alcohols in the stabilization step as suggested by Vispute et al. while other representative compounds in the bio-oil pass through the stabilization step unchanged.[51] The final conversion of the unreacted bio-oil representative compounds and the intermediate alcohols from the stabilization step to hydrocarbons then takes place in the final hydrotreatment step. The reaction pathway for acetol, one of the representative bio-oil compound in this study is shown in Figure 6-5. The hydrodeoxygenation reaction converts acetol to propylene glycol in the stabilization unit while the intermediate product, propylene glycol is converted to propane in the hydrotreater. Representative bio-oil compounds containing aromatic rings are modeled to yield two final hydrocarbon products, a fully deoxygenated aromatic hydrocarbon and a fully saturated aliphatic compound in a 0.45 to 0.55 ratio.

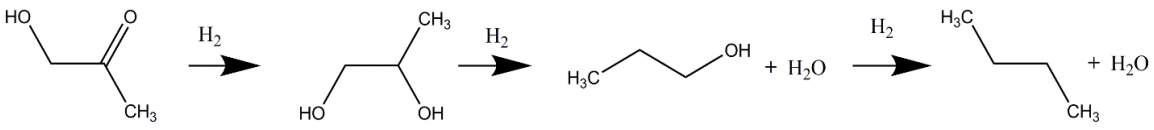

Stabilization unit

Hydrotreater

Figure 6-5. Upgrade of acetol to propane

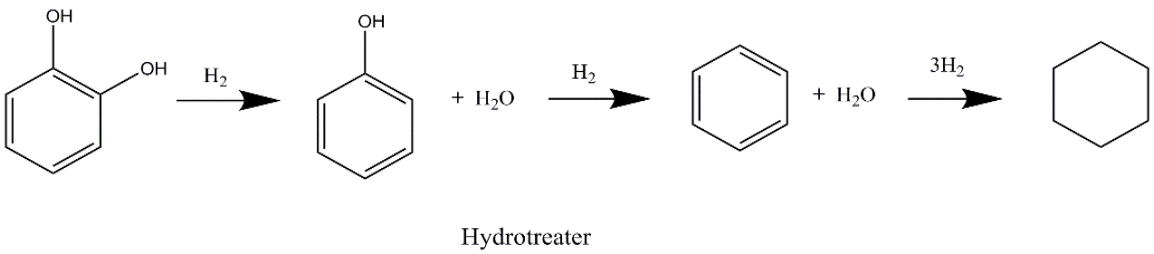

Figure 6-6. Upgrade of catechol to benzene and cyclohexane in the hydrotreater

As shown in Figure 6-6, the representative bio-oil compound catechol is modeled to only react with hydrogen in the hydrotreater to produce benzene and cyclohexane. In general, the major reaction pathway for the upgrade of bio-oil in this study was assumed to be through hydrodeoxygenation. Reactions such as decarbonylation, decarboxylation are also assumed to take place to produce intermediates that were subsequently converted to a hydrocarbon through hydrodeoxygenation.

Based on the described modeling approach, the hydrogen required to convert each representative compound to a hydrocarbon can be evaluated based on the weight fraction for each of the representative compounds in the bio-oil. The yield of hydrocarbon produced from the upgrade of the representative compound is also evaluated. The amount of the different hydrocarbon compounds in the final upgraded hydrocarbon

biofuel is subsequently evaluated. The hydrogen required for the upgrade step is estimated as the sum of the hydrogen needed for each representative compound.

The upgrade of bio-oil to a hydrocarbon biofuel is then modeled in Aspen Plus using a yield reactor. The yield factors required for modeling this reactor are evaluated by calculating the weight fraction of the compounds from the upgrade step based on our modeling approach. The product from the upgrade step includes the hydrocarbons formed for the hydrodeoxygenation reaction of the representative compounds as well as products such as water formed from these reactions. The operating conditions of 1200 psia, 140°C and 200 psia, 410°C utilized for the stabilization and hydrotreatment steps respectively in this study were obtained from literature.[52] The inputs and outputs for this reactor are shown in Table 6-5.

While this reactor was modeled and factored into this analysis, a more feasible economic scenario would include an "over the fence" arrangement, where the bio-oil from the NCW reactor, after separation in the Alfa-Laval centrifuge, would be shipped to a nearby refinery. The bio-oil would then be blended with the crude petroleum feed for hydrotreatment and further processing. However, in order to be acceptable to refiners, the oil would need an oxygen content of 10 wt% or less, which is therefore the target for the third scenario.

Table 6-5. HDO2 inputs and outputs

Unit Operation Material Streams In:					**Unit Operation Material Streams Out:**				
Influent mass flow rates	kg/hr	10k	10.5k	10.8k	Effluent mass flow rates	kg/hr	7.3k	7.9k	8.4k
Bio-Oil Composition (wt%)					Effluent composition from HDO2 unit (wt%) [40]				
Anisoles	wt.%	5.2%	6.2%	7.0%	Cyclohexane	wt.%	12.3%	11.1%	9.9%
Phenol	wt.%	12.8%	11.4%	10.0%	Benzene	wt.%	10.0%	9.1%	8.1%
Alkylphenols	wt.%	5.8%	7.8%	9.8%	Alkylcyclohexanes	wt.%	3.2%	4.3%	5.4%
Guaiacols	wt.%	2.0%	1.0%	0.3%	Alkylbenzenes	wt.%	2.6%	3.5%	4.4%
Catechols	wt.%	0.4%	0.6%	0.7%	Other	wt.%	1.8%	1.0%	0.2%
Other	wt.%	1.8%	1.0%	0.2%					
Total wt% of phenolic monomers	wt.%	28.0%	28.0%	28.0%					
*Remaining 72% is dimers, etc. that cannot be analyzed using GC/MS. Average MW of the bio-oil heavy fraction is 16-25 kDa.[30]									

6.4 Results & Discussion

This process was put through a profitability analysis, using Aspen software to estimate equipment costs and investment factors from Peters & Timmerhaus for operating costs.[46] Installation factors were also taken from Peters & Timmerhaus. The plant in Scenario 1 is based on the current state of technology, while Scenarios 2 and 3 assume technological improvements in the process. The plant is assumed to have an equivalent capacity factor of 89%, which is 325 days of online time. The cost of dry lignin was given by Verso Paper as $0.03/lb, or $60/metric ton.[59] There is no delivery cost, as the process includes a feed directly from the feed mill. The cost of electricity was assumed to be $0.07/kWh. Working capital is set as 15% of the fixed capital investment. Labor and maintenance are set as 2.3% of the total operating cost. The federal tax return and depreciation are calculated using the IRS MACRS and declining balance method, respectively. Because the location of the plant has not been determined, state tax is not included in our calculations.

In Table 6-6, a summary of the technoeconomic assessments for each scenario can be seen. The lignin feed is the same for each case and is based on a standard Swedish pulp mill production of 400 dry metric tons per day. The raw lignin feedstock costs $8.58 million per year.[59] However, the actual cost of lignin may be higher; it can be burned for fuel in the pulp mill or repurposed some other way, which might give it a higher value than used here. Scenario 1 is the basic case, which utilizes the current level of technology. The total biofuel yield in this case is 520 L/dry metric ton, while the BTEX

product yield is 134 L/dry metric ton. This results in annual production of 65 million L/yr and 16.8 million L/yr, respectively. Six thousand metric tons of carbon black can also be recovered from the process, and can be repurposed or burned in the plant for energy. The amount of carbon char decreases across the scenarios as the NCW reactor improves down to 2500 metric tons per year in Scenario 3, but this co-product was not credited anywhere in the economics for any scenario. A carbon conversion of 70% is achieved, by taking carbon in the product over carbon in the feed, and less than 1 g CO_2 equivalent/MJ are produced from the HTL reactor. The HTL equipment and operating costs listed are mostly from Knorr et al., Peters, and actual market costs.[46,49] Equipment costs are based on vendor quotes, while capital costs were adjusted using the Plant Cost Index.[49] Operating costs include fixed costs, such as employee salaries, and variable costs, such as utilities.[49] The net biofuel production cost is $0.41/L. Scenario 2 is based on optimal laboratory results, and sees a slight increase in the overall efficiency of the process, as well as the net cost. There is a biofuel production of 68 million L/yr, and an accompanying 17.4 million L/yr of BTEX produced. Scenario 2 results in a 74% carbon conversion; this improvement is caused by improving the NCW reactor conditions to decrease the solids yield and increasing separation efficiency in the LLE unit. The net cost for the biofuel in Scenario 2 is $0.43/L. The final scenario is based on target goals and projected technology improvements. These changes result in a total production of 70 million L/yr of biofuel and 18 million L/yr of BTEX products. A carbon conversion of 78% is achieved, a significant increase in recovery. The net biofuel production cost for Scenario 3 is $0.44/L. Across the three scenarios, there is an increase in production.

There is also a slight increase in the net cost per liter of biofuel, but this is accompanied by a decrease in the C/O ratio, an increase in the C/H ratio of the biofuel, and an increase in the amount of fuel processed and BTEX products produced alongside the fuel. The major cost improvements for these scenarios are due to the integration of the fuel production processes directly into the existing pulp mills for raw materials and refineries for fuel production. Figure 7 shows a column plot of the costs in millions of dollars, split into each section of the process for all three scenarios. The bulk of the installed capital costs are due to the hydrothermal liquefaction reactor and hydrodeoxygenation reactors. The installed capital costs also increase from $114 million to $124 million across the three scenarios. Net operating costs also increased from $18 million in Scenario 1 to $22 million in Scenario 3, due to increased utility and material demand. The amount of hydrogen necessary in the HDO reactors, for example, increases with the increased flow rates of both the aqueous phase and the bio-oil phase caused by improvements in NCW reactor operation. Based on this technoeconomic analysis, the minimum selling price (MSP) of the biofuel must be between $3.52 to $3.86 dollars per gallon, assuming the current BTEX value of $1 per liter. On the other hand, given the current diesel price of $2.88 per gallon, the MSP of BTEX must be between $1.65 and $2.00 per liter.[60]

Table 6-6. Summary results table

Process Details and Costs				
Feedstock Type	**Lignin**	**Scenario 1**	**Scenario 2**	**Scenario 3**
Envisioned Commercial Feed Rate (dry metric ton/day) *Basis: standard pulp mill (1million metric ton pulp/year),* e.g. Södra Cell Värö pulp mill, Sweden [8]	400			
Biofuel Yield (L/dry metric ton) [diesel blend] [44]		520	564	600
BioProduct Yield (L/dry metric ton) [BTEX] [42]		134	140	145
Annual Biofuel Production		65 M L/year	68 M L/year	70 M L/year
Annual BioProduct Production		16.8 M L/year	17.4 M L/year	18 M L/year
Recovered suspended carbon black		6000 metric ton/year	4000 metric ton/year	2500 metric ton/year
Carbon Conversion (%) (Products/feed)		70%	74%	78%
Lifecycle GHG emissions (only HTL)		<1 g CO_2 eq./MJ	<1 g CO_2 eq./MJ	<1 g CO_2 eq./MJ
Equipment Costs (2013$) [49]	**Description**	**Installed Capital Cost (million $)**		
Feedstock Storage and Handling (from pulp mill)	Pumps, tanks, mixing, heat exchangers	6.60	6.60	6.60
Biomass Deconstruction (recirculating PFR-HTL)	Pumps, pressure vessel, controls	47.60	49.98	51.87
Conversion – HDT reactor system [37]	Add to existing refinery as petrol replacement	1.00	1.05	1.09
Phenolic Recovery and Upgrading (LLE system) [42]	Alfa-Laval centrifuge, 3 stage LLE	10.73	11.27	11.69

Wastewater Treatment (>95% recycle)[46]	Small blowdown to pulp mill	2.00	2.10	2.18
Product and Feed Chemical Storage [46]	Alkali, capping agents, extracted phenols	3.40	3.57	3.70
HDO reactor for phenolics [40]	HP trickle bed system, pumps	37.25	39.11	40.59
Heat integration across pulp mill [46]	Pumps, heat exchangers, piping	5.30	5.44	5.56
Total Installed Capital (million$)		**113.88**	**119.44**	**123.87**
Total Installed Capital per Annual Liters		**1.75**	**1.75**	**1.76**
Operating Costs (2013$) [49]	**Description**	**$Million/yr**		
Feedstock Storage and Handling	Bio-oil storage and Shipping	5.12	5.55	5.91
Additional hydrogen for HDT/HDO reactors[40]	Makeup for additional renewable feed & BTEX	1.8	1.95	2.08
Alkali (800 kg.hr @ $240 metric ton) as catalyst. 95% recycled°	Option for BL alkali usage direct from pulp mill	1.44	1.56	1.66
Operating Costs (2013$) for LLE system [42,46]	Includes utilities of $8.23 million/yr for base case	16.75	18.17	19.33
Make-up LLE extractant, e.g. MIBK or EA°	Extractant recycled (~0.9% loss or 33760 ton/yr)	1.13	1.23	1.30
Capping agents (1 wt% of total dry feed)°	Make-up solvents ($1000/metric ton)	1.25	1.36	1.44
Waste Disposal [46]	Liquid purge to pulp mill	0.5	0.54	0.58

Process Steam [42]	Depolymerization integrated into pulp mill	3.27	3.55	3.77
Electricity ($0.07 kWh) [46]	Depolymerization, HDO, LLE	1.14	1.24	1.32
Labor and Maintenance [46]	Depolymerization, HDO, LLE	2.5	2.71	2.88
Total Operating Costs	**All units**	**34.9**	**37.9**	**40.3**
Co-product Credits	**BTEX compounds at ~$1/L**	**16.8**	**17.4**	**18**
Net Operating Costs		**18.1**	**20.5**	**22.3**
Net Biofuel Production Costs ($/Liters)		**$0.28**	**$0.30**	**$0.32**

° Actual Market Costs

Figure 6-7 shows a column plot of the installed capital costs for each scenario, divided into different sections of the plant. The HTL and the HDO reactors are the primary contributors to capital costs in all cases. Pulp mill and refinery costs are relatively low, since the operations are being integrated into existing mills and refineries. The total installed capital costs increase slightly across the three scenarios from $114 million to $123 million. This increase is due to increasing equipment sizes as the overall carbon conversion increases from 70% to 78%.

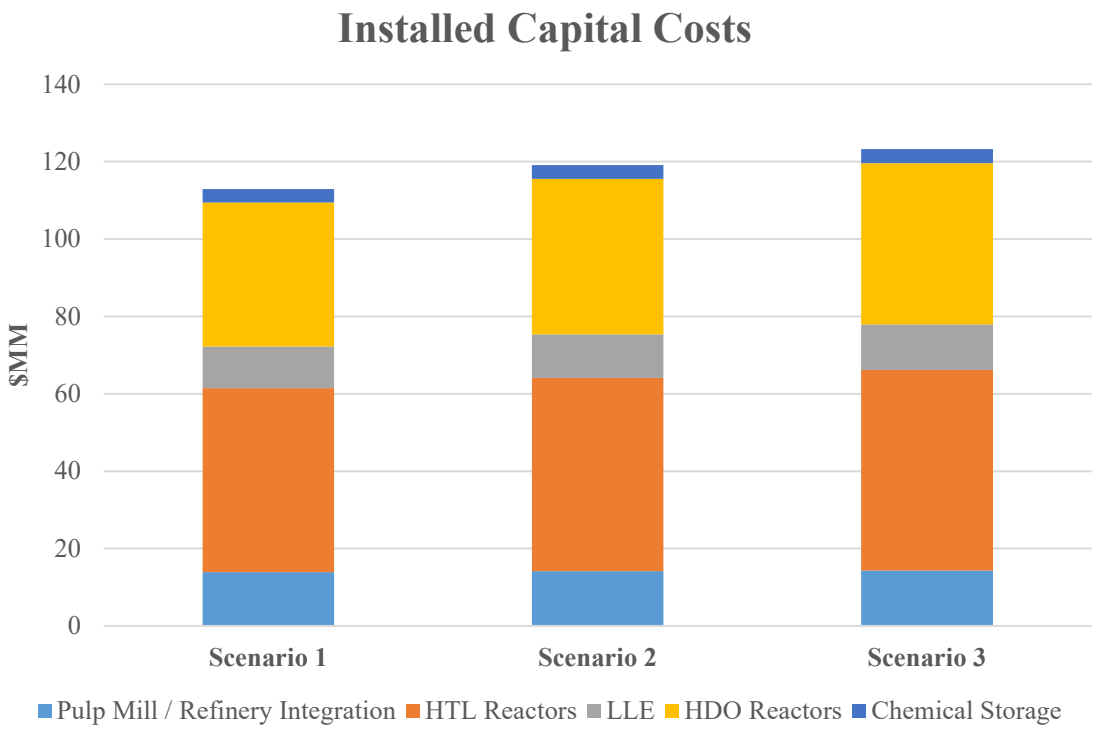

Figure 6-7. Column plot of installed capital costs

Figure 6-8 shows a similar column plot for the net operating costs across the three scenarios. Here, the LLE operation is the most significant cost. Pulp mill and refinery costs are also a significant fraction, specifically the bio-oil storage and shipping. The total operating costs increase from $34.9 million per year in Scenario 1 to $40.2 million per year in Scenario 3, again, due to the increased carbon conversion. However, with a co-product credit earned from BTEX generation, these costs drop from $18.1 million per year in Scenario 1 to $22.3 million per year in Scenario 3. It should be noted, however, that Scenario 3 is a hypothetical, and there may be diminishing returns for increased cost. At some point, any more carbon conversion might cost so much that it outweighs the revenue increase.

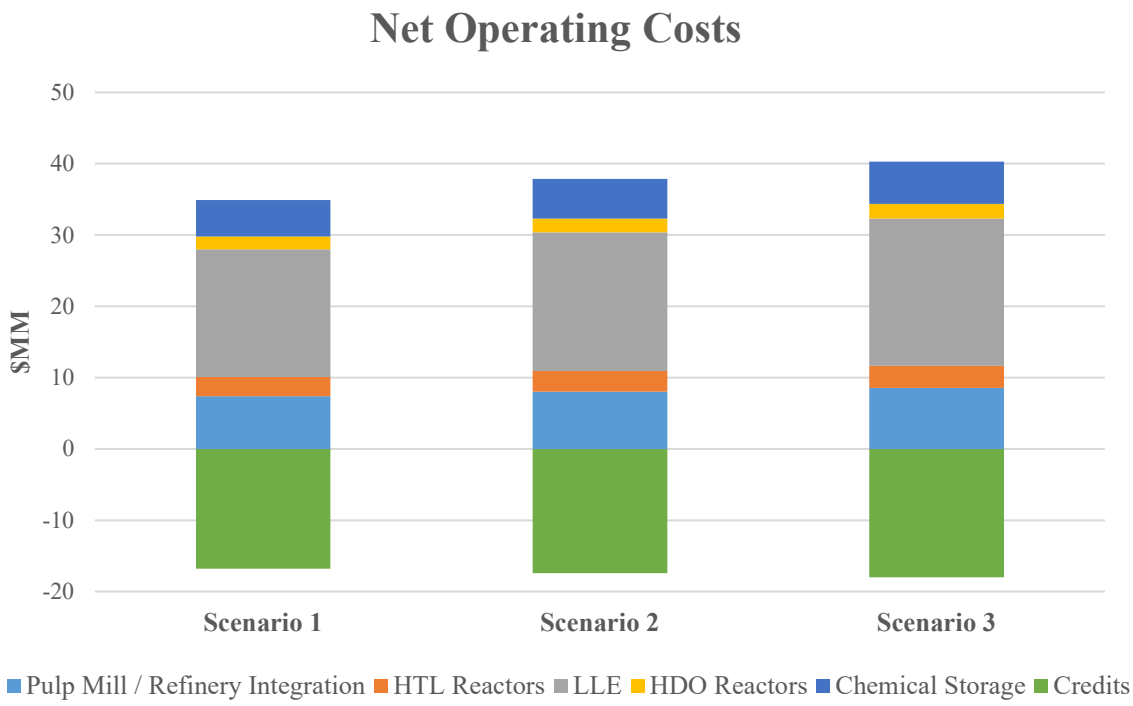

Figure 6-8. Column plot of operating costs

6.5 Sustainability & Life Cycle Assessments

While the economic viability of a process is important, it is also important to consider the environmental impact of a process. As with TEAs, areas of the process that need improvement can be pinpointed using the life cycle assessment (LCA) process. In the future, the goal is to also conduct formative and summative environmental LCAs on the conversion of lignin to biofuel and BTEX products. Like the TEA performed here, the main objectives would be to create an LCA model that is populated with literature or other baseline data, and then populate with experimentally-determined data as it becomes available to match the scenarios defined in the TEA modeling exercise. In this

manner, we have economic and environmental assessments that reflect sustainability information on the same optimal commercial development scenarios. These cradle-to-grave LCA studies will highlight environmental hotspots in the pathways and inform the direction of project research to address causes of high impact. The LCA studies will be conducted using framework and methodology following the ISO 14044:2006 standards.[ISO Standards] Pathway analyses will begin with lignin as a low-value material obtained from industrial processes in the forest products industry. Inputs to the LCA will be obtained from several sources including technical reports, peer-reviewed publications, and Aspen process simulations. Co-product allocation will be handled in accord with different regulatory requirements in the U.S. (system expansion) and EU (energy allocation). Inventories of environmental releases and resource consumption will be derived from the US LCI and from the ecoinvent™ database for the U.S. and EU-based studies, respectively. Impacts to be assessed will be global warming potential (IPCC 2013 100a method) and fossil energy demand. Energy return on energy invested will be determined. The LCA software tool SimaPro will be employed. Initial LCA modeling illustrates areas of large environmental impact in the overall process. The process model inputs for heat, power, and other process needs flow into the updated LCA models.

6.6 Conclusions

This technoeconomic analysis examined the production of biofuels with co-production of BTEX compounds via hydrothermal liquefaction of lignin from a pulp mill and

subsequent hydrotreatment of the products. This analysis considers a hydrothermal liquefaction process tied into the end of a pulp mill to use the lignin byproduct. This presents attractive commercial scenarios which could include collaboration between the pulp mill and the refinery, where bio-oil and possibly the BTEX co-product are shipped to the refinery and then blended with their crude oil. Tall oils and other pulp mill byproducts are already being utilized in a similar fashion, with similar transport scenarios as well. This allows the raw bio-oils to be directly incorporated into the refinery stream prior to hydrotreatment. This is attractive because it prevents green-field scenarios in either case.

Three scenarios were explored: the current level of technology available for commercialization, the state of the art level of research case, and an optimized, hypothetical case based upon the oxygen content and product composition goals defined by refiners.[37] Based on this analysis, the biofuel product costs $0.28-$0.32 per liter to produce, which includes a co-product credit from the BTEX, but not including installed equipment costs. The first scenario has $113.8 million in equipment costs and $34.9 million per year in total operating costs. A co-product credit of $16.8 million per year offsets the operating costs, for a net cost of $18.1 million per year to produce 65 million liters of biofuel and 16.8 million liters of BTEX per year. This scenario has a 70% carbon conversion, calculated by the moles of carbon in the product divided by the carbon in the lignin feed. Scenario 2 has $119.1 million in installed capital costs and $37.8 million per year in operating costs. The 17.4 million liters of BTEX produced

results in a co-product credit of $17.4 million per year. There are 68 million liters of biofuel produced per year, at a final cost of $0.30 per liter. This scenario had a carbon conversion of 74%. Finally, the third scenario had installed capital costs of $123.3 million and operating costs of $40.2 million per year. The co-product credit for this scenario is $18 million per year, for 18 million liters of BTEX produced per year. With 70 million liters of biofuel produced per year, the net cost per liter of biofuel is $0.32. The carbon conversion for this ideal scenario is 78%. Based on these results, the MSP of the biofuel is between $3.52 and $3.86 per gallon, and the MSP of BTEX is between $1.65 and $2.00 per liter.

Equipment and operating costs are based on current commercial plants and technology levels. The cost increase is tied to an increasing carbon conversion, from 70% in the first scenario up to 78% in the third scenario. The C/O and C/H ratios also improve from the first scenario to the third scenario, indicating an improvement in the final product quality as well. This improved recovery is tied to improving technology across the board, and therefore increases costs as well as the amount of extractant, hydrogen, etc. that are consumed by the process.

In this study, we examined the viability of producing BTEX as a co-product via separation and treatment of the aqueous organics. Our analysis shows that the hydrotreatment of phenolics to BTEX represents a significant fraction of the equipment cost. The liquid-liquid extraction step presents the most significant technological

challenge, as well as the highest annual operating costs. This technology needs further development; separation efficiencies need to be increased and the modeling also requires improvement. Overall, lignin and hydrothermal liquefaction show promise, as a potential biofuel feedstock and conversion process. Although BTEX is worth more than fuel, the technology is not advanced enough to produce BTEX without significant extra costs. Although overall carbon conversion is increased, the current state of the technology makes the incremental cost higher than the returns generated by the BTEX co-product.

6.7 References

[1] Hubbard, E., The utilisation of wood-waste. 1902: Scott, Greenwood & Company.

[2] Berl, E., Production of oil from plant material. Science, 1944. 99(2573): p. 309-312.

[3] Elliott, D.C., Historical developments in hydroprocessing bio-oils. Energy & Fuels, 2007. 21(3): p. 1792-1815.

[4] Nelson, D.A., et al., Application of direct thermal liquefaction for the conversion of cellulosic biomass. Industrial & engineering chemistry product research and development, 1984. 23(3): p. 471-475.

[5] Andersen, P.N., Kjeld, Philip-April 3, 1912, To October 24, 1989. 1990, Natl Forening Danmarks Natl Bank Havenengade 5, DK-1093 Copenhagen, Denmark. p. 137-147.

[6] Nielsen, R.P., G. Olofsson, and E.G. Søgaard, CatLiq–High pressure and temperature catalytic conversion of biomass: The CatLiq technology in relation to other thermochemical conversion technologies. Biomass and bioenergy, 2012. 39: p. 399-402.

[7] Wright, M.M., et al., Techno-economic analysis of biomass fast pyrolysis to transportation fuels. Fuel, 2010. 89: p. S2-S10.

[8] Valmet (2015). Personal communication.

[9] Pandey, M.P. and C.S. Kim, Lignin depolymerization and conversion: a review of thermochemical methods. Chemical Engineering & Technology, 2011. 34(1): p. 29-41.

[10] Carr, A.G., R. Mammucari, and N. Foster, A review of subcritical water as a solvent and its utilisation for the processing of hydrophobic organic compounds. Chemical Engineering Journal, 2011. 172(1): p. 1-17.

[11] Möller, M., et al., Subcritical water as reaction environment: fundamentals of hydrothermal biomass transformation. ChemSusChem, 2011. 4(5): p. 566-579.

[12] Toor, S.S., L. Rosendahl, and A. Rudolf, Hydrothermal liquefaction of biomass: a review of subcritical water technologies. Energy, 2011. 36(5): p. 2328-2342.

[13] Fang, Z., et al., Reaction chemistry and phase behavior of lignin in high-temperature and supercritical water. Bioresource Technology, 2008. 99(9): p. 3424-3430.

[14] Okuda, T., et al., Estimation of aboveground biomass in logged and primary lowland rainforests using 3-D photogrammetric analysis. Forest Ecology and Management, 2004. 203(1): p. 63-75.

[15] Saisu, M., et al., Conversion of lignin with supercritical water− phenol mixtures. Energy & Fuels, 2003. 17(4): p. 922-928.

[16] Pińkowska, H., P. Wolak, and A. Złocińska, Hydrothermal decomposition of alkali lignin in sub-and supercritical water. Chemical engineering journal, 2012. 187: p. 410-414.

[17] Yong, T.L.-K. and Y. Matsumura, Kinetic analysis of lignin hydrothermal conversion in sub-and supercritical water. Industrial & Engineering Chemistry Research, 2013. 52(16): p. 5626-5639.

[18] Lavoie, J.-M., W. Baré, and M. Bilodeau, Depolymerization of steam-treated lignin for the production of green chemicals. Bioresource technology, 2011. 102(7): p. 4917-4920.

[19] Miller, J., et al., Sandia National Laboratories Report SAND2002-1317. 2002, USA.

[20] Schmidl, C., et al., Chemical characterisation of fine particle emissions from wood stove combustion of common woods growing in mid-European Alpine regions. Atmospheric Environment, 2008. 42(1): p. 126-141.

[21] Unkelbach, G., et al. Catalyzed hydrothermal degradation of lignins from biorefineries to aromatic compounds. in 11th European Workshop on Lignocellulosics and Pulp. 2010.

[22] Azadi, P., et al., Liquid fuels, hydrogen and chemicals from lignin: A critical review. Renewable and Sustainable Energy Reviews, 2013. 21: p. 506-523.

[23] Roberts, D. and D. Harris, High-pressure char gasification kinetics: CO inhibition of the C–CO2 reaction. Energy & Fuels, 2011. 26(1): p. 176-184.

[24] Beauchet, R., F. Monteil-Rivera, and J. Lavoie, Conversion of lignin to aromatic-based chemicals (L-chems) and biofuels (L-fuels). Bioresource technology, 2012. 121: p. 328-334.

[25] Belkheiri, T., et al., Effect of pH on Kraft lignin depolymerisation in subcritical water. Energy & Fuels, 2016. 30(6): p. 4916-4924.

[26] Lehr, V., et al., Catalytic dehydration of biomass-derived polyols in sub- and supercritical water. Catalysis Today, 2007. 121(1): p. 121-129.

[27] Funkenbusch, L.T., Mullins, M.E., Salam, M.A., Olsson, L., Hydrotreatment of Pyrolysis Oil Model Compounds over Pt/Al_2O_3 and Pd/C Catalysts: Part I: Batch Reactors, *Industrial & Engineering Chemistry Research*, submitted September 2017.

[28] Goudriaan, F. and D. Peferoen, Liquid fuels from biomass via a hydrothermal process. Chemical Engineering Science, 1990. 45(8): p. 2729-2734.

[29] Boocock, D. and K. Sherman, Further aspects of powdered poplar wood liquefaction by aqueous pyrolysis. The Canadian Journal of Chemical Engineering, 1985. 63(4): p. 627-633.

[30] Belkheiri, T., Lignin Depolymerisation in Near-critical Water to Produce Biofuel and Chemicals: Effect of Co-solvent and PH. 2015, Department of Heat and Power Technology, Chalmers University of Technology.

[31] Ding, Z.-Y., S.N. Aki, and M.A. Abraham, Catalytic supercritical water oxidation: phenol conversion and product selectivity. Environmental science & technology, 1995. 29(11): p. 2748-2753.

[32] Joffres, B., et al., Thermochemical conversion of lignin for fuels and chemicals: A review. Oil & Gas Science and Technology–Revue d'IFP Energies nouvelles, 2013. 68(4): p. 753-763.

[33] Yan, N., et al., Selective Degradation of Wood Lignin over Noble‐Metal Catalysts in a Two‐Step Process. ChemSusChem, 2008. 1(7): p. 626-629.

[34] Elliott, D.C., et al., Hydrothermal liquefaction of biomass: developments from batch to continuous process. Bioresource technology, 2015. 178: p. 147-156.

[35] Belkheiri, T., et al., Kraft lignin depolymerization in near-critical water: effect of changing co-solvent. Cellulose Chemistry and Technology, 2014. 48(9-10): p. 813-818.

[36] Zhu, Y., et al., Techno-economic analysis of liquid fuel production from woody biomass via hydrothermal liquefaction (HTL) and upgrading. Applied Energy, 2014. 129: p. 384-394.

[37] Preem (2016). Personal communication.

[38] Levenspiel, O., Chemical reaction engineering. Industrial & engineering chemistry research, 1999. 38(11): p. 4140-4143.

[39] Maschietti, M., et al. Catalytic hydrothermal conversion of LignoBoost Kraft lignin for the production of bio-oil and aromatic chemicals. in International Chemical Recovery Conference. 2014.

[40] Winjobi, O., et al., Techno‐economic assessment of the effect of torrefaction on fast pyrolysis of pine. Biofuels, Bioproducts and Biorefining, 2016. 10(2): p. 117-128.

[41] Funkenbusch, L.T., Shonnard, D.R., Mullins, M.E., Metsa, J.C., Robinson, J., Kinetic Modeling of the Production of Hydrorenewable Diesel from Plant Oils, *Energy & Fuels*, in preparation for submission October 2017.

[42] Srettiwat, N. Simulation of separation unit for chemical products from lignin depolymerisation with economic evaluation using Aspen Plus. Department of Heat and Power Technology, Chalmers University of Technology, 2016.

[43] Funkenbusch, L.T., Mullins, M.E., Hydrotreatment of Pyrolysis Oil Model Compounds over Pt/Al2O3 and Pd/C Catalysts: Part II: Trickle Bed Reactors, Industrial & Engineering Chemistry Research, in preparation for submission October 2017.

[44] Nguyen, T.D.H. Catalytic Conversion of LignoBoost Kraft Lignin into Liquid Products in Near-Critical Water: The Effects of K_2CO_3 Concentration and Reaction Temperature. Department of Chemical and Biological Engineering, Chalmers University of Technology, 2014.

[45] Greminger, D.C., et al., Solvent extraction of phenols from water. Industrial & Engineering Chemistry Process Design and Development, 1982. 21(1): p. 51-54.

[46] Peters, M.S., et al., Plant design and economics for chemical engineers. Vol. 4. 1968: McGraw-Hill New York.

[47] chemengonline.com. (2017). The Chemical Engineering Plant Cost Index - Chemical Engineering. [online] Available at: http://www.chemengonline.com/pci-home.

[48] Bls.gov. (2017). U.S. Bureau of Labor Statistics. [online] Available at: https://www.bls.gov/.

[49] Knorr, D., J. Lukas, and P. Schoen, Production of Advanced Biofuels via Liquefaction-Hydrothermal Liquefaction Reactor Design: April 5, 2013. 2013, National Renewable Energy Laboratory (NREL), Golden, CO.

[50] Alfalaval.us. (2017). United States. [online] Available at: http://www.alfalaval.us/.

[51] Vispute, T., Pyrolysis oils: characterization, stability analysis, and catalytic upgrading to fuels and chemicals. 2011.

[52] Jones, S.B., et al., Process design and economics for the conversion of lignocellulosic biomass to hydrocarbon fuels: fast pyrolysis and hydrotreating bio-oil pathway. 2013, Pacific Northwest National Laboratory (PNNL), Richland, WA (US).

[53] Zacher, A.H., et al., A review and perspective of recent bio-oil hydrotreating research. Green Chemistry, 2014. 16(2): p. 491-515.

[54] Furimsky, E., Deactivation of molybdate catalyst during hydrodeoxygenation of tetrahydrofuran. Industrial & Engineering Chemistry Product Research and Development, 1983. 22(1): p. 34-38.

[55] Furimsky, E., Catalytic hydrodeoxygenation. Applied Catalysis A: General, 2000. 199(2): p. 147-190.

[56] He, Z. and X. Wang, Hydrodeoxygenation of model compounds and catalytic systems for pyrolysis bio-oils upgrading. Catalysis for sustainable energy, 2012. 1: p. 28-52.

[57] Huber, G.W., et al., Production of liquid alkanes by aqueous-phase processing of biomass-derived carbohydrates. Science, 2005. 308(5727): p. 1446-1450.

[58] Normalización, O.I.d., ISO 14044: Environmental Management, Life Cycle Assessment, Requirements and Guidelines. 2006: ISO.

[59] Verso Paper (2017). Personal communication.

[60] EIA.gov. (2017). *U.S. Gasoline and Diesel Retail Prices*. [online] Available at: https://www.eia.gov/dnav/pet/pet_pri_gnd_dcus_nus_w.htm.

7. Conclusions and Future Work

7.1 Conclusions

7.1.1 Plant Oils

A lumped parameter, Langmuir-Hinshelwood model was developed to model a multicomponent, multiphase, continuous reactor for the hydrotreatment of plant oils to produce renewable diesel fuel over a range of process conditions. Oleic acid, a common fatty acid found in plant oils, was used as a model compound over a Pt/Al_2O_3 catalyst, and Arrhenius rate constants were calculated using experimental data over the temperature range examined (250-375°C). The reactor was run under 6.7 bar of pressure, with argon and 5% hydrogen. The utility of this model was demonstrated by running a test case to match literature sources' hydrogen consumption and final product composition. The model also successfully predicts pathway shifts across a range of temperatures. With a small amount of experimental data and preliminary testing, this process-level model for plant oil hydrotreatment can predict product composition, hydrogen and energy consumption for a specific feedstock and set of reactor operating conditions in a way that commercial "black box" simulation programs, such as Aspen® and Unisim®, cannot. These predictions can be used to help design production facilities and perform analyses of a specific product composition target or biomass feedstock.

7.1.2 Pyrolysis Oils - Batch

The Langmuir-Hinshelwood model was adapted for the hydrotreatment of pyrolysis oil model compounds in a Parr batch reactor at Chalmers University. Experiments were run for four hours over a range of temperatures (250-350°C), at 50 bar of hydrogen, two different catalysts (Pt/Al_2O_3 and Pd/C), and with three common pyrolysis oil model compounds (anisole, m-cresol, and phenol). This study also considered two blends of model compounds; no interactions were seen between the compounds, therefore, the lumped parameter approach was deemed valid. Arrhenius rate constants were calculated using experimental data. When compared to an independent data set, the model fit the data with correlation coefficients ranging from 0.80 to 0.98. Once again, the model's ability to predict pathway shifts based on process conditions, especially temperature, is crucial for assessing the sustainability of the process, or for optimizing the reactor conditions.

7.1.3 Pyrolysis Oil - Continuous

In this part of the study, a continuous packed bed reactor was used in order to continue the earlier batch reactor work while also moving closer to reactors used in industry. First, a differential reactor was built in order to examine the intrinsic reaction kinetics of the system at low conversions and residence times. Powdered Pd/C and Pt/Al_2O_3 were tested as potential catalysts for this system. A pilot scale reactor was then constructed, with high conversions and a pellet Pt/Al_2O_3 catalyst. A similar suite of experiments was run with the pilot reactor to study rate kinetics in a more realistic system that included mass transfer limitations. Each reactor's data was fit to the Langmuir-Hinshelwood

model discussed in the previous chapter. When compared to the data, the model fit well (within 1%) for both reactors. However, this study demonstrated the need to perform a small set of experiments for each reactor of interest. Given a small set of preliminary experiments, however, this process-level model can be used to quickly and inexpensively analyze reactor conditions and catalysts for life cycle and technoeconomic assessments.

7.1.4 TEA

The technoeconomic analysis presented in this chapter studied the production of transportation fuel and commodity chemicals from the hydrothermal liquefaction and subsequent hydrotreatment of lignin, a byproduct from pulping processes. We considered a lignin depolymerization process in near-critical water, with a lignin feedstock directly from a pulp mill. Three scenarios were generated: a current technology level, a cutting edge technology level, and an idealized third case based on oxygen content goals set by refiners. Carbon conversion ranged from 70% in the first scenario to 78% in the third scenario. Equipment and operating costs were calculated for all three scenarios, using current commercial plants and technology levels, and were based on a production from 65 million liters to 70 million liters of biofuel produced per year. A per liter cost of $0.28 to $0.32 were calculated; this cost includes the commodity chemical co-product credit. The cost increase is due to the increasing carbon recovery, based on C/O and C/H ratios. As a result of the improved product quality, costs increase as the amount of consumables (extractant, catalyst, hydrogen, etc.) rises. Because this

process would be tied into the end of a pulp mill and, ideally, would have an "over the fence" arrangement with a refinery to process the bio-oil product, it presents an attractive commercial prospect, as green-field scenarios are avoided for both parties. In our study, however, the bio-oil hydrotreatment has been included in the cost analyses and, along with the phenolics hydrotreatment reactor, present a significant fraction of the installed equipment cost. The liquid-liquid extraction step has the highest annual operating costs of the process. The LLE technology also needs further research and development to increase separation efficiencies. Overall, however, this process shows promise as a source for biofuel and as a potential revenue source for pulp mills and refineries.

7.1.5 Overall Conclusions

Beginning with the batch reactor and moving to the continuous reactor, a Langmuir-Hinshelwood model has been developed to simulate the hydrotreatment of various biological oils. This model can accurately predict product distributions and selectivities, greenhouse gas emissions, heating or cooling load, and hydrogen consumption for a given input and set of reactor conditions. The major obstacle to this model is the lack of necessary kinetic rate information. This data must be collected for a specific catalyst in a continuous system large enough to test apparent activation energies, rather than the intrinsic rate kinetics seen in a smaller reactor where mass transfer limitations cannot be properly modeled. Although many hydrotreatment studies have been performed, both on plant and pyrolysis oil, there are very few studies that can be translated into rate kinetics

for this type of process-level model. Instead, studies need to be performed on the system of interest to tune and optimize the process conditions for a particular feedstock or product composition, or to improve sustainability. With only a few experimental tests, the hydrotreatment of many biological feedstocks can be modeled, including plant oils, pyrolysis oil, tall oil and algal oils. This process-level modeling can be incorporated into a complete biorefinery design or assessment of an entire process, as demonstrated in the techno-economic analysis in Chapter 6.

7.2 Recommendations for Future Work

The catalysts studied in this work are standard catalysts used in hydrotreatment. Ideally, however, novel catalysts designed especially for hydrodeoxygenation of biological feedstocks could be developed. These catalysts would need to be resistant to poisoning from water and minerals (ash) in the feedstock and coking. Optimal catalysts would also exhibit high activity for hydrodeoxygenation, without saturating the ring of the aromatic compound. For example, there has been promising work on supported pseudomorphic overlayer catalysts. Currently, this work has only been performed in the vapor phase, in small (<10 mm diameter) continuous reactors at near-atmospheric pressures, or small batch reactors.[1,2,3,4,5] Ideally, studies would be performed on a larger scale and at higher pressures, to more accurately approximate industrial hydrotreatment conditions. There is also some interest in reactions other than hydrotreatment. Condensation and dehydration reactions, for example, have been of some interest to produce various compounds from biological oils.[6]

A major barrier to this work is the separation and extraction efficiencies of the biological oils. Pyrolysis oil and hydrothermal liquefaction oil, for example, contain significant amounts of water that must be removed prior to hydrotreatment, as water is a serious catalyt poison. Separation technologies are costly, as discussed in Chapter 6, and the thermodynamics of the process are not well understood or modeled in commercial simulators. Improvements to this technology would be greatly beneficial. Another option is a stabilization step prior to hydrotreating, which would be at milder temperatures and with a less vulnerable catalyst; this approach is seen in the biofuel hydrotreatment reactor in Chapter 6.

An integrated biorefinery design can improve the feasibility of biological feedstocks for transportation fuel. Integration benefits both the supplier, who can dispose of process byproducts and generate revenue, and the refiner, who can blend the biofuels into their existing streams and improve their process sustainability. The kinetic model developed in this work can be used to help design and assess these biorefineries. It would also be advantageous to develop a specialized catalyst to handle blends of petroleum and bio-oils. Conventional petroleum catalysts are sulfided and require the presence of some sulfur in the reactor to maintain activity. Noble metal catalysts typically seen in bio-oil research are easily poisoned by sulfur and are too expensive to use at the scale necessary in industrial refiners. Some combination of the two would be ideal, and the novel catalyst research mentioned earlier shows promise.

7.3 References

[1] Lai, Q., C. Zhang, and J.H. Holles, Hydrodeoxygenation of guaiacol over Ni@Pd and Ni@Pt bimetallic overlayer catalysts. Applied Catalysis A: General, 2016. 528(Supplement C): p. 1-13.

[2] Latusek, M.P., et al., Correlation of H2 heat of adsorption and ethylene hydrogenation activity for supported Re@Pd overlayer catalysts. Journal of Catalysis, 2009. 263(2): p. 306-314.

[3] Skoglund, M.D., et al., Characterization of Ni@Pt and Co@Pt overlayer catalysts using adsorption, reactivity descriptors, and X-ray absorption spectroscopy. Applied Catalysis A: General, 2013. 467(Supplement C): p. 355-362.

[4] Zhang, C., Q. Lai, and J.H. Holles, Bimetallic overlayer catalysts with high selectivity and reactivity for furfural hydrogenation. Catalysis Communications, 2017. 89: p. 77-80.

[5] González-Borja, M.Á. and D.E. Resasco, Anisole and guaiacol hydrodeoxygenation over monolithic Pt–Sn catalysts. Energy & Fuels, 2011. 25(9): p. 4155-4162.

[6] Chheda, J. N.; Dumesic, J. A., An overview of dehydration, aldol-condensation and hydrogenation processes for production of liquid alkanes from biomass-derived carbohydrates. Catalysis Today 2007, 123 (1), 59-70.

8. Supplemental Information

8.1 Tabulated Pyrolysis Oil Literature Review

Table 8-1. Reactor Conditions & Type

Temperature (°C)	Pressure	Reactor Type	Reference
350	1 atm	batch	[1]
300	4 MPa	continuous	[2,3]
320	17 MPa	batch	[4]
400	7 MPa	batch	[5]
260-300	7 MPa	batch	[6]
300	2.85 MPa	continuous	[7]
300	0.14 MPa	continuous	[8,9,10,11]
250	6-9 MPa	batch	[12]
300	20 MPa	batch	[13]
240	4 MPa	batch	[14]
400	1 atm	continuous	[15]

Table 8-2. Model Compounds

Model Compound	Reference
Guaiacol	[2,3]

Guaiacol	[4]
Guaiacol	[5]
M-Cresol	[16]
Guaiacol	[17]
Cresol, Xylenol	[18]
Guaiacol	[19]
Phenol	[20]
Cresol, phenol, guaiacol, eugenol	[21]
2-methyltetrahydrofuran	[22]
Phenolic dimers	[23]
Guaiacol	[6]
Cresol, Xylenol	[7]
M-Cresol	[24]
Guaiacol	[8,9,11]
Eugenol	[10]
Anisole	[25]
Guaiacol, Anisole, Methylanisole, Cyclohexanone	[26]
Phenol, Methyl heptanoate	[12]
Phenol	[27]
Phenol, cresol, guaiacol	[28]
Anisole	[29]

Phenol in water	[30]
Guaiacol	[14]

Table 8-3. Catalyst & Catalyst Types

Catalyst / Catalyst Type	**Reference**
HZSM5	[31]
bimetallic	[1,32]
Sulfided CoMo	[33]
Sulfided CoMo	[2,3]
Nickel-based	[4]
Sulfided CoMo	[5]
Sulfided CoMo	[18]
Noble metal on support	[19]
ZSM5	[34]
CoMo, NiMo, sulfided	[6]
NiFe	[35]
Ni/ZSM5	[36]
Sulfided CoMo	[7]
Pt/SiO2	[24]
Pt/Al2O3	[8,9]
Pt/MgO	[11]

HY zeolite	[10]
Pt/Al2O3	[26]
Zeolites	[37]
Ni-Mo-B	[38]
Co-Mo-B	[39]
Ru/Al2O3, Ru/C	[13,27]
sulfided Mo	[28]
Ni on varying supports	[29]
Ni/HZSM5	[40]
Ni and NiCu on ZrO2-SiO2	[14,30]
Raney Ni (hydrogenation) & Nafion SiO2 (Bronsted acid)	[41]
Metal Phosphides	[42]
Noble metal catalysts	[43]
Ni/HZSM5	[44]
Ni/HZSM5, Ni/Al2O3-HZSM5	[45]
Pt/H-Beta	[15]

8.1.1 References

[1] A. R. Ardiyanti, S. A. Khromova, R. H. Venderbosch, V. A. Yakovlev, and H. J. Heeres, "Catalytic hydrotreatment of fast-pyrolysis oil using non-sulfided

bimetallic Ni-Cu catalysts on a δ-Al2O3 support," Applied Catalysis B: Environmental, vol. 117–118, pp. 105-117, 5/18/ 2012.

[2] V. N. Bui, D. Laurenti, P. Afanasiev, and C. Geantet, "Hydrodeoxygenation of guaiacol with CoMo catalysts. Part I: Promoting effect of cobalt on HDO selectivity and activity," Applied Catalysis B: Environmental, vol. 101, pp. 239-245, 2011.

[3] V. N. Bui, D. Laurenti, P. Delichère, and C. Geantet, "Hydrodeoxygenation of guaiacol: Part II: Support effect for CoMoS catalysts on HDO activity and selectivity," Applied Catalysis B: Environmental, vol. 101, pp. 246-255, 2011.

[4] M. Bykova, O. Bulavchenko, D. Y. Ermakov, M. Y. Lebedev, V. Yakovlev, and V. Parmon, "Guaiacol hydrodeoxygenation in the presence of Ni-containing catalysts," Catalysis in Industry, vol. 3, pp. 15-22, 2011.

[5] A. Centeno, E. Laurent, and B. Delmon, "Influence of the Support of CoMo Sulfide Catalysts and of the Addition of Potassium and Platinum on the Catalytic Performances for the Hydrodeoxygenation of Carbonyl, Carboxyl, and Guaiacol-Type Molecules," Journal of Catalysis, vol. 154, pp. 288-298, 7// 1995.

[6] E. Laurent and B. Delmon, "Study of the hydrodeoxygenation of carbonyl, carboxylic and guaiacyl groups over sulfided CoMo/γ-Al2O3 and NiMo/γ-Al2O3 catalysts. I: Catalytic reaction schemes," Applied catalysis. A, General, vol. 109, pp. 77-96, 1994.

[7] F. Massoth, P. Politzer, M. Concha, J. Murray, J. Jakowski, and J. Simons, "Catalytic hydrodeoxygenation of methyl-substituted phenols: Correlations of

kinetic parameters with molecular properties," The Journal of Physical Chemistry B, vol. 110, pp. 14283-14291, 2006.

[8] T. Nimmanwudipong, R. C. Runnebaum, D. E. Block, and B. C. Gates, "Catalytic conversion of guaiacol catalyzed by platinum supported on alumina: reaction network including hydrodeoxygenation reactions," Energy & fuels, vol. 25, pp. 3417-3427, 2011.

[9] T. Nimmanwudipong, R. C. Runnebaum, D. E. Block, and B. C. Gates, "Catalytic reactions of guaiacol: reaction network and evidence of oxygen removal in reactions with hydrogen," Catalysis letters, vol. 141, pp. 779-783, 2011.

[10] T. Nimmanwudipong, R. C. Runnebaum, S. E. Ebeler, D. E. Block, and B. C. Gates, "Upgrading of Lignin-Derived Compounds: Reactions of Eugenol Catalyzed by HY Zeolite and by Pt/γ-Al2O3," Catalysis letters, vol. 142, pp. 151-160, 2012.

[11] T. Nimmanwudipong, C. Aydin, J. Lu, R. C. Runnebaum, K. C. Brodwater, N. D. Browning, et al., "Selective Hydrodeoxygenation of Guaiacol Catalyzed by Platinum Supported on Magnesium Oxide," Catalysis letters, vol. 142, pp. 1190-1196, 2012.

[12] E.-M. Ryymin, M. L. Honkela, T.-R. Viljava, and A. O. I. Krause, "Competitive reactions and mechanisms in the simultaneous HDO of phenol and methyl heptanoate over sulphided NiMo/γ-Al< sub> 2</sub> O< sub> 3</sub>," Applied Catalysis A: General, vol. 389, pp. 114-121, 2010.

[13] J. Wildschut, F. H. Mahfud, R. H. Venderbosch, and H. J. Heeres, "Hydrotreatment of fast pyrolysis oil using heterogeneous noble-metal catalysts," Industrial & Engineering Chemistry Research, vol. 48, pp. 10324-10334, 2009.

[14] X. Zhang, T. Wang, L. Ma, Q. Zhang, Y. Yu, and Q. Liu, "Characterization and catalytic properties of Ni and NiCu catalysts supported on ZrO2–SiO2 for guaiacol hydrodeoxygenation," Catalysis Communications, vol. 33, pp. 15-19, 3/5/ 2013.

[15] X. Zhu, L. L. Lobban, R. G. Mallinson, and D. E. Resasco, "Bifunctional transalkylation and hydrodeoxygenation of anisole over a Pt/HBeta catalyst," Journal of Catalysis, vol. 281, pp. 21-29, 2011.

[16] A. J. Foster, P. T. Do, and R. F. Lobo, "The synergy of the support acid function and the metal function in the catalytic hydrodeoxygenation of m-cresol," Topics in Catalysis, vol. 55, pp. 118-128, 2012.

[17] A. G. Gayubo, A. T. Aguayo, A. Atutxa, R. Aguado, and J. Bilbao, "Transformation of Oxygenate Components of Biomass Pyrolysis Oil on a HZSM-5 Zeolite. I. Alcohols and Phenols," Industrial & Engineering Chemistry Research, vol. 43, pp. 2610-2618, 2004/05/01 2004.

[18] B. Gevert, J. Otterstedt, and F. Massoth, "Kinetics of the HDO of methyl-substituted phenols," Applied catalysis, vol. 31, pp. 119-131, 1987.

[19] A. Gutierrez, R. K. Kaila, M. L. Honkela, R. Slioor, and A. O. I. Krause, "Hydrodeoxygenation of guaiacol on noble metal catalysts," Catalysis Today, vol. 147, pp. 239-246, 10/15/ 2009.

[20] D.-Y. Hong, S. J. Miller, P. K. Agrawal, and C. W. Jones, "Hydrodeoxygenation and coupling of aqueous phenolics over bifunctional zeolite-supported metal catalysts," Chem. Commun., vol. 46, pp. 1038-1040, 2010.

[21] J. Horáček, G. Šťávová, V. Kelbichová, and D. Kubička, "Zeolite-Beta-supported platinum catalysts for hydrogenation/hydrodeoxygenation of pyrolysis oil model compounds," Catalysis Today, vol. 204, pp. 38-45, 2013.

[22] A. Iino, A. Cho, A. Takagaki, R. Kikuchi, and S. T. Oyama, "Kinetic studies of hydrodeoxygenation of 2-methyltetrahydrofuran on a Ni 2 P/SiO 2 catalyst at medium pressure," Journal of Catalysis, vol. 311, pp. 17-27, 2014.

[23] H. Kawamoto, S. Horigoshi, and S. Saka, "Pyrolysis reactions of various lignin model dimers," Journal of wood science, vol. 53, pp. 168-174, 2007.

[24] L. Nie and D. E. Resasco, "Kinetics and mechanism of m-cresol hydrodeoxygenation on a Pt/SiO 2 catalyst," Journal of Catalysis, vol. 317, pp. 22-29, 2014.

[25] R. C. Runnebaum, R. J. Lobo-Lapidus, T. Nimmanwudipong, D. E. Block, and B. C. Gates, "Conversion of anisole catalyzed by platinum supported on alumina: The reaction network," Energy & fuels, vol. 25, pp. 4776-4785, 2011.

[26] R. C. Runnebaum, T. Nimmanwudipong, D. E. Block, and B. C. Gates, "Catalytic conversion of compounds representative of lignin-derived bio-oils: a reaction network for guaiacol, anisole, 4-methylanisole, and cyclohexanone conversion catalysed by Pt/γ-Al2O3," Catalysis Science & Technology, vol. 2, pp. 113-118, 2012.

[27] J. Wildschut, I. Melian-Cabrera, and H. Heeres, "Catalyst studies on the hydrotreatment of fast pyrolysis oil," Applied Catalysis B: Environmental, vol. 99, pp. 298-306, 2010.

[28] Y. Yang, H. a. Luo, G. Tong, K. J. Smith, and C. T. Tye, "Hydrodeoxygenation of Phenolic Model Compounds over MoS< sub> 2</sub> Catalysts with Different Structures," Chinese Journal of Chemical Engineering, vol. 16, pp. 733-739, 2008.

[29] Y. Yang, C. Ochoa-Hernández, A. Víctor, P. Pizarro, J. M. Coronado, and D. P. Serrano, "Effect of metal–support interaction on the selective hydrodeoxygenation of anisole to aromatics over Ni-based catalysts," Applied Catalysis B: Environmental, vol. 145, pp. 91-100, 2014.

[30] X. Zhang, Q. Zhang, T. Wang, L. Ma, Y. Yu, and L. Chen, "Hydrodeoxygenation of lignin-derived phenolic compounds to hydrocarbons over Ni/SiO 2–ZrO 2 catalysts," Bioresource technology, vol. 134, pp. 73-80, 2013.

[31] J. D. Adjaye and N. N. Bakhshi, "Production of hydrocarbons by catalytic upgrading of a fast pyrolysis bio-oil. Part I: Conversion over various catalysts," Fuel Processing Technology, vol. 45, pp. 161-183, 12// 1995.

[32] A. R. Ardiyanti, S. A. Khromova, R. H. Venderbosch, V. A. Yakovlev, I. V. Melián-Cabrera, and H. J. Heeres, "Catalytic hydrotreatment of fast pyrolysis oil using bimetallic Ni–Cu catalysts on various supports," Applied catalysis A: general, vol. 449, pp. 121-130, 12/27/ 2012.

[33] E. G. Baker and D. C. Elliott, "Catalytic hydrotreating of biomass-derived oils," ACD, Div. Fuel Chem, vol. 32, pp. 257-263, 1987.

[34] K. L. Hew, A. M. Tamidi, S. Yusup, K. T. Lee, and M. M. Ahmad, "Catalytic cracking of bio-oil to organic liquid product (OLP)," Bioresource technology, vol. 101, pp. 8855-8858, 11// 2010.

[35] S. Leng, X. Wang, X. He, L. Liu, Y. e. Liu, X. Zhong, et al., "NiFe/γ-Al2O3: A universal catalyst for the hydrodeoxygenation of bio-oil and its model compounds," Catalysis Communications, vol. 41, pp. 34-37, 11/5/ 2013.

[36] A. J. Maia, B. Louis, Y. L. Lam, and M. M. Pereira, "Ni-ZSM-5 catalysts: Detailed characterization of metal sites for proper catalyst design," Journal of Catalysis, vol. 269, pp. 103-109, 1/1/ 2010.

[37] S. Vitolo, M. Seggiani, P. Frediani, G. Ambrosini, and L. Politi, "Catalytic upgrading of pyrolytic oils to fuel over different zeolites," Fuel, vol. 78, pp. 1147-1159, 1999.

[38] W.-y. Wang, Y.-q. Yang, J.-g. Bao, and H.-a. Luo, "Characterization and catalytic properties of Ni–Mo–B amorphous catalysts for phenol hydrodeoxygenation," Catalysis Communications, vol. 11, pp. 100-105, 2009.

[39] W. Wang, Y. Yang, H. Luo, T. Hu, and W. Liu, "Amorphous Co–Mo–B catalyst with high activity for the hydrodeoxygenation of bio-oil," Catalysis Communications, vol. 12, pp. 436-440, 2011.

[40] X. Zhang, T. Wang, L. Ma, Q. Zhang, and T. Jiang, "Hydrotreatment of bio-oil over Ni-based catalyst," Bioresource technology, vol. 127, pp. 306-311, 2013.

[41] C. Zhao, Y. Kou, A. A. Lemonidou, X. Li, and J. A. Lercher, "Hydrodeoxygenation of bio-derived phenols to hydrocarbons using RANEY® Ni and Nafion/SiO2 catalysts," Chemical Communications, vol. 46, pp. 412-414, 2010.

[42] H. Zhao, D. Li, P. Bui, and S. Oyama, "Hydrodeoxygenation of guaiacol as model compound for pyrolysis oil on transition metal phosphide hydroprocessing catalysts," Applied catalysis A: general, vol. 391, pp. 305-310, 2011.

[43] C. Zhao, J. He, A. A. Lemonidou, X. Li, and J. A. Lercher, "Aqueous-phase hydrodeoxygenation of bio-derived phenols to cycloalkanes," Journal of Catalysis, vol. 280, pp. 8-16, 2011.

[44] C. Zhao and J. A. Lercher, "Upgrading Pyrolysis Oil over Ni/HZSM-5 by Cascade Reactions," Angewandte Chemie, vol. 124, pp. 6037-6042, 2012.

[45] C. Zhao, S. Kasakov, J. He, and J. A. Lercher, "Comparison of kinetics, activity and stability of Ni/HZSM-5 and Ni/Al_2O_3-HZSM-5 for phenol hydrodeoxygenation," Journal of Catalysis, vol. 296, pp. 12-23, 2012.

8.2 Plant Oil Data

This section contains the GC/FID data from the oleic acid experiments with Pt/Al_2O_3. They depict the output composition of the pilot scale reactor at each temperature, after normalizing to account for the solvent, and the resulting concentration used in the kinetic modeling. The LC/MS data was already displayed in Chapter 2 and is not shown here.

Table 8-4. Oleic Acid Data for Pt/Al_2O_3 at 250°C

Residence Time (min)	Compound	Normalized Fraction	C (mol/L)
20.8	heptadecanol	0.0122	0.0027
21.35	octadecanol	0.0057	0.0012
21.95	oleic acid	0.9632	0.2082
22.05	stearic acid	0.0188	0.0041

Table 8-5. Oleic Acid Data for Pt/Al_2O_3 at 300°C

Residence Time (min)	Compound	Normalized Fraction	C (mol/L)
20.8	heptadecanol	0.0425	0.0091
21.35	octadecanol	0.0079	0.0017
21.95	oleic acid	0.9208	0.1991
22.05	stearic acid	0.0287	0.0062

Table 8-6. Oleic Acid Data for Pt/Al_2O_3 at 350°C

Residence Time (min)	Compound	Normalized Fraction	C (mol/L)
20.8	heptadecanol	0.0600	0.0130
21.35	octadecanol	0.0448	0.0096
21.95	oleic acid	0.8846	0.1912
22.05	stearic acid	0.0107	0.0023

Table 8-7. Oleic Acid Data for Pt/Al_2O_3 at 375°C

Residence Time (min)	Compound	Normalized Fraction	C (mol/L)
20.8	heptadecanol	0.1286	0.0278
21.35	octadecanol	0.0020	0.0004
21.95	oleic acid	0.4329	0.0936
22.05	stearic acid	0.4364	0.0943

8.3 Pyrolysis Oil Data – Batch

For the sake of brevity, only certain graphs/results were included in Chapter 4. The supplemental data presented here is the all of the data discussed. This data was taken using a GC/MSD, with calibration standards also taken in order to quantify the data.

8.3.1 Anisole on 500 mg Pt/Al_2O_3

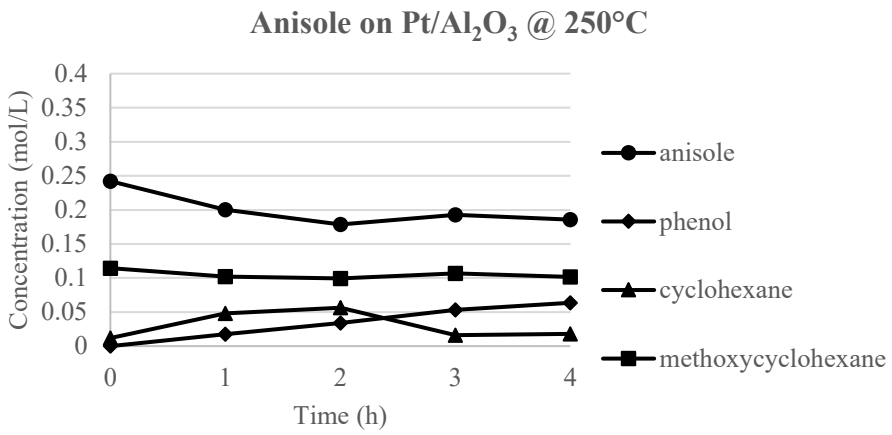

Figure 8-1. Batch Data for Anisole on 500 mg Pt/Al_2O_3 at 250°C

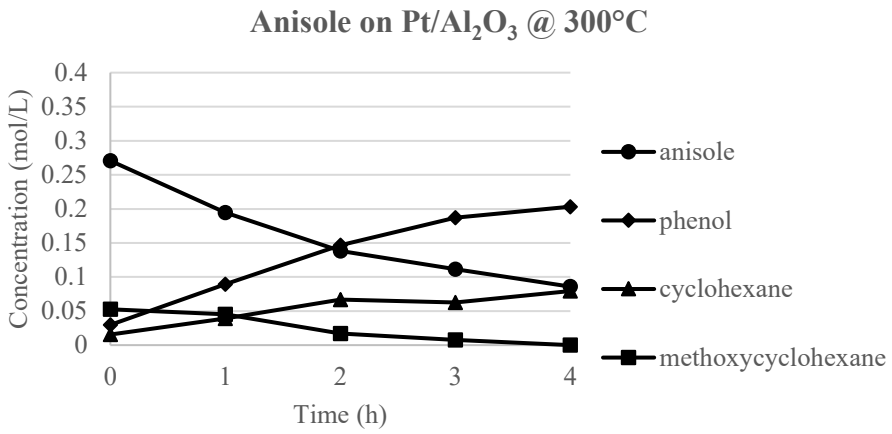

Figure 8-2. Batch Data for Anisole on 500 mg Pt/Al_2O_3 at 300°C

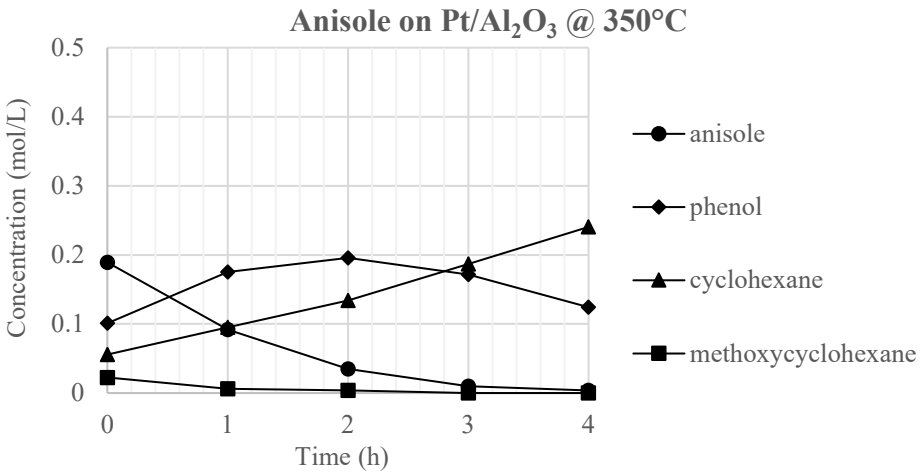

Figure 8-3. Batch Data for Anisole on 500 mg Pt/Al_2O_3 at 350°C

8.3.2 M-Cresol on 500 mg Pt/Al_2O_3

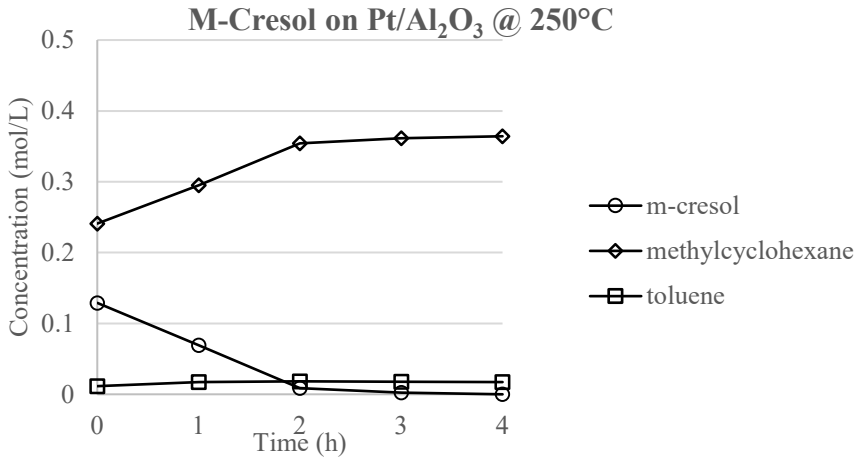

Figure 8-4. Batch Data for M-Cresol on 500 mg Pt/Al_2O_3 at 250°C

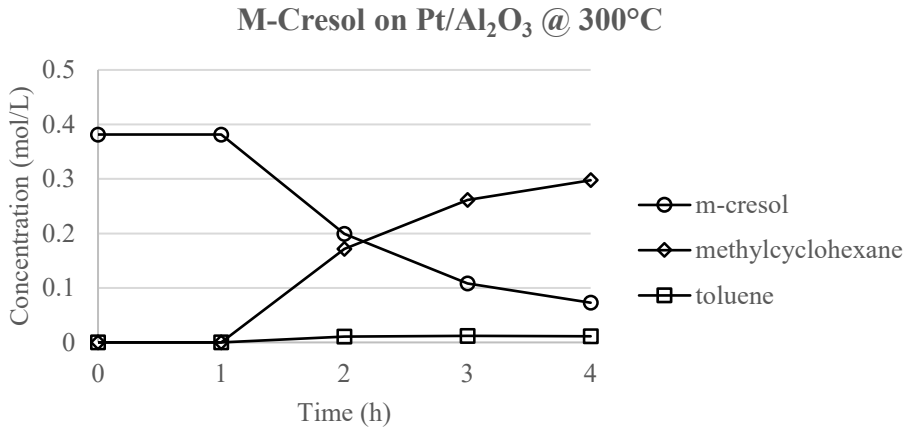

Figure 8-5. Batch Data for M-Cresol on 500 mg Pt/Al_2O_3 at 300°C

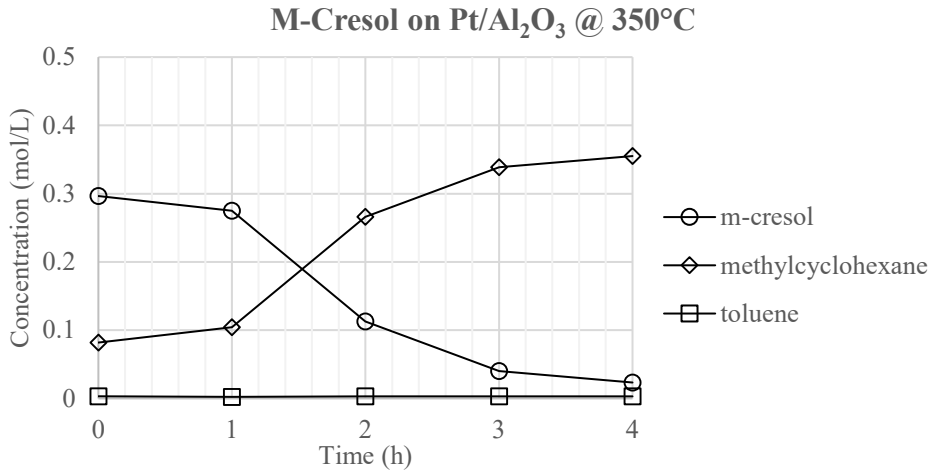

Figure 8-6. Batch Data for M-Cresol on 500 mg Pt/Al_2O_3 at 350°C

8.3.3 Phenol on 500 mg Pt/Al_2O_3

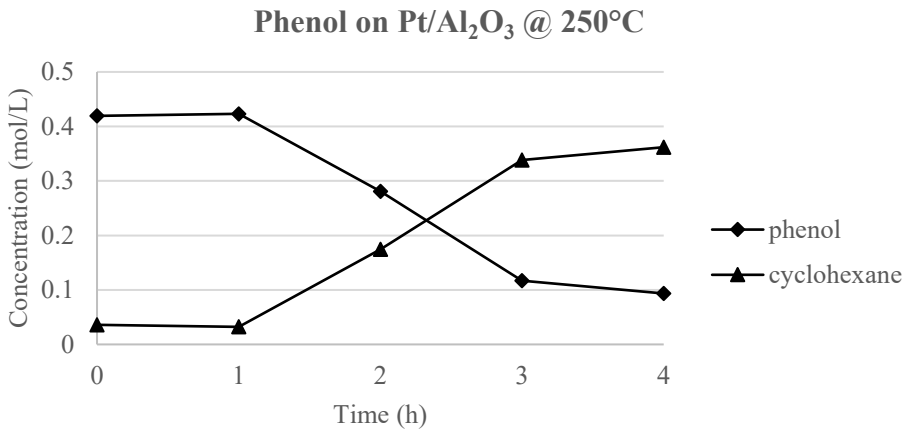

Figure 8-7. Batch Data for Phenol on 500 mg Pt/Al_2O_3 at 250°C

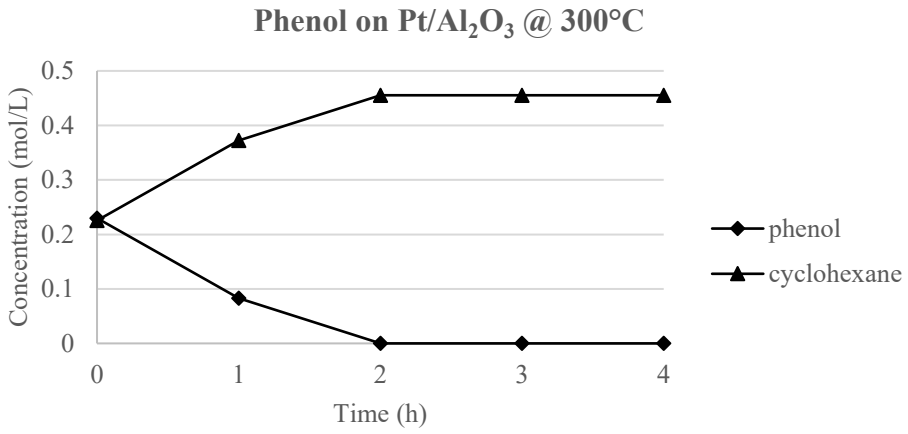

Figure 8-8. Batch Data for Phenol on 500 mg Pt/Al_2O_3 at 300°C

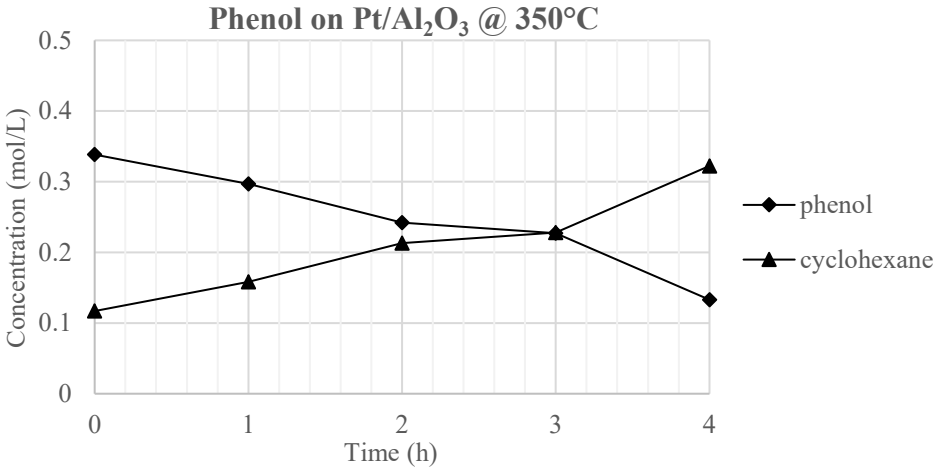

Figure 8-9. Batch Data for Phenol on 500 mg Pt/Al_2O_3 at 350°C

8.3.4 Anisole on 200 mg Pt/Al_2O_3

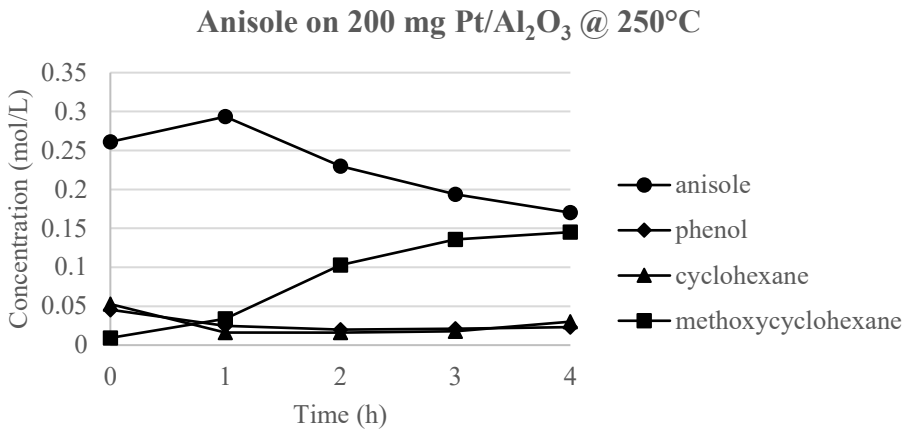

Figure 8-10. Batch Data for Anisole on 200 mg Pt/Al_2O_3 at 250°C

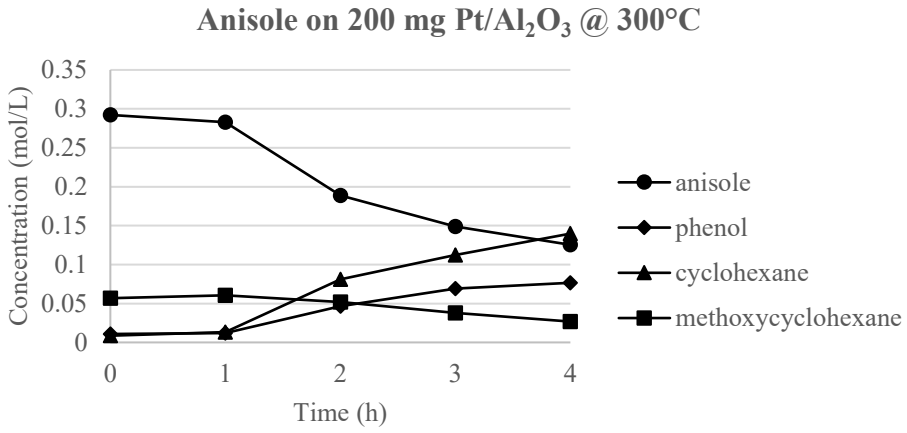

Figure 8-11. Batch Data for Anisole on 200 mg Pt/Al_2O_3 at 300°C

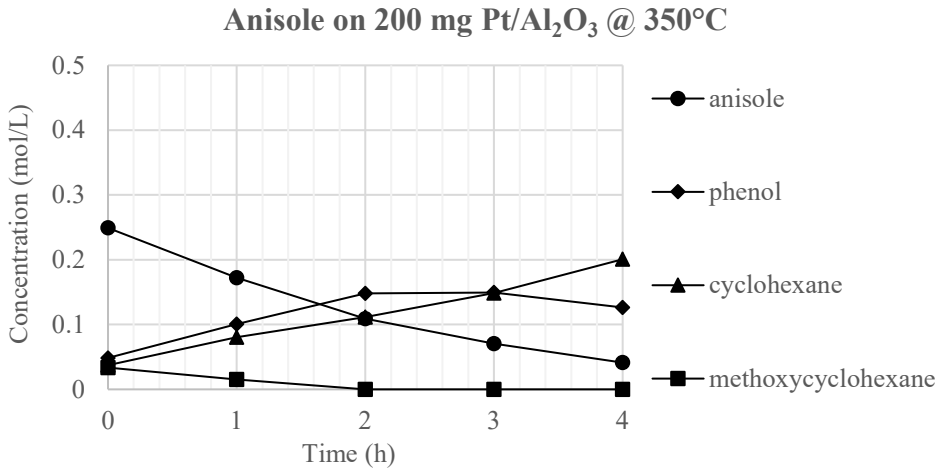

Figure 8-12. Batch Data for Anisole on 200 mg Pt/Al_2O_3 at 350°C

8.3.5 Anisole on 500 mg Pd/C

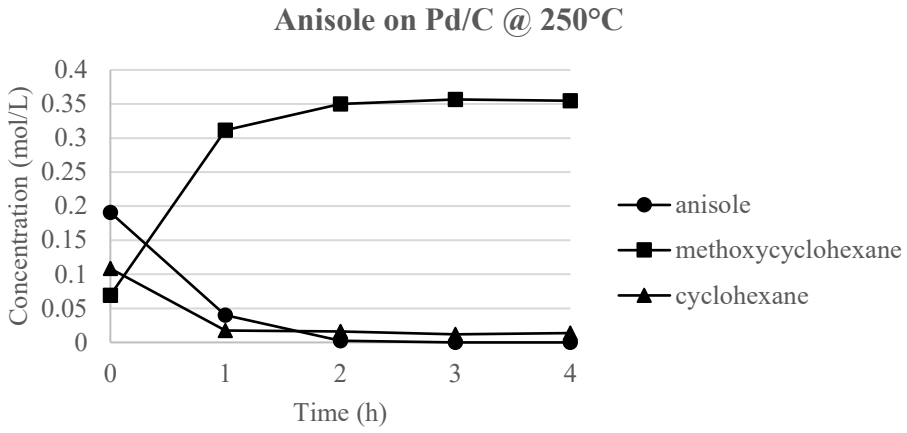

Figure 8-13. Batch Data for Anisole on 500 mg Pd/C at 250°C

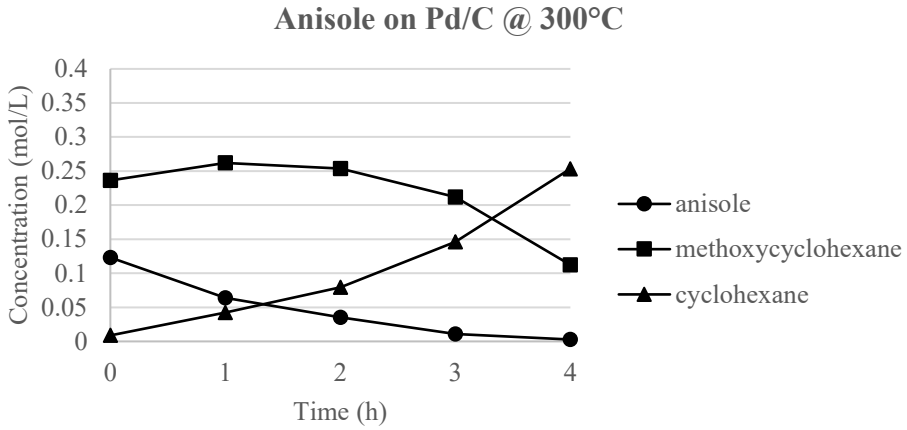

Figure 8-14. Batch Data for Anisole on 500 mg Pd/C at 300°C

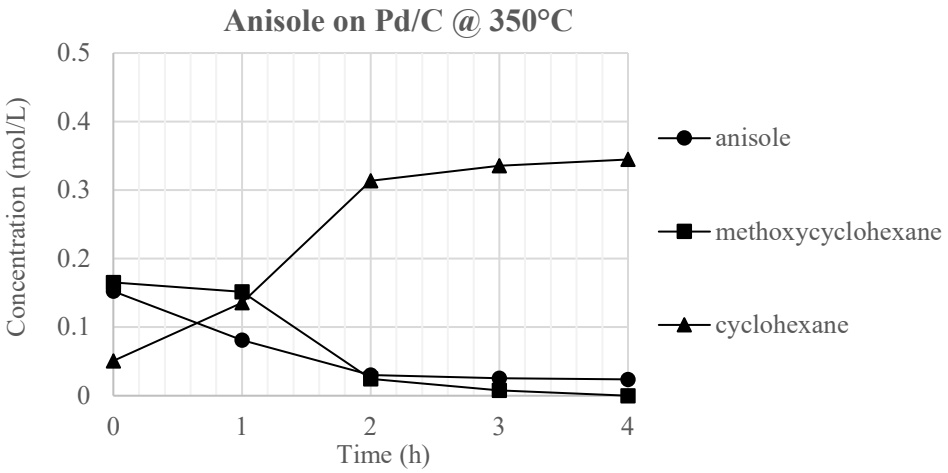

Figure 8-15. Batch Data for Anisole on 500 mg Pd/C at 350°C

8.3.6 Anisole & M-Cresol on 500 mg Pt/Al_2O_3

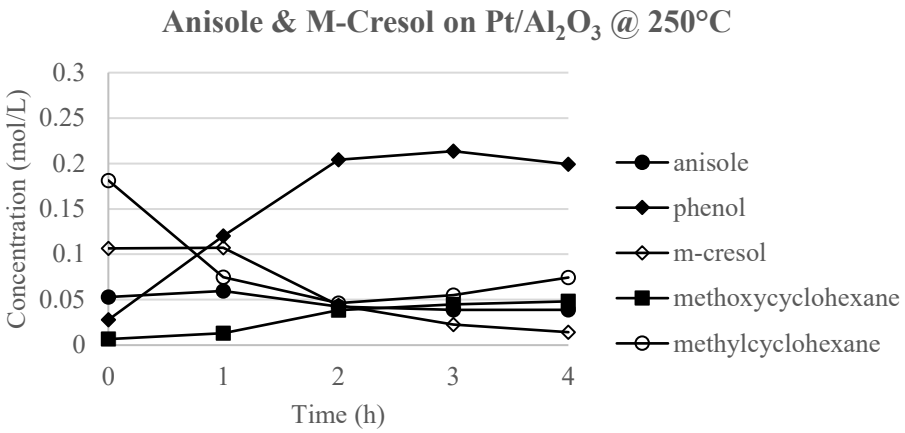

Figure 8-16. Batch Data for Anisole & M-Cresol Blend on 500 mg Pt/Al_2O_3 at 250°C

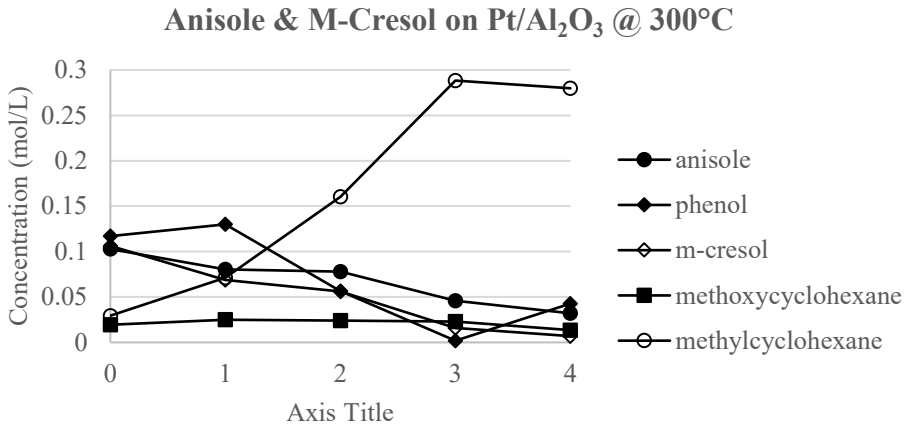

Figure 8-17. Batch Data for Anisole & M-Cresol Blend on 500 mg Pt/Al_2O_3 at 300°C

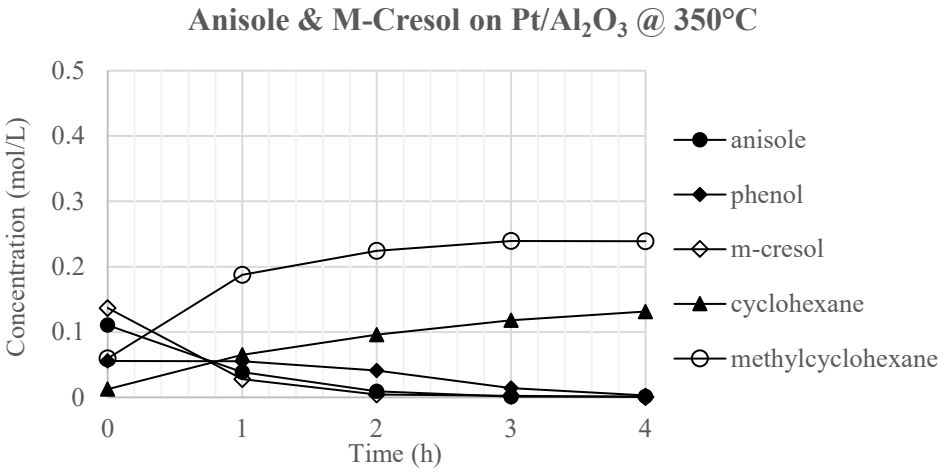

Figure 8-18. Batch Data for Anisole & M-Cresol Blend on 500 mg Pt/Al_2O_3 at 350°C

8.3.7 Anisole & Phenol on 500 mg Pt/Al_2O_3

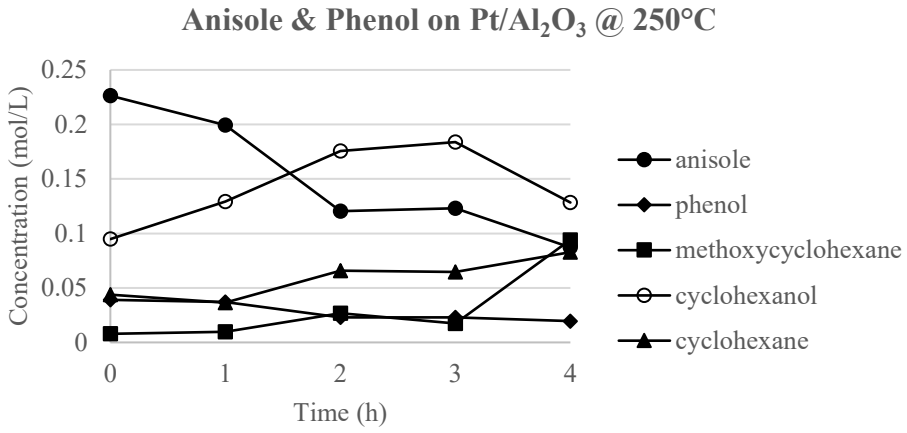

Figure 8-19. Batch Data for Anisole & Phenol Blend on 500 mg Pt/Al_2O_3 at 250°C

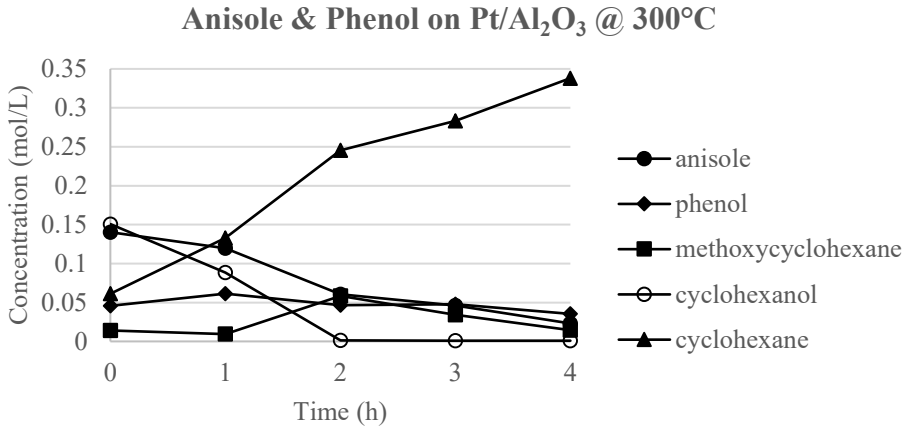

Figure 8-20. Batch Data for Anisole & Phenol Blend on 500 mg Pt/Al_2O_3 at 300°C

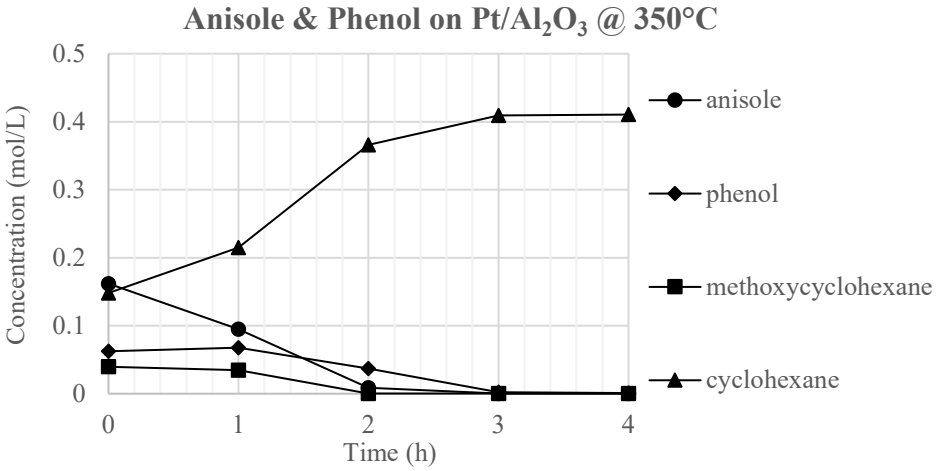

Figure 8-21. Batch Data for Anisole & Phenol Blend on 500 mg Pt/Al_2O_3 at 350°C

8.4 Pyrolysis Oil Data – Neat

The results presented in this section are from our initial experiments using pure model compounds in the differential reactor. While there are normalized fractions shown below, the results from this set of experiments are not reliably quantified and were not fit to the kinetic model.

8.4.1 Pd/C Results

8.4.1.1 Anisole

Table 8-8. Neat Anisole Data for Pd/C at 250°C

Peak	Compound	Normalized Fraction

2.23	benzene	0.0086
2.30	cyclohexene	0.0084
2.93	cyclohexanol	0.1076
3.10	anisole	0.8182
3.34	xylenol	0.0098
3.48	cresol	0.0473

Table 8-9. Neat Anisole Data for Pd/C at 300°C

Peak	Compound	Normalized Fraction
2.23	benzene	0.0049
2.30	cyclohexene	0.0106
2.93	cyclohexanol	0.0284
3.10	anisole	0.8981
3.23	phenol	0.0162
3.35	xylenol	0.0101
3.48	cresol	0.0262

Table 8-10. Neat Anisole Data for Pd/C at 350°C

Peak	Compound	Normalized Fraction
2.23	benzene	0.0190

2.3	cyclohexene	0.0170
2.93	cyclohexanol	0.0077
3.10	anisole	0.8953
3.23	phenol	0.0318
3.35	xylenol	0.0027
3.48	cresol	0.0145

8.4.1.2 Furfural

Table 8-11. Neat Furfural Data for Pd/C at 250°C

Peak	Compound	Normalized Fraction
2.90	furfural	1.0000

Table 8-12. Neat Furfural Data for Pd/C at 300°C

Peak	Compound	Normalized Fraction
2.90	furfural	0.9755
2.98	furylmethanol	0.0143
3.08	tetrahydrofurfuryl alcohol	0.0064
3.50	bifuran	0.0039

Table 8-13. Neat Furfural Data for Pd/C at 350°C

Peak	Compound	Normalized Fraction
2.39	tetrahydrofuran	0.0040
2.90	furfural	0.9761
2.98	furylmethanol	0.0199

8.4.1.3 Guaiacol

Table 8-14. Neat Guaiacol Data for Pd/C at 250°C

Peak	Compound	Normalized Fraction
3.26	phenol	0.0060
3.48	m-cresol	0.0092
3.56	p-cresol	0.0110
3.60	guaiacol	0.9738

Table 8-15. Neat Guaiacol Data for Pd/C at 300°C

Peak	Compound	Normalized Fraction
3.26	phenol	0.0079
3.60	guaiacol	0.9921

Table 8-16. Neat Guaiacol Data for Pd/C at 350°C

Peak	Compound	Normalized Fraction
3.26	phenol	0.0081
3.60	guaiacol	0.9919

8.4.1.4 M-Cresol

Table 8-17. Neat M-Cresol Data for Pd/C at 250°C

Peak	Compound	Normalized Fraction
3.28	methylcyclohexanone	0.1169
3.57	m-cresol	0.8831

Table 8-18. Neat M-Cresol Data for Pd/C at 300°C

Peak	Compound	Normalized Fraction
3.28	methylcyclohexanone	0.0608
3.57	m-cresol	0.9392

Table 8-19. Neat M-Cresol Data for Pd/C at 350°C

Peak	Compound	Normalized Fraction
3.28	methylcyclohexanone	0.1484

3.57	m-cresol	0.8516

8.4.2 Pt/Al_2O_3 Results

8.4.2.1 Anisole

Table 8-20. Neat Anisole Data for Pt/Al_2O_3 at 250°C

Peak	Compound	Normalized Fraction
2.23	benzene	0.0028
3.10	anisole	0.9893
3.36	methylanisole	0.0079

Table 8-21. Neat Anisole Data for Pt/Al_2O_3 at 300°C

Peak	Compound	Normalized Fraction
2.23	benzene	0.0354
2.30	cyclohexene	0.0077
3.04	cyclohexanone	0.1073
3.10	anisole	0.8210
3.23	phenol	0.0287

Table 8-22. Neat Anisole Data for Pt/Al_2O_3 at 350°C

Peak	Compound	Normalized Fraction
3.10	anisole	0.9849
3.27	benzyl alcohol	0.0072
3.38	methylanisole	0.0079

8.4.2.2 Furfural

Table 8-23. Neat Furfural Data for Pt/Al_2O_3 at 250°C

Peak	Compound	Normalized Fraction
2.90	furfural	0.9859
3.11	furyl methyl ketone	0.0118
3.47	bifuran	0.0024

Table 8-24. Neat Furfural Data for Pt/Al_2O_3 at 300°C

Peak	Compound	Normalized Fraction
2.90	furfural	0.9980
3.11	furyl methyl ketone	0.0010
3.47	bifuran	0.0010

Table 8-25. Neat Furfural Data for Pt/Al_2O_3 at 350°C

Peak	Compound	Normalized Fraction
2.90	furfural	0.9925
3.11	furyl methyl ketone	0.0049
3.42	bifuran	0.0026

8.4.2.3 Guaiacol

Table 8-26. Neat Guaiacol Data for Pt/Al_2O_3 at 250°C

Peak	Compound	Normalized Fraction
3.10	anisole	0.0119
3.58	cresol	0.0030
3.60	guaiacol	0.9852

Table 8-27. Neat Guaiacol Data for Pt/Al_2O_3 at 300°C

Peak	Compound	Normalized Fraction
3.26	phenol	0.0066
3.60	guaiacol	0.9934

Table 8-28. Neat Guaiacol Data for Pt/Al_2O_3 at 350°C

Peak	Compound	Normalized Fraction
3.10	anisole	0.0570
3.60	guaiacol	0.9430

8.4.2.4 M-Cresol

Table 8-29. Neat M-Cresol Data for Pt/Al_2O_3 at 250°C

Peak	Compound	Normalized Fraction
3.18	methylcyclohexanol	0.0069
3.21	methylcyclohexanone	0.0045
3.50	m-cresol	0.9887

Table 8-30. Neat M-Cresol Data for Pt/Al_2O_3 at 300°C

Peak	Compound	Normalized Fraction
3.18	methylcyclohexanol	0.0107
3.21	methylcyclohexanone	0.0052
3.50	m-cresol	0.9841

Table 8-31. Neat M-Cresol Data for Pt/Al_2O_3 at 350°C

Peak	Compound	Normalized Fraction
3.10	anisole	0.0134
3.57	m-cresol	0.9866

8.4.3 ZSM-5 Results

8.4.3.1 Anisole

Table 8-32. Neat Anisole Data for ZSM-5 at 250°C

Peak	Compound	Normalized Fraction
3.10	anisole	0.9890
3.48	cresol	0.0110

Table 8-33. Neat Anisole Data for ZSM-5 at 300°C

Peak	Compound	Normalized Fraction
2.30	cyclohexene	0.0050
3.06	cyclohexanone	0.5500
3.10	anisole	0.7205
3.23	phenol	0.0542
3.35	xylenol	0.0610

3.48	cresol	0.0360
3.58	trimethylphenol	0.0062

Table 8-34. Neat Anisole Data for ZSM-5 at 350°C

Peak	Compound	Normalized Fraction
2.30	cyclohexene	0.0111
3.10	anisole	0.7053
3.23	phenol	0.0819
3.35	xylenol	0.1257
3.48	cresol	0.0672
3.58	trimethylphenol	0.0089

8.4.3.2 Furfural

Table 8-35. Neat Furfural Data for ZSM-5 at 250°C

Peak	Compound	Normalized Fraction
2.90	furfural	0.9974
3.45	bifuran	0.0026

Table 8-36. Neat Furfural Data for ZSM-5 at 300°C

Peak	Compound	Normalized Fraction
2.90	furfural	0.9826
3.11	furyl methyl ketone	0.0110
3.50	bifuran	0.0064

Table 8-37. Neat Furfural Data for ZSM-5 at 350°C

Peak	Compound	Normalized Fraction
2.90	furfural	0.9880
3.11	furyl methyl ketone	0.0072
3.50	bifuran	0.0048

8.4.3.3 Guaiacol

Table 8-38. Neat Guaiacol Data for ZSM-5 at 250°C

Peak	Compound	Normalized Fraction
3.26	phenol	0.0043
3.48	m-cresol	0.0561
3.60	guaiacol	0.9397

Table 8-39. Neat Guaiacol Data for ZSM-5 at 300°C

Peak	Compound	Normalized Fraction
3.26	phenol	0.0038
3.48	m-cresol	0.0147
3.56	guaiacol	0.9815

Table 8-40. Neat Guaiacol Data for ZSM-5 at 350°C

Peak	Compound	Normalized Fraction
3.26	phenol	0.0081
3.60	guaiacol	0.9919

8.4.3.4 M-Cresol

Table 8-41. Neat M-Cresol Data for ZSM-5 at 250°C

Peak	Compound	Normalized Fraction
3.10	anisole	0.0107
3.57	m-cresol	0.9893

Table 8-42. Neat M-Cresol Data for ZSM-5 at 300°C

Peak	Compound	Normalized Fraction

3.10	anisole	0.0506
3.47	o-cresol	0.0066
3.57	m-cresol	0.9427

Table 8-43. Neat M-Cresol Data for ZSM-5 at 350°C

Peak	Compound	Normalized Fraction
3.10	anisole	0.0056
3.47	o-cresol	0.0071
3.57	m-cresol	0.9874

8.5 Pyrolysis Oil Data – Differential

The data in this section is from sets of experiments run in the differential reactor, using 5% (molar) model compound in dodecane. These were analyzed in the GC/FID, which was calibrated for proper quantification. The GC/MS was used to confirm peak identification, but was not used to quantify the data. Only the GC/FID data is presented here.

8.5.1 Pd/C

8.5.1.1 Anisole

Table 8-44. Differential Anisole Data for Pd/C at 250°C

Peak	Compound	Normalized Fraction
4.21	methoxycyclohexane	0.1393
5.25	anisole	0.8607

Table 8-45. Differential Anisole Data for Pd/C at 300°C

Peak	Compound	Normalized Fraction
4.21	methoxycyclohexane	0.2236
5.25	anisole	0.7764

Table 8-46. Differential Anisole Data for Pd/C at 350°C

Peak	Compound	Normalized Fraction
4.21	methoxycyclohexane	0.3350
5.25	anisole	0.6650

8.5.1.2 Guaiacol

Table 8-47. Differential Guaiacol Data for Pd/C at 250°C

Peak	Compound	Normalized Fraction
6.70	phenol	0.1171

8.30	guaiacol	0.8829

Table 8-48. Differential Guaiacol Data for Pd/C at 300°C

Peak	Compound	Normalized Fraction
6.70	phenol	0.4052
8.30	guaiacol	0.5948

Table 8-49. Differential Guaiacol Data for Pd/C at 350°C

Peak	Compound	Normalized Fraction
6.70	phenol	0.5560
8.30	guaiacol	0.4440

8.5.1.3 M-Cresol

Table 8-50. Differential M-Cresol Data for Pd/C at 250°C

Peak	Compound	Normalized Fraction
5.70	methylcyclohexanol	0.2925
8.40	m-cresol	0.7075

Table 8-51. Differential M-Cresol Data for Pd/C at 300°C

Peak	Compound	Normalized Fraction
5.70	methylcyclohexanol	0.5263
8.40	m-cresol	0.4737

Table 8-52. Differential M-Cresol Data for Pd/C at 350°C

Peak	Compound	Normalized Fraction
5.70	methylcyclohexanol	0.5939
8.40	m-cresol	0.4061

8.5.1.4 Phenol

Table 8-53. Differential Phenol Data for Pd/C at 250°C

Peak	Compound	Normalized Fraction
4.60	cyclohexanol	0.1045
6.90	phenol	0.8955

Table 8-54. Differential Phenol Data for Pd/C at 300°C

Peak	Compound	Normalized Fraction
4.60	cyclohexanol	0.1215

6.90	phenol	0.8785

Table 8-55. Differential Phenol Data for Pd/C at 350°C

Peak	Compound	Normalized Fraction
4.60	cyclohexanol	0.3028
6.90	phenol	0.6972

8.5.2 Pt/Al_2O_3

8.5.2.1 Anisole

Table 8-56. Differential Anisole Data for Pt/Al_2O_3 at 250°C

Peak	Compound	Normalized Fraction
4.21	methoxycyclohexane	0.0316
5.25	anisole	0.9684

Table 8-57. Differential Anisole Data for Pt/Al_2O_3 at 300°C

Peak	Compound	Normalized Fraction
4.21	methoxycyclohexane	0.0050
5.25	anisole	0.9950

Table 8-58. Differential Anisole Data for Pt/Al_2O_3 at 350°C

Peak	Compound	Normalized Fraction
4.21	methoxycyclohexane	0.0072
5.25	anisole	0.9928

8.5.2.2 Guaiacol

Table 8- 59. Differential Guaiacol Data for Pt/Al_2O_3 at 250°C

Peak	Compound	Normalized Fraction
6.70	phenol	0.0607
8.30	guaiacol	0.9393

Table 8-60. Differential Guaiacol Data for Pt/Al_2O_3 at 300°C

Peak	Compound	Normalized Fraction
6.70	phenol	0.1707
8.30	guaiacol	0.8293

Table 8-61. Differential Guaiacol Data for Pt/Al_2O_3 at 350°C

Peak	Compound	Normalized Fraction
6.70	phenol	0.4749

8.30	guaiacol	0.5251

8.5.2.3 M-Cresol

Table 8-62. Differential M-Cresol Data for Pt/Al_2O_3 at 250°C

Peak	Compound	Normalized Fraction
6.70	phenol	0.0245
8.40	m-cresol	0.9755

Table 8-63. Differential M-Cresol Data for Pt/Al_2O_3 at 300°C

Peak	Compound	Normalized Fraction
6.70	phenol	0.0252
8.40	m-cresol	0.9748

Table 8-64. Differential M-Cresol Data for Pt/Al_2O_3 at 350°C

Peak	Compound	Normalized Fraction
6.70	phenol	0.4436
8.40	m-cresol	0.5564

8.5.2.4 Phenol

Table 8-65. Differential Phenol Data for Pt/Al_2O_3 at 250°C

Peak	Compound	Normalized Fraction
4.60	cyclohexanol	0.0183
6.90	phenol	0.9817

Table 8-66. Differential Phenol Data for Pt/Al_2O_3 at 300°C

Peak	Compound	Normalized Fraction
4.60	cyclohexanol	0.0313
6.90	phenol	0.9687

Table 8-67. Differential Phenol Data for Pt/Al_2O_3 at 350°C

Peak	Compound	Normalized Fraction
4.60	cyclohexanol	0.0721
6.90	phenol	0.9279

8.6 Pyrolysis Oil Data – Pilot

This is the data from the pilot scale tests. These were continuous experiments using 5% (molar) model compound in dodecane over Pt/Al_2O_3 only. As with the differential

results in section 8.4, only the GC/FID data was used for quantification and is shown here.

8.6.1 Anisole

Table 8-68. Pilot Anisole Data for Pt/Al_2O_3 at 250°C

Peak	Compound	Normalized Fraction
1.95	cyclohexane	0.7125
5.20	anisole	0.2576
6.80	phenol	0.0299

Table 8-69. Pilot Anisole Data for Pt/Al_2O_3 at 300°C

Peak	Compound	Normalized Fraction
1.95	cyclohexane	0.8899
5.20	anisole	0.0886
6.80	phenol	0.0215

Table 8-70. Pilot Anisole Data for Pt/Al_2O_3 at 350°C

Peak	Compound	Normalized Fraction
1.95	cyclohexane	0.9070
5.20	anisole	0.0312

6.80	phenol	0.0618

8.6.2 Guaiacol

Table 8-71. Pilot Guaiacol Data for Pt/Al_2O_3 at 250°C

Peak	Compound	Normalized Fraction
1.95	cyclohexane	0.0078
6.80	phenol	0.0898
8.41	guaiacol	0.8324

Table 8-72. Pilot Guaiacol Data for Pt/Al_2O_3 at 300°C

Peak	Compound	Normalized Fraction
1.95	cyclohexane	0.1750
6.80	phenol	0.0128
8.41	guaiacol	0.8122

Table 8-73. Pilot Guaiacol Data for Pt/Al_2O_3 at 350°C

Peak	Compound	Normalized Fraction
1.95	cyclohexane	0.0829

6.80	phenol	0.1948
8.41	guaiacol	0.7222

8.6.3 M-Cresol

Table 8-74. Pilot M-Cresol Data for Pt/Al_2O_3 at 250°C

Peak	Compound	Normalized Fraction
1.95	cyclohexane	0.2765
6.80	phenol	0.0228
8.60	m-cresol	0.7007

Table 8-75. Pilot M-Cresol Data for Pt/Al_2O_3 at 300°C

Peak	Compound	Normalized Fraction
1.95	cyclohexane	0.6768
6.80	phenol	0.0253
8.60	m-cresol	0.2980

Table 8-76. Pilot M-Cresol Data for Pt/Al_2O_3 at 350°C

Peak	Compound	Normalized Fraction
1.95	cyclohexane	0.8054

6.80	phenol	0.1396
8.60	m-cresol	0.0550

8.6.4 Phenol

Table 8-77. Pilot Phenol Data for Pt/Al_2O_3 at 250°C

Peak	Compound	Normalized Fraction
1.95	cyclohexane	0.4875
6.80	phenol	0.5125

Table 8-78. Pilot Phenol Data for Pt/Al_2O_3 at 300°C

Peak	Compound	Normalized Fraction
1.95	cyclohexane	0.5095
6.80	phenol	0.4905

Table 8-79. Pilot Phenol Data for Pt/Al_2O_3 at 350°C

Peak	Compound	Normalized Fraction
1.95	cyclohexane	0.5194
6.80	phenol	0.4806